DISSERTATIONES PHYSICAE UNIVERSITATIS TARTUENSIS
33

PICOSECOND DYNAMICS OF OPTICAL EXCITATIONS IN GaAs AND OTHER EXCITONIC SYSTEMS

INDREK REIMAND

TARTU 2000

DISSERTATIONES PHYSICAE UNIVERSITATIS TARTUENSIS

33

DISSERTATIONES PHYSICAE UNIVERSITATIS TARTUENSIS
33

PICOSECOND DYNAMICS OF OPTICAL EXCITATIONS IN GaAs AND OTHER EXCITONIC SYSTEMS

INDREK REIMAND

TARTU UNIVERSITY
PRESS

The study was carried out at the Institute of Physics, Tartu University.

The dissertation was admitted on January 26, 2000, in partial fulfilment of the requirements for the degree of Doctor of Philosophy in physics (optics and spectroscopy), and allowed for defence by the Council of the Department of Physics, University of Tartu.

Supervisor: Prof. Jaak Aaviksoo, Institute of Experimental Physics, Tartu University

Opponents: Prof. Philippe Lavallard, Groupe de Physique des Solides, Université Paris 7;

Prof. Vladimir Hizhnyakov, University of Tartu

Defence: March 29, 2000 at University of Tartu, Tartu, Estonia.

Tartu Ülikooli Kirjastus
Tiigi 78, 50410 Tartu
Tellimus nr. 108

CONTENTS

LIST OF PUBLICATIONS INCLUDED IN THE THESIS

I. J. Aaviksoo, J. Kuhl, I. Reimand, "Time-resolved reflection of light from InP crystals", Solid State Comm., vol. 72, no. 1, p. 49 (1989).

II. J. Aaviksoo, J. Kuhl, I. Reimand, "Time resolved resonant reflection of light", Laser Optics of Condensed Matter, vol. 2, Plenum New York, pp. 61-69 (1991).

III. Я. Ю. Аавиксоо, И. Я. Рейманд, В. В. Россин, В. В. Травников, "Кинетика образования и энергетической релаксации экситонов в GaAs", Письма в ЖЭТФ, том 53, вып. 7, стр. 377, (1991).

IV. I. Reimand, J. Aaviksoo, "Surface polarization dynamics revealed by time-resolved resonant reflection of light", Opt. Commun., vol. 86, no. 2, p. 142, (1991).

V. Я. Ю. Аавиксоо, И. Я. Рейманд, В. В. Россин, В. В. Травников, "Гашение экситонной люминесценции горячими электронами в GaAs", ФТТ, том 33, вып. 8, стр. 2408, (1991).

VI. J. Aaviksoo, I. Reimand, V. V. Rossin, V. V. Travnikov, "Kinetics of free exciton luminescence in GaAs", Phys. Rev. B, vol. 45, no. 3, p. 1473, (1992).

VII. J. Aaviksoo, I. Reimand, V. Rossin, V. Travnikov, "Kinetics of free exciton formation and relaxation in GaAs", J. Lumin., vol. 53, p. 423, (1992).

VIII. D. Varding, I. Reimand, G. Zimmerer, "Time-resolved luminescence of exciton-polaritons in solid xenon", Physica Status Solidi B, vol. 185, no. 1, p.301, (1994).

IX. Я. Ю. Аавиксоо, И. Я. Рейманд, В. В. Россин, В. В. Травников, "Влияние экситон-электронного взаимодействия на кинетику экситонной люминесценсии", ФТТ, т. 36, № 5, стр. 1470, (1994).

X. С. О. Когновицкий, В. В. Травников, Я. Аавиксоо, И. Рейманд, "Рассеяние света электронами в области экситонного поглащения GaAs", ФТТ том 39, стр. 1011, (1997).

XI. I. Reimand, E. Gminder, M. Kirm, V. Kisand, B. Steeg, D. Varding, G. Zimmerer, "An analysis of electron-hole recombination in solid Xenon with time-resolved luminescence spectroscopy", Phys. Stat. Sol. (b), vol. 214, no 1, p. 81 (1999).

XII. I. Reimand, J. Aaviksoo, "Exciton interaction with hot electrons in GaAs" (**submitted** to Phys. Rev. B, October 1999).

1 INTRODUCTION

The interaction of light field with matter is one of the most general and fundamental problems in physics. Thanks to many practical applications, activity in this branch of physics has continuously maintained a very high level. A practical outcome of these investigations, namely lasers, is now a powerful tool in science and technology. The experimental possibilities have grown still further through the appearance of the ultra-short pulse lasers, which enables an even deeper understanding of many important and interesting aspects of the interaction of light with matter.

1.1 Secondary emission in the case of luminescence centres

The optical response of a material to incident light field is often called secondary emission (SE). In this notation the primary emission would be the oncoming light.

The secondary emission can be non-resonant and resonant. Non-resonant SE occurs when primary light does not excite any electronic states in the material. Non-resonant SE contains different scattering components, such as Raman and Rayleigh scattering, which are spectrally far from material resonance.

When a light pulse overlaps spectrally with the absorption band of the crystal, resonant secondary emission (RSE) may arise. Here the term *resonant* indicates that the exciting light generates *real* (not virtual) electronic transitions.

The RSE of impurity centres was theoretically analysed in [1–5]. The second-order perturbation formulae, obtained in [1, 3, 4] describe RSE as a superposition of two spectra: (1) a zero-phonon (Rayleigh) line of scattering and its vibrational replicas; (2) a zero-phonon (pure electronic) line of luminescence and its vibrational replicas [5].

From the point of view of relaxation criteria, the physical differences between the components of RSE are quite obvious. Scattering is part of the RSE emitted before the transverse relaxation, i.e. before the phase correlation with the excited light vanishes. Hot luminescence arises at the next relaxation stage, i.e. during the energetic relaxation towards the thermal equilibrium in the excited electronic state. Ordinary luminescence is an emission from the state, where both transverse and longitudinal relaxation are fully completed [4]. The transversal and longitudinal relaxation time constants (T_2 and T_1, respectively) will depend on the physical processes involved. The simplest case is an impurity in the crystal, which has one single local mode, but where an interaction with the lattice exists, and the vibrational relaxation processes are rapid in comparison with the optical lifetime of the electronic state. In this case T_2 is determined by the interaction with the thermal bath only, and T_1 is the vibrational relaxation time.

In a simple case all impurity centres can be treated independently. The overall crystal RSE is just an incoherent superposition of individual centres. In the case of exciting a crystal with luminescence centres with a low intensity light (when emission from individual centres remains linear), the T_2 and T_1 are independent of the intensity, and the RSE may be concerned linear — excited centres do not *feel* each other. An interaction between the impurities starts from a concentration of about 10^{18} cm^{-3} [6].

Under certain limiting conditions the phenomenological time constants T_2 and T_1 are directly measurable from the experimentally registered RSE. In most practical cases the RSE has a more complicated time-frequency kinetics that involves T_2, T_1 and excitation conditions as parameters [7].

Although RSE may have a greater magnitude in the vicinity of crystal resonance, it is important to bear in mind, that a non-resonant SE will always exist, and may have an interference with the coherent part of RSE.

1.2 Secondary emission in the case of exciton resonance

A theory of RSE of the excitons weakly coupled with phonons is developed in [8, 9]. Phenomenological T_2 and T_1 times, which play a decisive role in describing the RSE in localised systems, are replaced by the lifetime of the polariton states (with a fixed wave number k) and the decay time of the polariton distribution function at the corresponding energy. A frequency- and geometry-dependent radiative process replaces the radiative decay constant, which characterises electronic transition in the impurity case.

The processes responsible for phase and energy relaxation are quite different from the impurity centre, and are generally not exponential. The kinetics of the RSE (including both scattering and luminescence) of polariton systems can be regarded as a unique optical process resulting from multiple scattering of photon-coupled excitons by vibrations.

An important feature is that in the exciton case, the Rayleigh' scattering forms only reflected (back scattered) and transmitted (forth-scattered) beams; in all other directions the interference is destructive. This is explained by the fact that exciton is a collective excitation of the crystal, with the translational symmetry, and is, thereby, characterised by a good wave number; as opposed to the impurity centre case. Generally, a strict physical distinction of scattering from the rest of RSE at exciton resonance is often difficult or even meaningless. However, RSE in the form of reflection results from pure (Rayleigh') scattering, giving us information about the processes leading to a phase coherence loss [10].

As in the case of impurities in a crystal, the frequency-dependent kinetics of RSE of exciton resonance reveals information about the material parameters. A major difference lies in the fact that some processes in exciton kinetics are essentially non-linear. The polariton propagation and the radiation from the crystal surface are some examples. Exciton energy exchange with other excitons

in GaAs has been found to be important already at concentrations of 10^{14} cm^{-3} [11]. And last but not least, exciton creation from charge carriers has a bimolecular character (proportional both to electrons' and holes' concentration) with a quadratic dependence on the particle number. Thus the understanding of all the processes involved is still qualitative, and is under continuing investigation.

1.3 Excitations generated by light in a pure crystal

An absorbed photon in a pure non-metallic crystal generates a free electron-hole pair or an exciton. Due to the energy and momentum conservation law the initial excess energy (relative) shares of electron and hole are inverse proportional to their masses. At this point the relaxation starts. In the course of the relaxation other excitations may arise, such as phonons, excitons etc.
As mentioned earlier, the process of excitation evolution has several non-linear aspects already at low excitation intensities. However, if the initial light excitation is strong, various additional essentially non-linear effects may take place. These non-linear effects are out of scope of the present work, but let us mention them and give some relevant scale for estimating their importance.

- If the exciting light field is very strong (about 10^9 W/cm^2), the dynamic Stark' effect takes place. In this case the electromagnetic field modifies the crystal resonance itself. When the field disappears, the shift caused by the dynamic Stark' effect also disappears, indicating to the generation of virtual excitations (real excitations would have lifetime) by the light field. For the exciton line it is only the shift caused by the dynamic Stark' effect that is registered (first observation reported in [12]), the splitting of the line is not observed [13].
- If the concentration of the created electron-hole plasma is in the order of, or higher than the Mott' density then the conduction band re-normalisation takes place shifting the band-gap energy due to a reduced screening length. At the Mott' density screening length is equal to 0.84 excitons Bohr' radius, band-gap is shifted to exciton energy and exciton becomes metastable. However, the energy of exciton line does not shift [14, 15], even for densities significantly greater than Mott' density. The Mott' density depends strongly on the temperature of the excited plasma and for GaAs at $kT=E_B$ $n_{Mott}=3*10^{16}$ cm^{-3} [15] (k – Boltzmann coefficient, E_B – excitons Bohr' energy).
- If the exciton concentration is high, biexcitons may form. When two excitons are close together, the two-exciton wavefunction can be either a symmetric or anti-symmetric combination of exciton wave-functions. The symmetric combination has a lower energy and forms the bound state of biexciton. In GaAs, however, the biexciton binding energy is extremely low (0.13 meV [16]), and biexcitons do not play a major role in the secondary emission.

In the current work only low intensity excitations are regarded and these effects are not considered.

1.4 Relaxation dynamics of optical excitations

If a semiconductor crystal is at a thermodynamic equilibrium, its excitation by a short light pulse is followed by several stages of relaxation before it regains its thermodynamic equilibrium. The carrier relaxation can be classified into four temporally overlapping regimes (in growing order of characteristic time-scale) [13]:

a) Coherent regime. An ultra-short laser pulse creates an excitation in the semiconductor with a well-defined phase relationship within the excitation and with the electromagnetic field that created the excitations. The laser pulse can create either real or virtual excitations. The scattering processes, which destroy the coherence, are extremely fast in semiconductors, and pico- and femtosecond techniques are required to study this regime. Typical scattering processes are carrier-carrier scattering, intervalley scattering ($\Gamma \rightarrow L, X$) and hole-optical-phonon scattering.

b) Non-thermal regime. In most cases of excitation the crystal by light, the distribution of the free electron-hole pairs or excitons after the destruction of coherence is very likely to be non-thermal, i.e. the distribution function of excitations can not be characterised by a temperature. Investigation of this regime provides information about various processes (such as carrier-carrier or exciton-exciton and electron-optical-phonon scattering) that bring the non-thermal distribution to a hot, thermalised distribution.

c) Hot-excitation regime. Carrier-carrier (or exciton-exciton) scattering is primarily responsible for a redistribution of the energy within the carrier (exciton) system, and leads to a thermalised distribution. The temperature is usually higher than the lattice temperature, and may be different for different sub-systems (electrons, holes, excitons). The thermalisation times depend strongly on many factors including the carrier density. Typically, the electrons and holes thermalise among themselves in hundreds of femtoseconds, while the electrons and holes achieve a common temperature in a couple of picoseconds. These times depend strongly on the concentration of charge carriers ($\tau \sim n^{-2}$). The thermalised electron-hole pairs reach lattice temperature in hundreds of picoseconds, through interaction with various phonons in the semiconductor. This time does not depend on the carriers' concentration, at least in the low concentration limit.

d) Isothermal regime. At the end of hot-excitation regime, all the carriers, phonons and excitons are in equilibrium with each other, i.e. can be described by the same temperature, that of lattice. However, there is still an excess of excitations as compared to the thermodynamic equilibrium. These excess electron-hole pairs (or excitons) recombine either radiatively or non-

radiatively, and the semiconductor returns to the thermodynamic equilibrium.

The time-scales for the above-mentioned regimes depend on various conditions, especially on the crystal temperature and the subsystem considered (charge carriers or excitons), and therefore are not provided here.

1.5 Main objectives of the present study

The main objectives of the present study were (**in bold**):

For the purposes of investigating the coherent stage of the resonant secondary emission (RSE) of semiconductor crystals by means of picosecond time-resolved spectroscopy,

- **To study the reflection of light from the surfaces of semiconductor crystals at exciton resonance; to analyse the dynamical processes leading to the loss of the phase coherence of polaritons and other mechanisms of polarisation decay.**

To understand the sophisticated interaction between various excitations in crystals in the process of the energy relaxation and to distinguish between different contributions of exciton photoluminescence (PL) kinetics

- **To study the low-temperature exciton PL kinetics in semiconductor and other monocrystals with picosecond time-resolution; to analyse the dynamical processes governing the exciton formation and PL.**

To estimate the applicability of the models used, to get some feedback from the other groups concerned with a similar research, and to add some quantitative information to otherwise a very qualitative picture of the processes involved

- **To relate the material exciton-resonance parameters to the results of experimental measurements.**

For the purposes of gaining some new knowledge from experiment by using novel experimental methods

- **To develop experimental techniques for investigating the dynamics of low intensity optical excitations**

2 THEORY AND EXPERIMENTAL

2.1 Basic concepts

2.1.1 Excitons

At a low temperatures in pure crystals excitons constitute the final state in the energy relaxation of the photo-excited crystal.

The concept of the exciton as a quantum of excitation propagating in an insulating crystal originated with Frenkel (1931) and Peierls (1932). Frenkel considered N identical atoms in a crystal, in which one atom is raised to an excited state of energy E_1. In the absence of inter-atomic coupling, the wave function of the crystal is $\Phi_j = A\phi_1\phi_2...\varphi_j...\phi_N$, where ϕ_i represents the ground state of atom i, φ_i its excited state, and A is the antisymmetrization operator. Clearly Φ_j is N-fold degenerate, since the excitation can be on any atom. Introduction of inter-atomic coupling lifts this degeneracy. The problem is analogous to that of N coupled oscillators and has a well-known solution: a band of N normal modes with Bloch-type wave functions.

Frenkel's model is appropriate in the limit when both excited electron and hole are located in the same atom. In the opposite limit, when the electron and hole are separated by many inter-atomic spacings, we can use the effective mass approximation (EMA), as was first shown by Wannier (1937).

In the ordinary single particle band theory, the lowest excited state of an insulator consists of an electron at the absolute minimum of the (normally empty) conduction band and a hole at the absolute maximum of the (normally filled) valence band. This state is at the energy E_g, the bandgap, above the ground state. Near these extrema, the kinetic energies of the electron and the hole are positive quadratic functions of the change in momentum $\hbar(\vec{k} - \vec{k}_m)$, where $\hbar\vec{k}$ is the momentum at the extremum.

The electron and hole attract each other. If they are so far apart that the atomic structure of the crystal can be ignored, their mutual potential can be written $V(\vec{\rho}) = -e^2/\varepsilon\rho$, where $\vec{\rho}$ is the electron-hole separation and ε is the macroscopic dielectric constant. The Coulomb potential gives rise to an infinite series of discrete hydrogenic bound states, with energies given by

$$E_n(\vec{k}) = -\frac{e^4\mu}{2\hbar^2\varepsilon^2 n^2} + \frac{\hbar^2 K^2}{2M}$$

where n=1,2,...,∞, $\mu^{-1}=(m_e^*)^{-1}+(m_h^*)^{-1}$, $M=m_e^*+m_h^*$, m_e^* and m_h^* are effective masses of the electron and hole, $\hbar\vec{K}$ is the momentum of the center of mass,

and E_n is measured from the band edge E_g. The analogy with H atom lets us use "exciton Bohr radius" $a_x = \hbar^2 \varepsilon / \mu e^2$ and "exciton Rydberg energy" $E_x = \hbar^2 / 2\mu a_x$ [17].

In conclusion an exciton forms a resonance lying energetically below the conduction band and being the final point of optical excitation, and having essential oscillator strength. Wannier excitons are well described by H-atom model.

2.1.2 Polaritons

The interaction of light (photons) with material resonances (excitons) brings about the formation of new excitations called polaritons [18, 19, 20]. In classical electrodynamic theory, light in a homogeneous dielectric medium is described by the dielectric constant ε, which can be calculated from microscopic theory. In the case of excitons ε is well modelled as a response of a set of Lorentz oscillators and one has

$$\varepsilon(\omega) = \varepsilon_0 + \frac{4\pi\alpha\omega_0^2}{\omega_0^2 - \omega^2 - i\omega\Gamma} \qquad (1)$$

where ε_0 is the dielectric constant due to higher lying resonances, α the polarizability, ω_0 the frequency, and Γ the phenomenological damping rate of the material resonance [21]. If coupling of the local oscillators (spatial dispersion) is relevant, ω_0 is replaced by

$$\omega_0 = \omega_0^0 + \frac{\hbar k^2}{2m_*} \qquad (2)$$

where m_* is the effective mass of excitons, and ε is , hence, wave vector dependent $\varepsilon = \varepsilon(\omega, k)$ [22]. By solving the homogeneous wave equation $\varepsilon(\omega, k) = c^2 k^2 / \omega^2$ one gets the dispersion curve of the new normal waves in the medium; the polaritons.

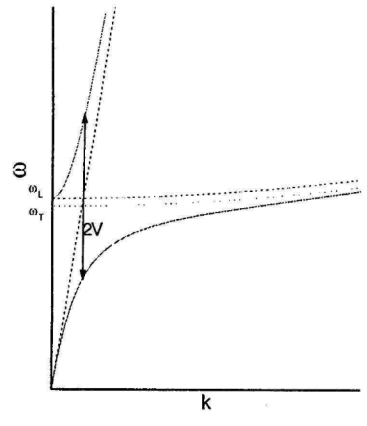

Figure 1. Schematic dispersion curve of polaritons. ω_L and ω_T denote longitudinal and transversal exciton frequency.

Quantum theory regards polariton as a superposition of a photon state and an exciton state with a common wave vector k, which forms an eigenstate of the coupled exciton-photon Hamiltonian. The general shape of the polariton dispersion curve is given in figure 1. The splitting of the dispersion curves at exact resonance $k = k_0 = \sqrt{\varepsilon_0 \omega_0 / c}$ is given by

$$2V = \sqrt{\frac{4\pi\alpha}{\varepsilon_0}}\omega_0$$

and reflects the coupling strength of excitons and photons. Another important parameter is the LT-splitting (the width of the stop band)

$$\omega_L - \omega_T = \Delta_{LT} = \frac{4\pi\alpha\omega_0}{2\varepsilon_0} \tag{4}$$

which is proportional to the polarizability α of the resonance. The oscillator strength F and the dipole moment D, which are often used to characterise the resonance, are related to the polarizability by the following relations

$$\alpha = \frac{e^2}{\omega_0^2 m v} F = \frac{2}{3\hbar\omega_0 v} D^2 \tag{5}$$

where v is the volume of the unit cell.

A notable consequence of spatial dispersion, compared to the case of local media, is the presence of additional (polariton) waves propagating in the crystal at given ω. If the system is infinite (no boundary), any linear combination of polariton waves can be taken as a propagating excitation in the crystal. If the system is bounded, the amplitudes of each component of reflected and transmitted waves are found by solving Maxwell equations using conventional Maxwell boundary conditions for the dielectrics. With an additional polariton wave propagating in the crystal one needs an additional boundary condition (ABC). Most frequently the Pekar ABC is used, which assumes that polarisation vanishes at the surface: $P(r,t)\big|_{\Sigma} = 0$ [23]. Generally, a microscopic calculation of ABC is needed.

The polariton description is useful regardless of the exciton mode (Wannier-Mott or Frenkel).

2.2 Transient reflection of light

The term *transient reflection* in the current work denotes transient phenomena at reflection and not *transient reflectivity*, which ordinarily denotes transients arising due to a non-linear modification of the reflectivity itself (e.g. see [24]). Reflection is a constructive interference of Rayleigh' scattering, therefore it may also be considered from the viewpoint of the secondary emission (SE). If the spectrum of the oncoming light covers exciton-resonance of the crystal, then both resonant and non-resonant terms of the SE are present. The resonant terms of the reflection depend on particular exciton-resonance parameters. We can talk about reflection as long as a coherent ensemble of polaritons is present near the surface of the crystal.

To understand the way a resonance modifies the temporal shape of a reflected light pulse to the best of advantage, one should consider the processes in the spectral domain. The temporal and spectral representations of the light pulse are connected by Fourier' transforms [25]:

$$F(\omega) = \int_{-\infty}^{\infty} f(t) e^{-i\omega t} dt \tag{6}$$

$$f(t) = \frac{1}{2\pi} \int_{-\infty}^{\infty} F(\omega) e^{i\omega t} d\omega \tag{7}$$

where f(t) and F(ω) are temporal and spectral representations of the light pulse. Reflection spectra of crystals are generally understood proceeding from the Fresnel formula for the reflection coefficient $r(\omega)$. For right angle reflection:

$$r(\omega) = \frac{1 - n(\omega)}{1 + n(\omega)} \tag{8}$$

where $n(\omega)$ is the complex refraction index of the material. In the vicinity of a resonance the reflection should show transient behaviour for pulse excitation as a straightforward consequence of the frequency dependence of the reflection coefficient. In the linear approximation, the reflected pulse $E_R(t)$ is related to the initial pulse $E_I(t)$ through the Fourier integral:

$$E_R(t) = \frac{1}{2\pi} \int e^{-i\omega t} E_I(\omega) r(\omega) d\omega \tag{9}$$

where $E_R(\omega)$ is the spectrum of the initial pulse.

Due to large size of Wannier-Mott excitons, at the crystal surface an interface layer (with a characteristic thickness in order of the exciton radius) should exist, where exciton population "feels" the surface. The most illustrative explanation of the effect is that excitons can not go closer to the surface than their radius. This exciton-free or "dead" layer effect is found to play an essential role in steady-state light reflection experiments from semiconductor surface in the vicinity of exciton resonance [26]. This dead layer effectively adds another boundary to the crystal, and the resultant reflection coefficient will have

additional terms. Fortunately, in the case of Brewster' angle incident beam ($\alpha = \arctan\sqrt{\varepsilon_0}$, parallel polarised beam), at the vacuum-dead-layer boundary no reflection remains at all, and at the dead-layer-bulk-crystal boundary it is the exciton resonance alone that determines all the reflection (if there is no exciton then there is no reflection, due to Brewster' condition). Or in other words, under the Brewster' angle only the resonant part of reflection persists, whereas the non-resonant component is eliminated.
Following formula (9), the transient properties of reflection were first analysed by Elert in ref. [27] for the case of a local media and for a truncated sinusoidal waveform as the incident pulse. It was shown that the transients generated by the fast front of the incident wave appear at early times in the reflected waveform; however, they do so with a characteristic duration, comparable with the light period. Later, transient reflectivity was analysed in [28] for a spatially dispersive media, but again with a truncated waveform. The observability of transient reflection under experimentally available conditions (realistic incident light pulses) was analysed in [29]. The analysis has revealed that transient behaviour of coherent polarisation can be observed on a 1 ps time scale, both in transmission and reflection, provided that the exciting pulse possesses sharp temporal structures (leading or trailing edges), which are shorter than the characteristic reaction time of the system.

2.3 Samples

In the present study the following samples were investigated experimentally.

InP and CdSe
The epitaxial InP sample (FS920, 2.3 μm thick) revealed a characteristic excitonic reflection dip and the luminescence spectrum of the sample exhibited a well-pronounced free-exciton emission band. The sample was obtained from J. Kuhl at Max-Planck-Institut für Festkörperforschung, Stuttgart.
The vapor grown thin platelets of CdSe exhibited well-pronounced steady-state reflection and polariton emission spectra. The sample was obtained from V. Travnikov at Institute of Physics and Technology, S.-Petersburg.

GaAs
The sample R560 used in reflection experiments was a liquid phase epitaxy grown bulk crystal with an impurity concentration of about 10^{14} cm^{-3}. The sample was obtained from J. Kuhl at Max-Planck-Institut für Festkörper-forschung, Stuttgart.
The sample G13 used in luminescence experiments was an ultra pure vapour phase epitaxy grown GaAs bulk crystal with a residual donor concentration of about 10^{12} cm^{-3} [30]. The sample was obtained from V. Travnikov at Institute of Physics and Technology, S.-Petersburg.

Solid Xe
The crystal was grown directly at the experiment site (at HASYLAB, Deutsches Elektronensynchrotron, Hamburg) under nearly thermal equilibrium conditions at T=118 K with a growing rate of $\approx 10^3$ nm/min, the preparation time was up to 18 hours. The crystal-growth set-up is described in detail in [31]. As a result, a bulk clear sample with a thickness up to ~1 mm, was obtained.

2.4 Experimental

Time-resolved reflection experiments on InP, GaAs and CdSe.
The experimental set-up was based on a synchronously pumped dye laser: Styryl-9M, average power 10 mW, pulse duration Δt=3.6 ps (FWHM of the autocorrelation function ACF), spectral width $\Delta\nu$=6 cm^{-1} at ν_L=12221.5 cm^{-1}. The reflected pulses were analysed by measuring their cross-correlation functions (CCF) with the incident pulses using synchronous detection technique. The experiment was performed by J. Aaviksoo and J. Kuhl at Max-Planck-Institut für Festkörperforschung, Stuttgart. The experimental for the case of GaAs is published in [32].

Luminescence experiments on GaAs
The excitation source was a mode locked Kr^+ or Ar^+ ion laser (Spectra-Physics Model 171-01 or –09 with a mode locking rate f=41 MHz and an average power P_{av}=1 W), which pumped the Styryl-8 dye laser (Spectra-Physics Model 375). The dye laser emitted pulse train with a repetition rate f=82 or f=4 MHz (cavity dumping) and it was frequency tuned by a 2-plate Lyot' filter. The laser linewidth $\Delta\lambda_{laser}$=0.2 nm and pulse length Δt=3 ps (measured by using auto-correlation technique). The pulse mean power was measured by a Newport power meter (model 880) and regulated by a variable optical density neutral filter. Both focused and unfocused beams were used in experiments.
The sample was immersed into liquid Helium in a cryostate UTREKS at a temperature below He λ-point (T≈2 K).
The emission kinetics was measured through a monochromator pair (MDR-23) in the subtractive dispersion mount. For temporal resolution the time correlated single photon counting technique was used (photomultiplier Hamamatsu R928, constant-fraction discriminator ORTEC M583 and time-to-amplitude converter (TAC) ORTEC M567). An analog signal was digitised for a pulse-height-analysis by a data-acquisition computer board (Meilhaus Electronic PC26AT, with self-made add-ons for featuring pulse amplitude analyse). The apparatus function of the total experimental set-up was Δt=200 ps and $\Delta\lambda$=0.1 nm.
In the experiments with an additional laser excitation a modulated (quasi-CW) diode laser of λ=670 nm or λ=815 nm illuminated the sample. The modulation was meander-like with rate f=50 kHz, which exceeds the maximum photon count rate, allowing us to disregard the influence of dead times dependent on

the modulation phase. Two luminescence kinetics were recorded simultaneously for both cases: with and without an additional CW excitation. In this experiment the laser beams were focused to a slit-like profile with dimensions 0.04×0.9 mm^2. The scheme of the experiment is shown in fig. 2.

To our best knowledge, no one has reported using an such experimental set-up to investigate exciton luminescence. The novelty of the scheme is in joining the time-correlated photon-counting (TCPC) method with the modulation. This set-up allows us to investigate the *difference* of two TCPC profiles (corresponding to the phases of modulation) with reduced noises, compared to simply subtracting two separately measured profiles.

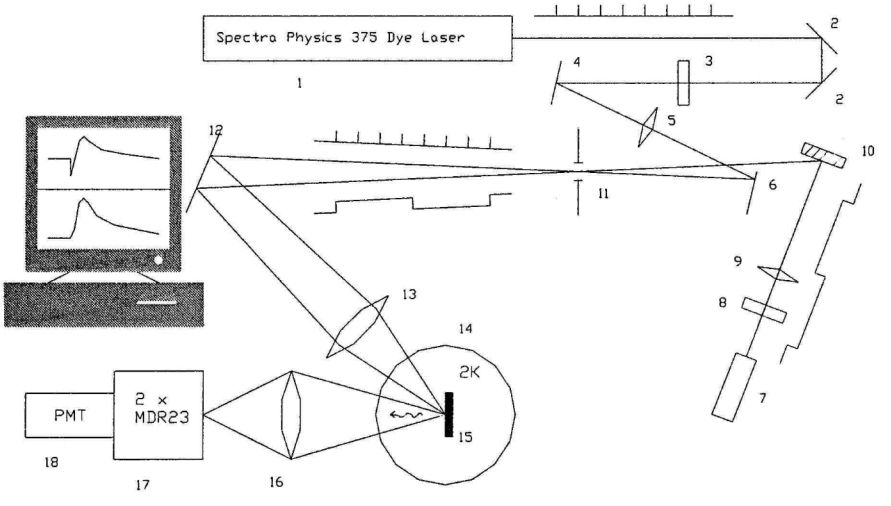

Figure 2. Experiment scheme. 1 – picosecond pulse laser, 2, 4, 6, 12 – mirrors, 3, 8 – shutters, 5, 9, 13, 16 - lenses, 7 – meander-like modulated diode laser, 10, 11 – grating and slit for purifying the diode laser spectrum, 14 – cryostat, 15 – the sample, 17 – a pair of monochromators, 18 – photomultiplying tube. Schematic time profiles of exciting light are drawn at laser beams (see text for timing parameters). In computer screen typical luminescence kinetics are shown: upper curve – diode lasers ***on*** phase, lower curve – diode lasers ***off*** phase.

Luminescence experiments on solid Xe

The experimental set-up is based on the pulsed nature of synchrotron radiation (pulse width Δt=130 ps). Spectrally, the incident beam was selected by a primary monochromator with $\Delta\lambda$=0.25 nm. For temporal resolution the time-correlated single photon counting technique was used. The spectral and temporal resolution (FWHM) of the registering system was $\Delta\lambda$=1.5 nm and Δt=0.4 ns, respectively.

The experiment was performed by D. Varding, G. Zimmerer et. al. at HASYLAB, Deutsches Elektronensynchrotron (DESY), Hamburg.

3 COHERENT OPTICAL RESPONSE OF LIGHT FROM SEMICONDUCTOR SURFACES

3.1 Theoretical considerations

The optical properties of the crystal in the vicinity of exciton resonance are described by a dielectric function $\varepsilon(\omega,k)$ [22, 33], written in the form:

$$\varepsilon(\omega,k)=\varepsilon_0+\frac{4\pi\alpha\omega_0^2}{\omega_0^2-\omega^2-i\omega\Gamma+\hbar\omega_0k^2/m_*} \tag{10}$$

which accounts for the actual resonance at ω_0 with the polarizability $4\pi\alpha$, the dephasing rate Γ, and the effective mass m^*. The influence of higher-lying resonances is included through ε_0.

The reflection coefficient can be calculated proceeding from the dielectric function and making use of appropriate boundary conditions. In the general case of oblique incidence, three waves (two transverse and one longitudinal) are excited in a nonlocal medium [34]. The explicit expression for $r(\omega)$ has been calculated for Pekar ABC in [35]. The reflected pulse amplitude from the material surface is given by formula (9).

So, a good knowledge of the material parameters (ω_0, $4\pi\alpha$, Γ, m^* and ε_0) allows us to calculate the reflected pulse in quite a straightforward way. However, from an experimentalist viewpoint, there is no straightforward way of getting material parameters from an experimentally recorded reflection.

For explaining the measured reflection pulses, the Resonant Secondary Emission (RSE) concept can be used. In this concept the reflected pulse is, in fact, a constructive interference of resonant Rayleigh Scattering. The crystal is emitting the (reflected) beam as long as a coherent ensemble of polaritons exists in the surface layer of the crystal. The processes leading to the loss of such an ensemble are: polariton transforming to photon at the crystal boundary (characterised by the oscillator strength or polarizability), moving of a polariton package into the crystal (characterised by the exciton effective mass) and a dissipative interaction with the lattice (characterised by the damping factor). Thus in formula (10) the corresponding parameters contemplate the influence of distinct processes. We can make an attempt analysing the effects of these processes (parameters) on the temporal shape of the reflected pulse.

To extract the analysis from the exact form of an incident pulse it is beneficial to consider the material response:

$$r(t)=\frac{1}{2\pi}\int e^{-i\omega t}r(\omega)d\omega\,. \tag{11}$$

Under reasonable assumptions (the higher-lying resonances determining the ε_0 term in (10) are well separated from exciton resonance), it can be shown that it

is possible to separate the resonant and non-resonant parts of a material response (for details see ref. IV):

$$r(t) = r_0(t)\delta(t) + \int e^{-i\omega t} R(\omega) d\omega \,. \qquad (12)$$

Here $r_0(t)$ is the non-resonant response depending only on ε_0, and $R(\omega)$ is the resonant part in the spectral domain, vanishing far from resonance, $R(t)$ will be the resonant part of the material temporal response. We will look for the envelope function $R'(t)$, which will be the absolute value of $R(t)$ without the fast oscillating term like $cos(\omega_0 t)$.

In order to relate the experimental features to the elementary processes responsible for the transients in the reflection we analysed the limiting cases for the Brewster angle incidence, each of which demonstrates a specific decay mechanism:

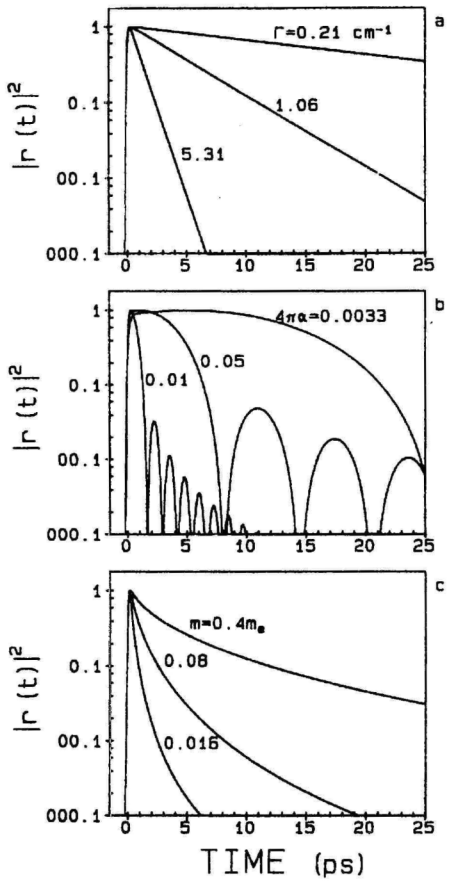

Figure 3. Characteristic decay curves of the reflection response in three limiting cases: (a) polarisation dephasing ($4\pi\alpha\to 0$, $m_*\to\infty$), (b) radiative decay ($m_*\to\infty$, $\Gamma=0$), and (c) polarisation propagation ($4\pi\alpha\to 0$, $\Gamma=0$) for $\varepsilon_0=12.1$, $\omega_0=11441\,cm^{-1}$, and $\varphi=\varphi_B$.

i) Radiative decay of the polarization due to $4\pi\alpha\neq 0$ ($m_*\to\infty$, $\Gamma=0$). For a normal angle incidence and $\varepsilon_0=1$, the analytical solution is

$$R'(t) = 2\frac{J_1(\Delta_{LT}/2)}{t} \qquad (13)$$

where J_1 is the first-order Bessel function. For an arbitrary ε_0 and angle of incidence no closed form expression for R'(t) can be obtained, however the decay always shows the same oscillatory features. The time-scale of the decay can be characterised by a time constant found as the first momentum of $R'(t)^2$:

$$\bar{\tau}_\Delta = \frac{\int R'(t)^2 t\,dt}{\int R'(t)^2\,dt} \qquad (14)$$

For InP ($\varepsilon_0=12.1$) a numerical calculation yields $\bar{\tau}_\Delta(ps) = 20.9\Delta_{LT}(cm^{-1})$. The proportionality constant varies between 15 and 23 in the region $\varepsilon_0=1$ to $\varepsilon_0=15$.

ii) Dephasing of the polarisation due to $\Gamma\neq 0$ ($4\pi\alpha\to 0$, $m_*\to\infty$). Within this limit an analytical solution can be reached [29].

$$R(\omega) = \frac{\Delta_{LT}}{4}\frac{\varepsilon_0 - 1}{\varepsilon_0}(\omega_0 - \omega - i\Gamma/2)^{-1}$$

giving us a purely exponential response

$$R'(t) = \frac{\Delta_{LT}}{4}\frac{\varepsilon_0 - 1}{\varepsilon_0}\exp(-\Gamma t/2)$$

iii) Spatial dispersion due to $m_*\neq\infty$ ($4\pi\alpha\to 0$, $\Gamma=0$). No analytic solutions can be obtained. A set of computed response functions in dependence on m_* are depicted in figure 3c. The response is decaying non-exponentially and the first momentum $\bar{\tau}_m$ is proportional to the effective mass of the excitons. The proportionality factor depends weakly on ε_0 and for $\varepsilon_0=12.1$ (InP) $\bar{\tau}_m(ps) = 30.3m_*$ (free electron masses).

If these limits do not apply, the reflection response is a complicated interplay of all the three decay mechanisms. In general, they are not independent. However, these mechanisms can be regarded as quasi-independent as far as the first momentum $\bar{\tau}$ of response is calculated. To characterise the intermediate situations simulated by computer calculations, the following empirical formula has been found:

$$\bar{\tau}^{-1}(ps) = \frac{\Delta_{LT}(cm^{-1})}{20.9} + \Gamma(ps^{-1}) + \frac{1}{30.3 m_*(m_e)} \qquad (16)$$

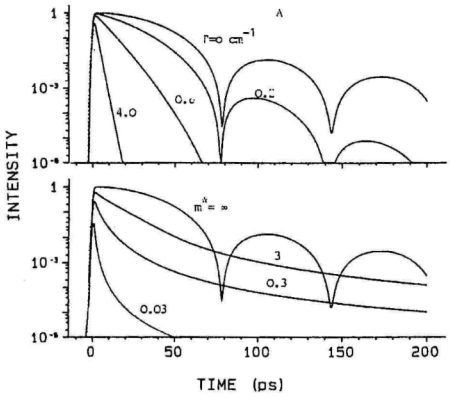

Figure 4. Calculated transient reflection for intermediate situations. A: Dependence on Γ for case $m^*=\infty$, B: Dependence on m^* for case $\Gamma=0$. Other material parameters are taken from GaAs.

Some examples of the calculated kinetic curves in the case of the intermediate situations are depicted in figure 4. A comparison of the approximated values according to (16) is given in [IV].

In conclusion, it can be shown theoretically that the non-resonant terms in crystals dielectric permeability cause an extremely fast component in the reflection response. The resonant response is influenced by three physical processes, dependent on appropriate resonance parameter: (i) dephasing of the polarization characterised by the damping factor Γ, (ii) radiative decay characterised by the polarizability $4\pi\alpha$ and (iii) polarization propagation characterised by the effective mass. By means of numerical modelling has been concluded that these processes can be regarded quasi-independent and a simple phenomenological formula gives a fairly good estimate to the duration of experimentally measured reflection response.

3.2 Experimental results and discussion

3.2.1 GaAs

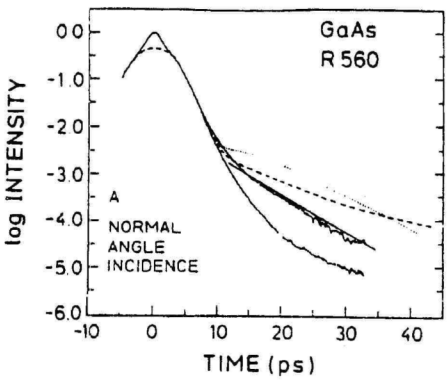

Figure 5. Experimental Cross-Correlation Function (CCF) of reflected and incident pulses for a GaAs (solid lines: upper – weak pulse, lower – high intensity excitation). Dotted line – theoretical fit neglecting spatial dispersion; dashed line – fit including spatial dispersion. Straight solid line – slope of 5.4 ps. The sharp peak is the coherence peak of the correlation signal.

The measured temporal shape of the normal incidence reflected pulse from a GaAs crystal, is shown in figure 5. The general shape of the reflected pulse profile can be divided into a non-resonant contribution, which follows the exciting pulse, and a resonant reflection, which is responsible for the delayed tail. We have tried to model the observed decay by making use of the two sets of material parameters, which were used in [36] to fit the steady-state reflection spectrum (fig. 5 dotted and dashed lines). An overestimation (three times) of the long scale intensity of the pulse tail is evident. Comparing the two models, we can see that the model with no spatial dispersion predicts a "concave" nature of the non-exponential decay, which is not observed experimentally and cannot be altered by varying the parameters of the model. The inclusion of spatial dispersion predicts a "convex" shape of the non-exponential tail and is evidently more appropriate for describing the observed transients. The fit of the experimental curve can be considerably improved by a slight increase of the damping parameter. The strong dependence of the transients on the incident intensity is evidently caused by the increased damping due to induced exciton-exciton collisions.

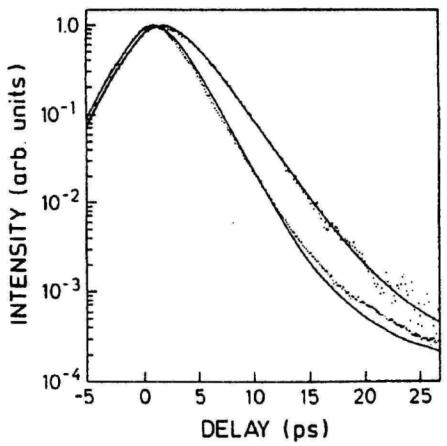

Figure 6. Experimental CCF of the reflected pulses (dotted) and theoretical fits to the data at two excitation intensities (30 μW upper curve, 1000 μW lower curve) for InP under Brewster angle incidence.

The measured time resolution of the Brewster angle incidence reflected pulse from an InP crystal is shown in figure 6. The measured CCF show clearly that the reflected pulses are delayed and have tails which extend several picoseconds beyond the exciting pulses. The reflected pulse shape and delay depends also on the incident pulse intensity. In the fitting procedure the following InP parameters were taken from literature: ε_0=12.1, ω_0=11441 cm^{-1} and $4\pi\alpha$=2.3*10^{-3} [37]. The damping constant Γ and the effective mass of excitons m_* were varied in the curve fitting procedure. The fitting yielded two results: 1) No reasonable fit could be reached neglecting spatial dispersion, whereas the inclusion of spatial dispersion provided a good fit over three orders of magnitude of the reflection decay. 2) At higher excitation intensities the decay curves could be modelled by increasing the dephasing rate, however, the fit was clearly worse than in the low intensity limit.

3.2.3 CdSe

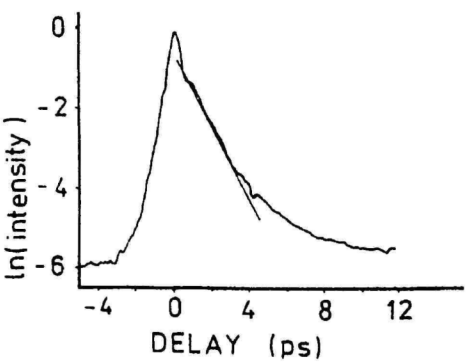

Figure 7. Experimental CCF of the reflected pulse from a CdSe crystal under normal-angle incidence. Straight line – the slope of 1.2 ps.

A CdSe crystal was studied near the lowest exciton resonance at ω_0=14729 cm^{-1}. The time-resolved normal-angle incidence reflection curve is presented in figure 7. The incident laser pulse had a autocorrelation FWHM of 650 fs. The reflected pulse includes an ultra-fast response at zero delay (non-resonant part of the reflection response), and a long non-exponential tail. Using formula (16) with material parameters, taken from literature (ε_0=8, Δ_{LT}=1.3...0.5 meV and Γ=0.05 meV)

[38] the estimate $\bar{\tau} \cong 1ps$, which is close to the experimental value of $\bar{\tau} = 1.2ps$ (plotted in the figure too). Spatial dispersion seems to be responsible for the strongly non-exponential character of the decay.

In this chapter, for the first time experimentally observed time-resolved reflection from GaAs, InP, and CdSe, revealing distinct material-dependent temporal features has been analysed and interpreted. We have observed the *reflection time of light*, lying in the picosecond timescale.
In the limit of our experiment, these material- dependent features may be described by the formula (16).

4 DYNAMICS OF OPTICAL EXCITATIONS IN GaAs AND SOLID Xe

4.1 Theoretical considerations

At low temperatures in pure crystals excitons constitute the final state in the energy relaxation of the photo-excited crystal.

According to the energy and momentum conservation rules on excitation at a given excess energy (relative to conduction band energy) E_{excess}, the electrons and holes (with effective masses m_e and m_h) get an initial kinetic energy E_e and E_h, respectively

$$E_{e,h} = \frac{m_{h,e}}{m_e + m_h} E_{excess}. \tag{17}$$

An intuitive and commonly accepted picture of this process is that very early on in the semiconductor-light interaction, the *e-h* pairs coherently oscillate between their respective bands. Then they start to scatter among themselves and with other elementary excitations of the crystal. As they lose coherence they form non-equilibrium distributions which eventually evolve into thermalised ones, following a Maxwell-Boltzmann distribution with a temperature that depends on the initial excess energy. Finally the hot carriers cool down to the lattice temperature and, later on, recombine. In intrinsic semiconductors, two dominant scattering mechanisms are involved, carrier-carrier scattering (CCS) and carrier-phonon scattering (CPS). The former conserves the *e-h* total kinetic energy, but redistributes it. The latter allows an energy exchange with lattice, and plays a major role in the cool-down process [39].

Shortly after the generation, (in case of GaAs faster than 100fs [40]) an energetically broad distribution of charge carriers is formed. At this point of particle evolution the processes cannot be described using Boltzmann rate equations. It is only for times much longer than an oscillation period of the elementary excitation involved in the interaction, when the reaction of the "reservoir" can be described by the Fermi's golden rule. For GaAs the respective response times are in order of 100 fs [39]. However, within the first picoseconds a Maxwell-Boltzmann distribution is formed with a characteristic temperature ($T_{e,h}$ electron and hole temperatures, respectively) [41] and, from this point on, the processes may be described by the Boltzmann rate equations.

4.1.1 Boltzmann rate equations

On the picosecond time-scale like in our experiments, a system of electrons, holes and excitons we can describe by their respective concentrations $n_{e,h,x}$ and temperatures $T_{e,h,x}$.

$$\frac{dn_{eh}}{dt} = G - \frac{n_{eh}}{\tau_{eh}} - \sigma n_{eh}^2 \tag{18}$$

$$\frac{dn_x}{dt} = -\frac{n_x}{\tau_x} + \sigma n_{eh}^2 \tag{19}$$

$$\frac{2}{3k}\frac{dE_{eh}}{dt} = GT_g - \frac{n_{eh}}{\tau_{eh}}T_{eh} - \left\langle \frac{\overline{dE_{eh}}}{dt} \right\rangle_{ph} - \sigma n_{eh}^2 T_{eh} + \gamma m_{eh} n_x (T_x - T_{eh}) \tag{20}$$

$$\frac{2}{3k}\frac{dE_x}{dt} = -\frac{n_x}{\tau_x}T_x - \left\langle \frac{\overline{dE_x}}{dt} \right\rangle_{ph} + \sigma n_{eh}^2 (T_{eh} + T_B) - \gamma m_{eh} n_x (T_x - T_{eh}). \tag{21}$$

Here T_g is the charge carrier temperature at excitation and T_B is the temperature corresponding to the exciton Rydberg' energy. γ stands for the exciton probability to lose energy by colliding with a charge carrier (we considered thermal exchange, not exciton dissociation). For γ we used the hydrogen-electron collision efficiency $\gamma_0 = 20a_0\frac{h}{m_e}$, taken from [42], multiplied by the mean energy exchange fraction at a collision $\frac{2m_e}{m_e + m_x}$.

$$\gamma = 40a_0\frac{h}{m_e + m_x},$$

a_0 is the Bohr radius of the excitons.

$\left\langle \frac{\overline{dE}}{dt} \right\rangle_{ph}$ is particle's total mean energy loss rate in all the scattering processes on phonons. For charge carriers we considered deformation potential and piezoelectric LA phonon and polar LO phonon scattering, for excitons deformation potential LA scattering, the corresponding rates were taken from literature [43 ,44].

$$\left\langle \frac{dE_e}{dt} \right\rangle_{op} = \sqrt{2m_e(\hbar\omega_{LO})^3}\frac{e^2}{\hbar^2}(\varepsilon_\infty^{-1} - \varepsilon_0^{-1})\left[\exp(-\frac{\hbar\omega_{LO}}{k_B T_e}) - \exp(-\frac{\hbar\omega_{LO}}{k_B T_L})\right] \tag{22}$$

$$\left\langle \frac{dE_e}{dt} \right\rangle_{pe} = \frac{32\sqrt{\pi}e^2 e_{14}^2\sqrt{m_e^3}a\sqrt{k_B T_e}}{\sqrt{2}\hbar^2\varepsilon_0^2\rho}\frac{T_e - T_L}{T_e} \tag{23}$$

$$\left\langle \frac{dE_e}{dt} \right\rangle_{ac} = \frac{8\sqrt{2}D^2\sqrt{m_e^5(k_B T_e)^3}}{\sqrt{\pi^3}\hbar^4\rho}\frac{T_e - T_L}{T_e} \tag{24}$$

$$\left\langle \frac{dE_x}{dt} \right\rangle_{ac} = \frac{8\sqrt{2}D_x^2\sqrt{m_x^5(k_B T_x)^3}}{\sqrt{\pi^3}\hbar^4\rho}\frac{T_x - T_L}{T_x}. \quad (25)$$

Here subscripts *op*, *pe*, *ac* denote optical phonon, piezo-electric, and acoustic deformation potential scattering processes, respectively; ε_0 and ε_∞ - high and low frequency dielectric permeabilities, $\hbar\omega_{LO}$ – optical phonon energy, e_{14} – piezoelectric constant, a – geometric factor of the order of unity, D – deformation potential, T_L – lattice temperature, ρ - mass density of the crystal. The hole temperature rates can be found, replacing the corresponding subscripts.

For the bimolecular coupling constant σ we used a formula from Ref. [45], which we modified for the case when the charge carriers have a temperature, different from the lattice temperature:

$$\sigma(T_e) = \frac{16\sqrt{2}D^2e^6m_h^2\sqrt{m_h m_e}}{3\sqrt{\pi}\hbar^4\rho\varepsilon^3 s m_x}\frac{1}{(kT_L)^{0.5}(kT_e)^{1.5}} \quad (26)$$

To our knowledge this is the only model describing the exciton creation cross section depending on the (carriers effective) temperature. In our calculations the essential feature was the temperature behaviour of the cross section ($\sigma \propto T_e^{-1.5}$), which follows from the acceptable assumption of charge carriers Boltzmann' distribution. For 2D case in QW, the dependence $\sigma \propto T_e^{-1}$ is used [46].

To simplify the set of equations we will take $n_h = n_e$. This is justified while the creation of charge carriers by photons as well as exciton generation from charge carriers is a pair-wise process (the crystals under the investigation are compensated as well).

Next, we will take T_h=T_L. This is justified while under our experimental conditions (exciting well below the optical phonon energy) the main energy loss rate is due to acoustic phonon scattering. The corresponding rate is proportional to $m^{5/2}$. If holes are significantly heavier than electrons (in case of GaAs m_e=0.06 and m_h=0.54 free electron masses), then the holes are relaxing in temperature significantly faster than electrons. For GaAs the holes energy relaxation time will be smaller than our experimental time resolution allowing us to perform the above-mentioned simplification.

We will use this set of Boltzmann' equations in interpreting some experimental results of exciton PL kinetics. The model has too many parameters and too heavy simplifications to enable quantitatively matching fits. However, qualitatively this model is able to explain most of the features, registered by us experimentally.

4.1.2 Monte-Carlo calculations

An approach allowing a detailed treatment of individual processes (in contrast to Boltzmann rate equations operating with parametrised distribution functions) is the Monte-Carlo simulation. The Monte-Carlo method is a technique which obtains a probable approximation to the solution of a problem by using statistical sampling techniques [47]. Knowing the probabilities of possible individual events, this method constructs a lot of possible life-stories of excitations. The exact event is always chosen randomly (as in roulette, that is why the method is named after Monte-Carlo) according to given probabilities. If the number of calculated life-stories is sufficiently large, we get a statistical behaviour of an ensemble of excitations.

To author's knowledge, the most comprehensive free-carrier and exciton relaxation simulation in optically excited semiconductors is given in [48]. The processes included into the model are carrier generation from light pulse, carrier-carrier-, carrier-phonon-, exciton-phonon-scattering, and exciton creation from carriers. However, it is worth noting that the results concerning the exciton luminescence rise time in GaAs, given in [48, figure 8], are neither observed in our experiments nor have been reported in literature. This fact indicates that even such a sophisticated calculation does not model all the processes, and the method should be used with a more focused problems, having a specific goal in mind.

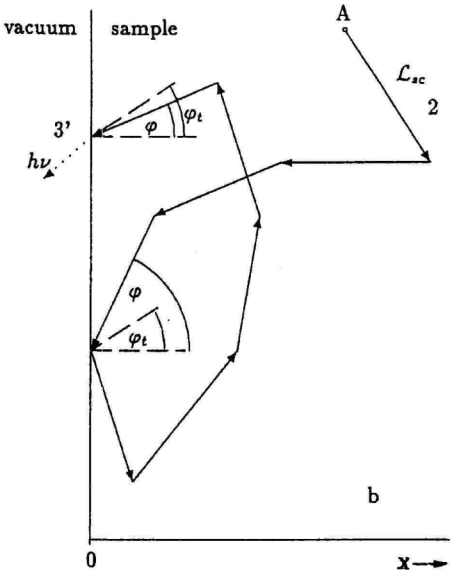

Figure 8. A schematic model of exciton transport to the sample/vacuum interface and transmission into vacuum. For details see text.

We used Monte-Carlo simulations for describing the diffusion-like movement of thermalised exciton-polaritons in solid Xe in case of excitation into exciton band. An assumption is made that excitons relax to the crystal temperature with a in a period of time, shorter than our experimental temporal resolution. The x-axis is perpendicular to the sample/vacuum interface. At time zero, a bottleneck exciton-polariton was created at a certain depth, x, below the surface (A in fig. 8). The damping of the exciting light along the x-axis according to Beer's law was taken into account as a weight function for the individual events. Then, the particle will move with group velocity v_g, in an arbitrary direction (φ - the angle between the moving direction of polariton and x-axis). After a scattering length L_{sc}, the direction was changed arbitrarily. Trapping and non-radiative

loss processes were taken into account by an appropriate life-time (probability to survive is $exp(-t/\tau)$). If φ is smaller than the angle of total reflection, then the polariton close to vacuum-crystal interface has a probability to leave the crystal, equal to the reflection coefficient R. All the exciton-polaritons decaying in this way at the crystal surface were registered including their time-correlation to time zero (excitation process). In this way, the decay curves of free exciton luminescence were constructed. The resultant fits (fig. 16) are shown and discussed in the section of experimental results.

4.2 Experimental results

Experimentally exciton photoluminescence (PL) kinetics was registered at low temperatures in two systems: GaAs and Xe. Excitation into the exciton band as well as into the conduction band was considered.

4.2.1 Exciton luminescence kinetics of GaAs

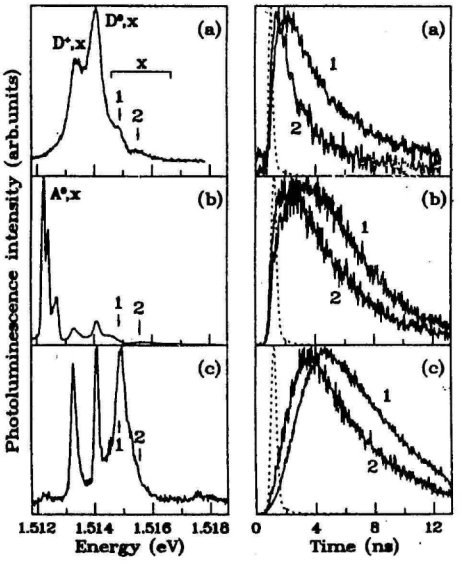

Figure 9. Time-integrated PL spectra (left) and corresponding kinetics (right) of different GaAs samples. (a) n^0-GaAs, $N_D \sim 10^{14}$ cm^{-3}, (b) p^0-GaAs, $N_A \sim 10^{14}$ cm^{-3}, (c) sample G13, $N_D \sim 10^{12}$ cm^{-3}. The dashed line represents the excitation pulse. The excitation energy is 1.554 eV. Traces 1 and 2 correspond to the luminescence energies denoted by arrows on the spectra.

The time-integrated exciton luminescence spectra and the corresponding kinetics of different GaAs samples at T=2 K are depicted in figure 9. The kinetics was measured at the energy of lower and upper polariton branches (denoted by arrows). In all the samples a slowing of the onset with decreasing polariton luminescence energy is observed. The onset of the polariton luminescence depends essentially on the impurity concentration. It is usually assumed [49] that the energy relaxation of electrons in GaAs with energy smaller than the energy of optical phonon is governed by an emission of acoustical phonons. This process, however, is rather slow because of the small value of the electron effective mass (according to the calculations carried out by Ulbrich [43] the energy relaxation rate via the emission of acoustical phonons for the electron temperature T_e=10 K is determined to be S~0.1 meV/ns). The observed impurity concentration dependence in our experiments clearly points to the role of extrinsic processes in the electron energy relaxation. A noticeable decrease in Δt_{max} and the appearance of a fast

initial rise with an increasing impurity concentration is caused by an enhancement of the electron energy relaxation rate due to inelastic impurity scattering.

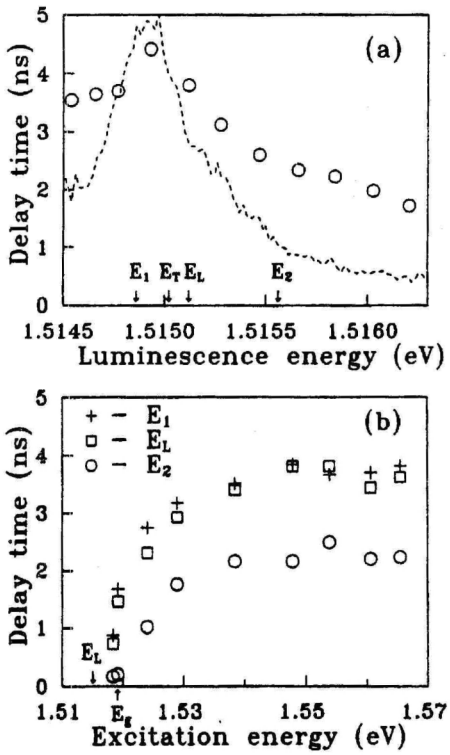

Figure 10. The dependence of the luminescence maximum time delay on (a) the luminescence energy and (b) excitation energy for sample G13. (a) The excitation energy is 1.554 eV; the dashed line represents the polariton luminescence spectrum. (b) Luminescence energies correspond to those denoted in (a). E_L and E_T are longitudinal and transverse exciton energies, respectively.

The dependence of the delay time of the pulse maximum Δt_{max} on the luminescence energy of sample G13 is shown in figure 10. This dependence reveals the effect of a polariton bottleneck due to a reduced energy relaxation rate in the vicinity of the exciton resonance [50]. Unlike the results concerning the polariton bottleneck in CdS [51, 52], the decay time here depends weakly on the luminescence energy. In the ultra-pure sample G13 this decay time reaches the value of 4-5 ns. A weak dependence of the luminescence onset on the luminescence energy was earlier reported in [53] and attributed to an energy-dependent diffusion of polaritons from the bulk to the surface. To determine the contribution of the polariton diffusion to the observed delayed onset of the polariton luminescence we measured the temporal evolution of the exciton luminescence accompanied with LO-phonon emission. Because of the small absorption coefficient and high group velocity, spatial distribution of polaritons should not affect the time behaviour of this emission. No essential difference in the onset of the luminescence at the exciton resonance and corresponding energies of the LO-phonon replica was found in sample G13. This fact rules out the contribution of the polariton diffusion to the observed delayed onset of luminescence.

The luminescence onset essentially depends on the excitation energy, so that Δt_{max} is increased (approximately 2 ns) with increasing the excitation energy above the band gap for all the luminescence energies (fig. 10b). It is natural to attribute this part of the delay time to the energy relaxation of electrons. However, we could not resolve the process of exciton formation from cold

electrons and holes (the values of the delay time are practically the same for the excitation at the band edge and $n=2$ excited state of free exciton.
In this section the luminescence time evolution of the ultra pure GaAs exciton luminescence was investigated experimentally as a function of excitation density and energy. For the first time rise-time of bulk GaAs exciton PL has been registered.

4.2.2 Exciton interaction with hot electrons in GaAs

The rise of PL is a sophisticated interplay of excitation relaxation populating luminescent excitons, and exciton heating processes by interaction with charge carriers depopulating luminescent excitons. If the next exciting light pulse generates hot charge carriers before the exciton PL of the previous pulse decays, a quenching of PL may take place (fig. 11). This effect of luminescence quenching in GaAs was for the first time reported in our paper [VI].

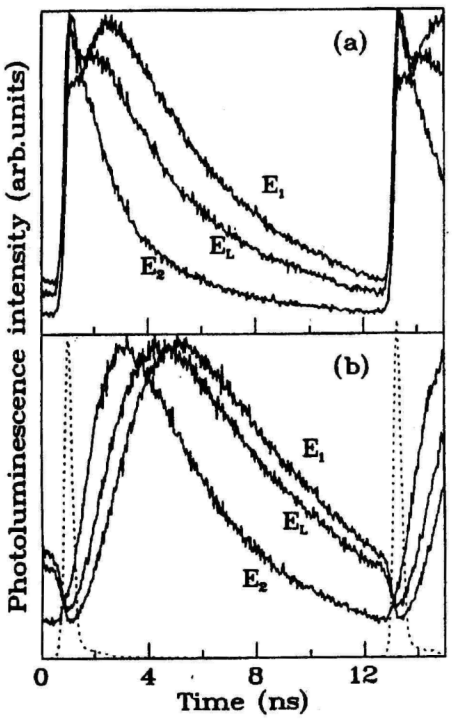

Figure 11. Time behaviour of the polariton luminescence of sample G13 at a high repetition rate. Excitation energy is (a) 1.520 eV, equal to the energy gap and (b) 1.554 eV. The dashed curves represent the excitation pulses. Traces are measured at the luminescence energies denoted in Fig. 9.

To investigate the exciton-charge-carrier interaction, an experiment was performed with an additional (step-like modulated) CW background excitation, generating a stationary exciton luminescence. PL kinetics curves were recorded simultaneously for cases without and with a background excitation, corresponding to the phase of modulation.
In figure 12 luminescence kinetics curves have been shown for three different pulse intensities. The pulse photon energy is E_g+15 meV, well below the optical phonon (E_{LO}=36 meV) replica of the band (E_g - electron conduction band energy). The solid line marks the temporal dependence of the luminescence when both (diode and pulsed) lasers are exciting the crystal. The dashed line marks the luminescence for the case when the crystal is excited only by a pulse-laser.
At the lowest pulse intensity (part a) of 10 mW/cm^2 (about 10^{14} excited electrons per cubic cm per pulse) a stationary luminescence is emitted by the crystal until the pulse fires. In

response to the pulse, the luminescence momentarily (below the temporal resolution of the experiment) decreases and afterwards slowly relaxes to a stationary one. The integral of "hole" in luminescence is approximately 80% of the integral of luminescence in case the exciting is performed only with the pulsed laser. In other words, the amount of excited electrons, being able to create one registered exciton is able to "kill" 1.8 otherwise registered excitons. The difference kinetics is shown in the upper part of fig. 13.

It is remarkable feature is that no maximum appears in kinetics, although additional excitations were injected by pulse. Where do the excitons disappear? It is possible to show that if the excitons were destroyed forever, the time constant τ, fitted from difference kinetics, has to be equal with the exciton decay (losses) time τ_x. In fact, τ=2 ns and τ_x=4 ns (measured by exciting excitons directly). Consequently, excitons were not destroyed forever but just excited to higher-energetic states and they will later also be involved in luminescence.

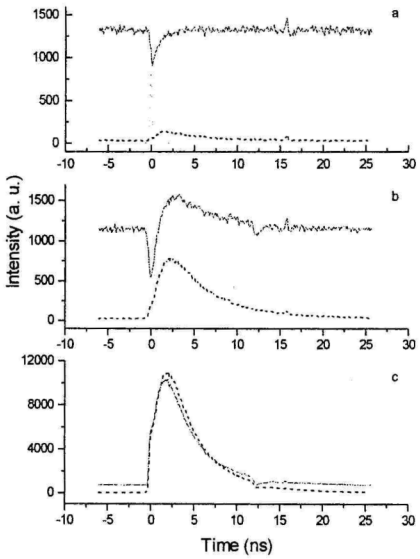

Figure 12. Temporal behaviour of PL of GaAs for excitation by pulsed laser with (solid line) and without (dashed line) CW laser illumination in case of three pulsed laser intensities: a - 0.01 W/cm^2, b - 0.2 W/cm^2 and c – 1 W/cm^2. The incident pulse is depicted by dots on part a.

A qualitative analysis says that if the losses during the round trip are smaller than in the stationary case, then the PL kinetics excited by both lasers will always have a maximum. The absence of a maximum in luminescence (at the excitation of both lasers) lets us to conclude that the averaged losses (both non-radiative and radiative) at these upper states are bigger than in the stationary case.

At an intermediate intensity of 0.2 W/cm^2 (fig. 12 b) when excited both by a diode and pulsed laser, at the moment of pulse excitation the stationary luminescence also decreases, but later the luminescence grows higher than the stationary one. For the pulsed-only excitation, a steep rise of luminescence occurs followed by a slower component. Often this steep step-like or even spike-like behaviour in luminescence kinetics is attributed to an experimental artefact (scattered exciting laser pulse), but in the current experiment we do not see the feature in the other simultaneously registered kinetics – indicating to the real nature of the effect. We think that the step-like behaviour may be caused by a small fraction of excitons created by a LO-

phonon mediated process (the initial hot distribution of charge carriers generated by photons with an excess energy of 15 meV may have enough a high-energy tail). The relative share of the step-like feature increases with the pulse intensity, as it should be in a bimolecular process, confirming the interpretation. The LO-mediated exciton generation is important in GaAs QW structures [54, 55]. Monte-Carlo calculations made by Selbmann et al. [48] predicted an essential share of the LO-process in exciton creation also in bulk GaAs. In an earlier experiment of ours [VI] we, as well as the authors of ref. [56] have not seen a distinct evidence of LO-phonon mediated exciton generation in bulk GaAs. This may be caused by the fact that in the experiments of [VI, 56] the excitation intensity is about an order of magnitude lower and the bimolecular process (depending on the carrier concentration as n^2) had too small probability. In our earlier unpublished measurements, we often saw this spike-like behaviour, but attributed it to a scattered laser light.

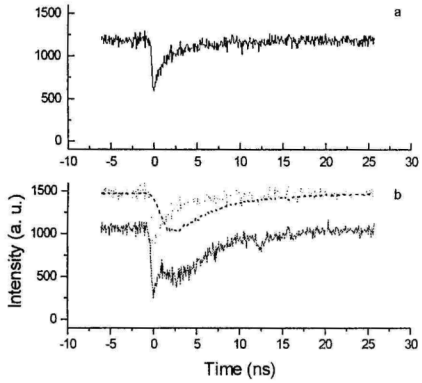

Figure 13. Solid lines: temporal behaviour of PL difference kinetics at low (0.01 W/cm2 – upper part) and intermediate pulse intensity (0.2 W/cm2 – lower part). Dotted line -- the contribution of reduced exciton coupling with photons due to an exciton temperature change, dashed line – contribution of reduced exciton generation rate due to electron temperature change.

The difference kinetics in the case of an intermediate pulse intensity is shown in the lower part of fig. 13. A two-component structure is clearly seen. At the moment of excitation, a similar luminescence quenching is going on as in the low-intensity case. Later on, another component, roughly proportional to the exciton luminescence signal, also reveals itself. We interpret the further component as a contribution of a smaller exciton coupling with photons due to an exciton temperature change (photons can be emitted only at $k \approx 0$, at an elevated temperature the share of such excitons decreases). The other component is possibly due to a changed exciton generation rate with an electron temperature increase.

At a high pulse intensity of 1 W/cm^2 (fig. 12 c), no initial decrease takes place. Instead, at the first moment a step-like rise in luminescence is found for both cases. A striking fact is that the maximum luminescence intensity, if exciting with both light sources, is smaller than if exciting only with a pulsed laser. There are no changes in the character of difference kinetics (not shown), compared with the intermediate pulse intensity, except that the slower component reveals a different (slower) shape than the corresponding pulsed-only luminescence. This seems to be natural,

considering the bimolecular process of exciton formation and the reduced exciton generation rate at a higher carrier temperature.

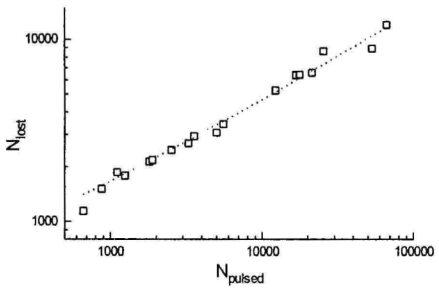

Figure 14. Open squares: fraction of excitons "getting lost" when an additional CW excitation is present compared to the luminescence intensity for a pulsed excitation. With the dotted line a fit $q \propto \sqrt{N_{pulsed}}$ is shown.

In figure 14 the number of lost excitations (N_{lost}) depending on N_{pulsed} is shown, calculated by the formula:
$N_{lost} = N_{stationary} + N_{pulsed} - N_{both}$
where $N_{stationary}$ is the integral of stationary luminescence when excited only with a diode laser, N_{pulsed} is the integral of luminescence when excited only with a pulsed laser and N_{both} is the integral when both excitations are used. We do not have an explanation to the dependence, but it is interesting to note that N_{lost} depends on N_{pulsed} as square root. The dotted line in fig. 14 marks the dependence $N_{lost} = a + b*(N_{pulsed})^{1/2}$. For checking the interpretation, model calculations according to rate equations (18)-(21) were performed. As already mentioned in section 4.1.1 no quantitative fit is achievable. However, the model qualitatively explains the experimental features (fig. 5 in [XII]). At a low pulse intensity no maximum appears in luminescence with a CW background excitation. At a high excitation the luminescence without background CW excitation has a higher intensity than the luminescence with that. As we could not find a good possibility for the model to take into account the proposed LO phonon mediated exciton creation mechanism, it does not reproduce initial steep rise.

In this section the time evolution of the exciton luminescence from an ultra-high purity GaAs crystal has been investigated as a function of excitation density and energy. The effect of quenching of exciton luminescence by light has been found experimentally. For investigating the quenching effect, special experiments with additionally excited charge carriers were performed. The analysis of the results indicates clearly the importance of considering exciton creation from *hot* charge carriers and exciton-carrier *heat exchange* effects.

4.2.3 Exciton luminescence kinetics in solid Xe

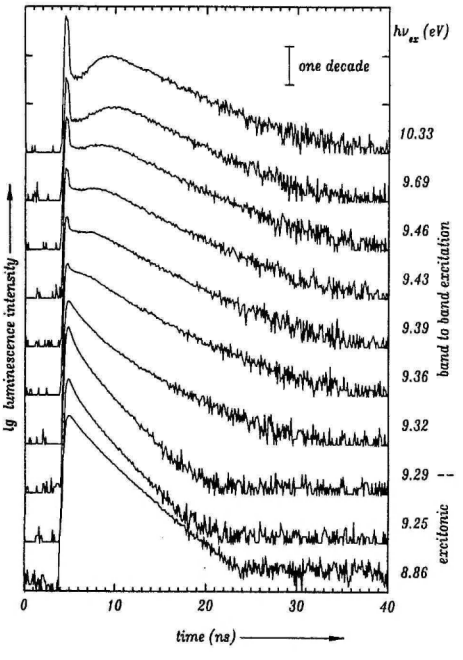

Figure 15. Decay curves of the free exciton in solid Xe, measured at different photon energies of excitation. The values are given at each curve. T=4.7 K.

The decay of excitons in solid Xe was investigated recording time- and spectrally resolved photoluminescence (PL) as a function of temperature and photon energy of excitation. In figure 15 the experimental decay curves of the free exciton PL in solid Xe are presented at fixed temperature of 4.7 K. The photon energy of excitation is varied between 8.86 and 10.33 eV. Below the band-gap energy E_g=9.33 eV, excitons of the Γ(3/2) series are created. Above 9.33 eV, the situation is not so clear because the continuum (free electron-hole pairs) of the Γ(3/2) series overlaps with the Γ(1/2) exciton series. Starting from 8.86 eV, with increasing photon energy of excitation, the non-exponential decay behaviour gets more and more pronounced. Above 9.3 eV, the overall decay is slowed down, and with a further increase in the photon energy of excitation, a cascade-like temporal behaviour develops additionally to a spike-type luminescence signal displaying the apparatus function.

No rise-time in the luminescence was detected in case of exciting below the band-gap, indicating that exciton-polaritons reach thermal quasi-equilibrium in the bottleneck of the dispersion curve already within an apparatus temporal resolution. For modelling the experimental results a Monte-Carlo simulation was performed, described in section 4.1.2. The group velocity of polariton was substituted by the exciton one $v_g = \sqrt{\frac{3kT}{m_x}}$. The material parameters L_{sc}, R, α (absorption coefficient), $m_x = m_e^* + m_h^*$, used by simulation were taken from literature [57, 58, 59]. The only fitting parameter remained was the (trapping and non-radiative) loss rate $\Gamma=1/\tau$.

The simulation gives remarkably good fits with the experimental data for all the measured curves depending on the excitation energy (below band-gap). The fitted value of the trapping rate $\Gamma=4.5\times10^8$ s^{-1}.

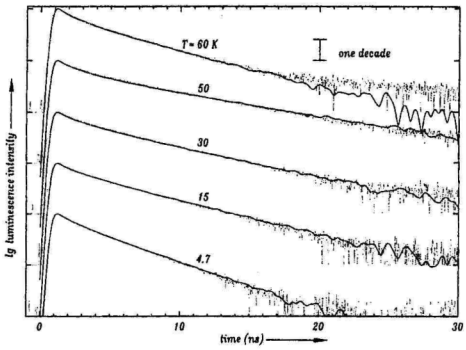

Figure 16. Measured exciton PL in Solid Xe at different temperatures (dots) and according Monte-Carlo simulations.

In figure 16 the experimental decay curves of the free exciton are presented (the dotted line) with the Monte-Carlo simulated fits (the solid line). The photon energy of excitation was fixed to $h\nu$=8.86 eV. The temperature varied between 4.7 and 60 K. The fit is good, however, an adjustment of Γ was necessary for modelling the experiment. The Γ dependence on the temperature can be attributed to the dependence of non-radiative processes (see [VIII]).

For modelling the experimental data with an exciting photon energy above the band-gap the charge-carrier relaxation and exciton formation was modelled by Boltzmann rate-equations (18)-(21). Then the evolution of excitons was calculated by the equation

$$\frac{dn_{ex}}{dt} = \sigma(T_e) n_e n_h v_{rel}(T_e) - R(t), \quad (27)$$

The *R(t)* follows from the Monte-Carlo simulation for the case when the was luminescence excited with a photon energy 9.29 eV (just below the band-gap value). In this way, all further relaxation processes within the exciton manifold including non-radiative decay-channels are taken into account. The model was solved numerically and the results are plotted in figure [17].

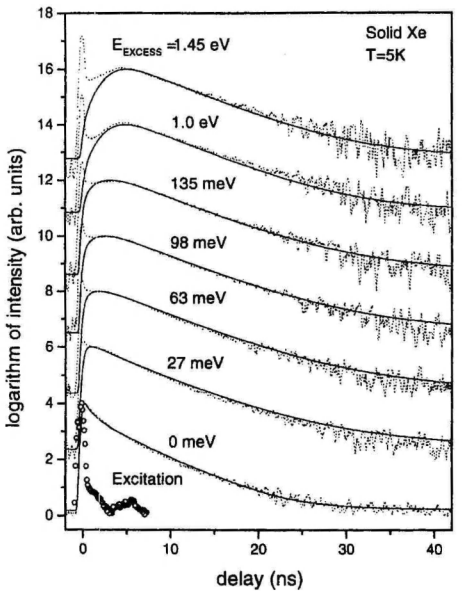

Figure 17. Decay curves of free exciton line of solid Xe at T=5 K, excited with different photon excess energies (indicated on each curve). The dotted lines are measurements, the full curves are the result of model calculations. The apparatus function is marked with open circles.

In spite of many simplifications we can conclude that our measured free exciton decay curves can be fitted by model calculations taking into account only scattering on acoustic phonons. The evolution of the electron temperature in time governs the observed kinetics through the strong variation of the recombination cross-section. Our results on thermalization of hot photoelectrons agree with findings of earlier investigations using other methods (conductivity measurements).

5 SUMMARY AND THE MAIN THESES PROPOSED

In accordance with the main objectives of the present study, the resonant secondary emission of excitons was investigated experimentally and theoretically.

The main results of the study can be summarised as follows (**the main theses are presented in bold**).

Time-resolved reflection of light from the surfaces of semiconductor crystals has been studied:

1. **For the first time, experimentally observed time-resolved reflection from GaAs, InP, and CdSe, revealing distinct material-dependent temporal features, has been analysed and interpreted. We have observed the *reflection time of light.***
2. **By theoretical analysis, it has been demonstrated that the non-resonant terms in the crystals dielectric permeability cause an extremely short component in the reflection response while the resonant terms correspond to the longer component.**
3. **The resonant contribution of the reflection can be described by three distinct physical processes, dependent on the corresponding exciton-resonance parameter: (i) dephasing of the polarization characterised by the damping factor Γ, (ii) radiative decay characterised by the polarizability $4\pi\alpha$ and (iii) polarization propagation characterised by the effective mass. A simple phenomenological formula incorporating these parameters allows a fairly good reproduction of the duration of the experimentally measured reflection response.**

Time evolution of the exciton luminescence from an ultra-high purity GaAs crystal has been investigated as a function of excitation density and energy:

4. **For the first time, rise times of exciton photoluminescence signal of bulk GaAs have been registered.**
5. **The effect of quenching of exciton luminescence by light has been established experimentally.**

For investigating the quenching effect, special experiments with additionally excited charge carriers were performed. In order to analyse the results, a model based on Boltzmann kinetic equations is proposed, which gives a qualitative description of the experimental effects.

6. **The analysis of the results clearly indicates to the importance of considering exciton creation from *hot* charge carriers and exciton-carrier *heat exchange* effects.**

The decay of excitons in solid Xe was investigated by registering the time and spectrally resolved luminescence as a function of the temperature and photon energy of the excitation. For interpreting the results Monte-Carlo type simulations were performed:

7. **The free-exciton luminescence decay curves are of non-exponential nature and indicate to the importance of phonon scattering at exciton-polariton transport to the sample/vacuum interface. The analysis of the formation kinetics of exciton luminescence also indicates (as in the case of GaAs) to the importance of considering exciton creation from *hot* charge carriers.**

In general, our analysis of the results of exciton photoluminescence shows that:

8. **In contrast to luminescence kinetics from colour centres, already in the case of low excitation intensities (in the order of 10^{14} cm^{-3}) the PL kinetics is essentially non-linear. Thanks to these photonic non-linearity possibilities, *a low intensity light-by-light gate* can be developed.**

In the experimental aspect of the work:

9. **A novel time-resolved dual channel modulated luminescence correlation technique method was worked out for investigating interaction between excitations. On the one hand, this method has the typical advantages of modulation schemes (such as eliminating the effects of dead time and slow time-scale drifts), and, on the other hand, the typical advantages of time-correlated single photon counting (such as registering the signal *in the time domain* and having the best possible noise characteristics).**

6 REFERENCES

1. I. J. Tehver, V. V. Hizhnyakov, Eesti NSV Tead. Akad. Toimet. Füüs. Mat., vol. 15, p. 9, (1966).
2. K. K. Rebane, *Impurity Spectra of Solids*, Plenum Press, New York – London, 1970.
3. V. V. Hizhnyakov, K. K. Rebane, I. J. Tehver, in *Light Scattering Spectra of Solids*, ed. G. B. Wright, Springer, New York, 1968.
4. K. K. Rebane, I. J. Tehver, V. V. Hizhnyakov, in *Theory of Light Scattering in Condensed Matter*, eds. B. Bendow, J. Birman, V. Agranovich, Plenum Press, New York (1976).
5. K. Rebane, P. Saari, J. Lumin., vol. 16, p. 223, (1978).
6. И. Ю. Техвер, В. В. Хижняков, ЖЭТФ т. 69, № 2, с. 599, (1975).
7. J. Aaviksoo, A. Freiberg, T. Reinot, S. Savikhin, J. Lumin., vol. 35, p. 267, (1986).
8. J. Toyozawa, J. Lumin., vol. 12/13, p. 13, (1976).
9. V. V. Hizhnyakov, A. V. Sherman, phys. stat. sol. (b), vol. 85, p. 51, (1978).
10. J. Aaviksoo, J. Lumin., vol. 48/49, p. 57, (1991)
11. L. Shultheis, J. Kuhl, A. Honold, C. W. Tu, Phys. Rev. Lett., vol. 57, no 13, p. 1635, (1986).
12. A. Mysyrovich, D. Hulin, A. Antonetti, A. Migus, W. T. Masselink, H. Morkoc, Phys. Rev. Lett, vol. 56, p. 2748, (1986).
13. J. Shah, *Ultrafast Spectroscopy of Semiconductors and Semiconductor Nanostructures*, Springer, 1996.
14. G. W. Fehrenbach, W. Schäfer, J. Treusch, R. G. Ulbrich, Phys. Rev. Lett., vol. 49, no. 17, p. 1281, (1982).
15. R. Zimmermann, K. Kilimann, W. D. Kraeft, D. Kremp, G. Röpke, Phys. stat. sol. (b), vol. 90, p. 175, (1978).
16. W. F. Brinkman, T. M. Rice, P. Bell Phys. Rev. B, vol. 8, p. 1570, (1973).
17. M. D. Sturge in *Excitons*, edited by E. I. Rashba and M. D. Sturge (North-Holland publishing, Amsterdam, 1982).
18. U. Fano, Phys. Rev., vol 103, p. 1202, (1956).
19. J. J. Hopfield, Phys. Rev., vol. 112, p. 1555, (1958).
20. V. M. Agranovich, Sov. Phys JETP, vol. 10, p. 307, (1960).
21. R. Loudon, *The quantum theory of light* (Clarendon, Oxford, 1973).
22. V. M. Agranovich, V. L. Ginzburg, Crystal optics with spatial dispersion and excitons (Springer, Berlin, 1984).
23. С. И. Пекар, *Кристаллооптика и добавочные световые волны*, Наукова думка, Киев 1982.
24. *Semiconductors probed by ultrafast laser Spectroscopy*, vol. 1 and 2, ed. R. R. Alfano Academic Press, New York (1984).

25. Л. М. Сороко, *Основы голографии и когерентной оптики*, Наука, Москва, 1971, стр. 49.
26. J. L. Birman in *Excitons*, eds. E. I. Rashba, M. D. Sturge, North-Holland Publishing Company, Amsterdam 1982, p. 48.
27. D. Elert, Ann. Phys. ser. 5, vol. 7, p. 65, (1930).
28. G. P. Agrawal, J. L. Birman, D. N. Pattanayak, A. Puri, Phys. Rev. B, vol. 25, p. 2715, (1982).
29. J. Aaviksoo, J. Lippmaa, J. Kuhl, J. Opt. Soc. Amer. B, vol. 5, p. 1631, (1988).
30. V. G. Golubev. Y. V. Zhiliajev, I. V. Ivanov-Omskii, G. R. Markarjan, A. V. Osutin, V. E. Tschelnokov, FTP vol. 21, no 10, p. 1771 (1987).
31. W. Laasch, H. Hagedorn, T. Kloiber, G. Zimmerer, phys. stat. sol. (b) vol. 158, p. 753, (1990).
32. J. Aaviksoo, J. Kuhl, IEEE J. Quant. Electr. **QE-25**, 2523, (1989).
33. S. V. Branis, K. Arya, J. L. Birman, in *Laser optics of condensed matter*, eds. J. L. Birman, H. Z. Cummins, A. A. Kaplyanskii, Plenum Press, New York, 1988, p. 303.
34. В. М. Агранович, В. Л. Гинзбург, *Кристаллооптика с учетом пространственной дисперсии и теория экситонов*, (Наука, Москва 1965).
35. I. Broser, M. Rosenzweig, R. Broser, M. Richard, E. Birkicht, Phys. Stat. Sol. (b), vol. 90, p. 77, (1978).
36. D. D. Sell, S. E. Stokowski, R. Dingle, J. V. DiLorenzo, Phys. Rev. B, vol. 9, p. 4568, (1973).
37. F. Evangelisti, J. U. Fishbach, A. Frova, Phys. Rev. B, vol. 9, p. 1516, (1974).
38. T. Itoh, P. Lavallard, J. Reydellet, C. Benoit à la Guillaume, Solid State Commun., vol. 37, p. 925, (1981).
39. S. Bar-ad, P. Kner, M. V. Marquezini, D. S. Chemla, K. El Sayed, Phys. Rev. Lett. Vol. 77, no. 15, p. 3177, (1996).
40. A. Leitenstorfer, C. Fürst, A. Laubereau, W. Kaiser, G. Tränkle, G. Weimann, Phys. Rev. Lett. Vol. 76, no. 9, p. 1545, (1996).
41. D. W. Snoke, W. W. Rühle, Y.-C. Lu, E. Bauser, Phys. Rev. B, vol. 45, no. 19, p. 10797, (1992).
42. Erginsoy, Phys. Rev. **79**, 1013 (1950).
43. R. Ulbrich, Phys. Rev. B, vol. 8, no. 12, p. 5719, (1973).
44. W. C. Tait, R. L. Weiher, Phys. Rev., vol. 178, p. 1404, 1969.
45. V. N. Avakumov, V. I. Perel, I. N. Yassievich, Sov. Phys. JETP 51, 626 (1980).
46. R. Kumar, A. S. Vengurlekar, S. S. Prabhu, J. Shah, L. N. Pfeiffer, Phys. Rev. B 54, 4891 (1996).
47. *McGraw-Hill dictionary of scientific and technical terms*, McGraw-Hill, 1978.

48. P. E. Selbmann, M. Gulia, F. Rossi, E. Molinari, P. Lugli, Phys. Rev. B, vol. 54, no. 7, p. 4660, (1996).
49. R. Höger, E. O. Gögel, J. Kuhl, K. Ploog, H. J. Queisser, J. Phys. C, vol. 17, p. L905. (1984).
50. Y. Toyozawa, Prog. Theor. Phys. Suppl. 12, p. 111, (1959).
51. F. Askary, P. Y. Yu, Phys. Rev. B, vol. 11, p. 3071, (1983).
52. Я. Ю. Аавиксоо, Я. Э. Липпмаа, А. М. Фрейберг, С. Ф. Савиххин, ФТТ, т. 31, стр. 203, (1989).
53. T. Steiner, M. L. W. Thewalt, E. S. Koteles, J. P. Salerno, Phys. Rev. B, vol. 34, p.1006, (1984).
54. P. W. M. Blom, P. J. van Hall, C. Smit, J. P. Cuypers, J. H. Wolter, Phys. Rev. Lett. **71**, 3878 (1993).
55. M. Gulia, F. Rossi, E. Molinari, P. E. Selbmann, P. Lugli, Phys. Rev. B **55**, R16049 (1997).
56. M. Gurioli, P. Borri, M. Colocci, M. Gulia, F. Rossi, E. Molinari, P. E. Selbmann, P. Lugli, Phys. Rev. B **58**, R13403 (1998).
57. G. Zimmerer, in: Exited-State Spectroscopy in Solids, Ed. U.M.Grassano, N. Terzi, North-Holland Publ. Co., Amsterdam, p. 34 (1987).
58. R. Kink, M. Selg, phys. stat. sol. (b), vol. 96, p. 101, (1981).
59. I. Ya. Fugol, Adv. Phys. vol. 37, p. 1, (1988).

7 SUMMARY IN ESTONIAN

GaAs ja teiste eksitonsüsteemide optiliste ergastuste pikosekundiline dünaamika

Kokkuvõte

Käesolevas töös on teoreetiliselt ja eksperimentaalselt uuritud eksitonide resonantset sekundaarkiirgust (**põhitulemused on esitatud poolpaksus kirjas**). Ajalise lahutusega valgusimpulsside peegeldumise uurimisel pooljuhtide pinnalt saime järgmised tulemused.

1. **Esimest korda on analüüsitud ja interpreteeritud katses ajalise lahutusega registreeritud valgusimpulsside peegeldusi GaAs, InP ja CdSe pinnalt, millel on uuritavast ainest sõltuvad iseärasused. Me oleme näinud valguse kristallilt *peegeldamise aega*.**
2. **Teoreetilise analüüsiga on näidatud, et kristalli dielektrilise läbitavuse mitteresonantne osa põhjustab peegelduse koste äärmiselt kiiret komponenti, resonantne osa vastab koste aeglasemale komponendile.**
3. **Koste resonantne osa määratakse kolme füüsikalise protsessi poolt, mis sõltuvad vastavatest resonantsi parameetritest: (i) polarisatsiooni defaseerumine, mida iseloomustab kustumistegur Γ; (ii) kiirguslik kustumine, mida iseloomustab polariseeritavus $4\pi\alpha$; ja (iii) polarisatsiooni levimine, mida iseloomustab eksitoni efektiivne mass. Eksperimendis mõõdetud peegelduse koste kestust saab küllalt hästi hinnata lihtsa fenomenoloogilise valemiga, mis sisaldab vastavaid parameetreid.**

Eksitonide luminestsentsi ajalist arengut kõrge kvaliteediga GaAs kristallis on uuritud sõltuvalt ergastuse energiast ja tihedusest.

4. **Esmakordselt on mõõdetud ja avaldatud eksitonide luminestsentsi tõusuaeg GaAs mahulises kristallis.**
5. **Katseliselt on avastatud eksitonide luminestsentsi kustutamise efekt valguskiirguse abil.**

Kustutamise efekti uurimiseks on teostatud spetsiaalsed luminestsentsi uurimise katsed kristallis täiendavalt ergastatud laengukandjatega. Katsetulemuste analüüsimiseks on esitatud Boltzmanni kineetilistel võrranditel põhinev mudel, mis kirjeldab kvalitatiivselt eksperimendi efekte.

6. **Analüüs näitab selgelt, et protsesside kirjeldamisel tuleb arvestada eksitonide formeerimist *kuumadest* laengukandjatest ja eksitonide-laengukandjate *soojusvahetust*.**

Tahke Xe kristallis on ajalise ja spektraalse lahutusega uuritud eksitonide luminestsentsi kineetikat sõltuvalt kristalli temperatuurist ja ergastuse energiast.

Katsetulemuste interpreteerimiseks on teostatud Monte-Carlo tüüpi mudelarvutusi.

7. **Vaba eksitoni luminestsentsi kustumise kineetika on selgelt mitte-eksponentsiaalne. See kineetika osutab vajadusele arvestada eksiton-polaritonide hajumist foononitel nende transpordil kristalli sisemusest pinnale. Eksitonide luminestsentsi tõusu analüüs näitab (nagu ka GaAs puhul) vajadust arvestada eksitonide formeerumist *kuumadest* laengukandjatest.**

Eksitonide fotoluminestsentsi uuringute tulemused näitavad üldiselt et:

8. **Erinevalt lisanditsentrite luminestsentsist on eksitonide fotoluminestsents oluliselt mittelineaarne juba madalate ergastusintensiivsuste korral (suurusjärgus 10^{14} cm^{-3}). Tänu sellisele mittelineaarsusele võib osutuda võimalikuks *madala intensiivsusega töötavate valgus-valgus-loogikaelementide* loomine.**

Töö eksperimentaalses osas:

9. **Kristalli ergastuste vastasmõju uurimiseks on välja töötatud uudne kahekanaliline moduleeritud luminestsentsi mõõtmise korrelatsioon-tehnika. Sel metoodikal on ühelt poolt modulatsioontehnika tüüpilised eelised (nagu "kadunud aja" korrigeerimine ja triivide mõju kõrvaldamine) ja teiselt poolt tüüpilised aeglahutusega footonite loendamise eelised (signaal mõõdetakse kohe ajaliselt, parima võimaliku müra statistikaga).**

8 ACKNOWLEDGEMENTS

The author is especially grateful to his long-time supervisor professor Jaak Aaviksoo for his kind support and everything else.
The author is indebted to Prof. Viktor V. Travnikov and Dr. Viktor V. Rossin for collaboration and for supplying the samples; and to Prof. Georg Zimmerer for providing the possibilities of visiting his group.
The author thanks all his colleagues from the Laboratory of Crystal Spectroscopy for their kind co-operation and helpful discussions.

9 PUBLICATIONS

I

J. Aaviksoo, J. Kuhl, I. Reimand,
"Time-resolved reflection of light from InP crystals",
Solid State Comm., vol. 72, no. 1, p. 49 (1989).

Solid State Communications, Vol. 72, No. 1, pp. 49-51, 1989.
Printed in Great Britain.

0038-1098/89$3.00+.00
Pergamon Press plc

TIME-RESOLVED REFLECTION OF LIGHT FROM InP CRYSTALS

J. Aaviksoo[a)]*, J. Kuhl[a)] and I. Reimand[b)]
[a)]Max-Planck-Institut für Festkörperforschung, Heisenbergstr. 1,
7000 Stuttgart 80, FRG
[b)]Institute of Physics, Estonian Acad. Sci.,Riia 142, 202400 Tartu, Estonia/USSR
(received 12. July, 1989 by M. Cardona)

The reflection dynamics of picosecond light pulses is investigated under the Brewster angle of incidence near the lowest exciton resonance in InP. The reflected pulses acquire a nonexponential tail which follows the resonant polarization decay in the reflecting surface layer. Both finite effective mass of excitons and dephasing must be included in the theoretical model to yield a numerical fit of the experimental data. The observed intensity dependence of the reflection dynamics can be understood by an enhanced dephasing process due to exciton-exciton collisions.

* Alexander von Humboldt Fellow. Permanent address:
Institute of Physics, Estonian Acad.Sci., Riia 142, 202400 Tartu, Estonia/USSR

1. Introduction

Reflection spectra of direct-gap semiconductors show distinct structures near excitonic resonances. This structure results in a corresponding transient behavior of resonantly reflected ultrashort optical pulses in the time domain. The effect of transient reflection has been theoretically analyzed[1-3] and was recently demonstrated experimentally on GaAs crystals[4] . Pulsed excitation is shown to induce resonant (and nonresonant) polarization in the reflecting surface layer of the crystal, which in turn, reemits light in the form of a reflected pulse. Time-resolved studies of the reflected pulse shape thus provide a direct means to follow the polarization dynamics in the surface layer. It was shown[4] that three decay channels of the surface polarization can be distinguished: pure optical dephasing, radiative decay, and polarization propagation due to spatial dispersion. As a matter of fact, extrinsic surface effects probably enhanced recombination and scattering of excitons caused by charged surface states, did not allow a numerical fit of the experimental data for GaAs crystals, however.

The present communication reports time-resolved reflection measurements on InP crystals. The general features of the reflection kinetics of InP are similar to those of GaAs. However, it is additionally possible to reach a good numerical fit for InP and thus differentiate quantitatively between the different decay channels of the surface polarization.

2. Experimental

The experimental set-up was based on a synchronously pumped dye laser: Styryl-9M, average power 10 mW, FWHM of the autocorrelation function (ACF) Δt = 5.2 ps, spectral width $\Delta\nu$=6 cm^{-1}. The reflected pulses were analyzed by measuring their cross-correlation functions (CCF) with the incident pulses using synchronous detection technique. The ACF of the pulses had long tails which extended beyond the usual sech^2-pulse shape approximation. This could be traced back to intracavity water vapour absorption and dispersion effects, which strongly limit picosecond pulse generation in the near-infrared. The laser beam was focused onto the epitaxial InP sample to a $\sim$ 0.1 mm spot by a f=250 mm lens. All the measurements were carried out in an immersion cryostat below the λ-point (T=2K) of liquid helium.

The epitaxial InP samples (FS920, 2.3μm thick) revealed a characteristic excitonic reflection dip at 11441.7 cm^{-1} in accordance with earlier reflection measurements[5] and the luminescence spectrum of the sample exhibited a well pronounced free-exciton emission band.

3. Results and Discussion

The reflection experiments were carried out under the Brewster angle of incidence (β =arctan $\sqrt{\epsilon_0}$, where ϵ_0 is the nonresonant dielectric susceptibility), in order to eliminate the nonresonant contribution to the reflection amplitude. Besides getting rid of the instantaneous nonresonant response, the Brewster angle of incidence suppresses also the influence of the dead layer. By this means the resonant contribution of the bulk to the reflection could be investigated independently. The experimental results are depicted in Fig. 1. The measured CCF show clearly that the reflected pulses are delayed and have tails which extend several picoseconds beyond the exiting pulses. The other apparent feature is the dependence of pulse shape and delay on incident light intensity.

The interpretation of the time-resolved data may proceed from the Fourier analysis of the reflection spectrum as far as linear processes are concerned[1-4] . The reflected pulse is therefore a convolution of the incident pulse with the Fourier transform of the reflection amplitude $r(\omega)$. The latter may be calculated using the modified Fresnel formulae[6] proceeding from the dielectric susceptibility $\epsilon(\omega)$, which includes spatial dispersion and dephasing in the usual form. These formulae allow also for dead layer and oblique angle of incidence. We have

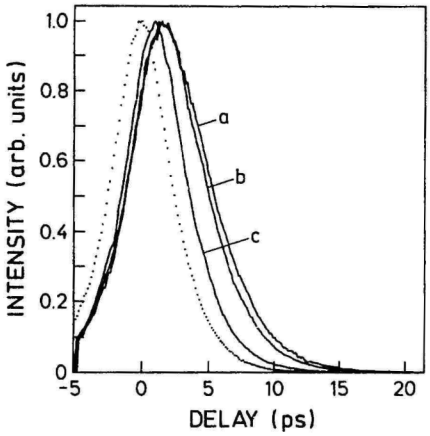

1. ACF of the incident pulses (dotted line) and CCF of the reflected pulses at different excitation intensities: (a: 10μW incident laser power, b: 100 μW, c: 1000 μW angle of incidence $\beta = 73.96°$, T=2K).

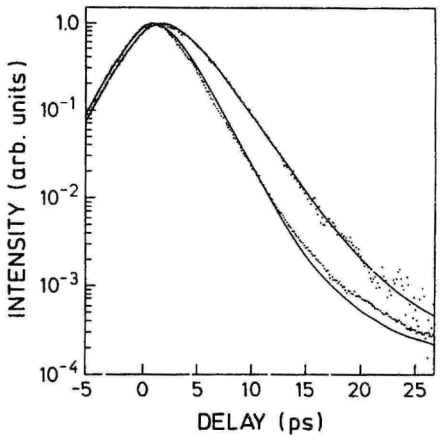

2. Logarithmic plot of experimental cross-correlation functions of the reflected pulses (dotted) and theoretical fits to the data (continuous line) at two excitation intensites (incident laser power 30 μW - upper and 1000 μW lower curves).

used the following values of the InP material parameters: $\epsilon_0 = 12.1$,[7] transverse exciton frequency $\nu_0 = 11441.0$ cm^{-1}, exciton polarizability[5] $4\pi\alpha = 2.3 \cdot 10^{-3}$. The homogeneous linewidth $\Gamma = \frac{1}{\pi \cdot T_2}$ and the effective mass of excitons M were varied in the curve fitting procedure.

The incident pulse shapes were computed from the measured ACF under the assumption of symmetric transform-limited pulses, and convoluted with the model reflection response r(t) to give the reflected pulse $E_R(t)$. The corresponding CCF were then compared to the experimental curves. The fitting procedure yielded two important results: 1) no reasonable fit could be obtained neglecting spatial dispersion ($M = \infty$), whereas inclusion of spatial dispersion provided a good fit over three orders of magnitude of the reflection decay, and 2) at higher excitation intensities the decay curves could be modeled by increasing the dephasing rate, however, the fit was clearly worse than in the low intensity limit. These facts are illustrated in Fig. 2.

The exciton effective mass, determined from the measurements at lowest incident laser power of 10 μW ($1.3 \cdot 10^9$ photons/cm^2 pulse) was M=$(0.2 \pm 0.05)m_e$, where m_e is the free-electron mass. This value is distinctly smaller than the theoretical result $M_{th} = 0.32m_e$ calculated with Kane's formula for the effective masses for two degenerate exciton bands with d-like valence bands[8] using the Luttringer parameters of Ref.9. Our experimental result coincides however, with the value determined from the steady state reflection spectrum[5] . For our time-resolved experiments the spatial dispersion model provides a distinctly better theoretical description than a"classical" model without dispersion. The homogeneous linewidth $\Gamma = 1.5cm^{-1}$ obtained from a fit of the time-resolved spectra with the spatial dispersion model is considerably higher, however, than the value $\Gamma = 0.4cm^{-1}$ reported for the fit of that model to frequency domain spectra. In fact, our value for Γ is even close to the homogeneous linewidth determined previously from the spectral lineshape with the "classical" model ($\Gamma = 2.6$ cm^{-1} and $\Gamma = 1.6$ cm^{-1})[5,10] .

We have not measured the reflection spectra of our samples under the Brewster angle of incidence and therefore no direct comparison of the spectral curves could be made. We note, however, two important features of the transient reflection measurement which increase the reliability of our curve fitting data. First, we could eliminate the dead layer effect reducing the number of free-parameters in the model, and second, the dephasing time T_2 is directly reproduced in the decay of the reflected pulses making an unambiguous interpretation much simpler.

In conclusion, in the case of InP crystals transient reflection near the lowest exciton resonance can be well-described by the straightforward linear response model proceeding from the dielectric susceptibility function including spatial dispersion. The transient reflection effect in this case includes pulse delay and the appearance of slowly decaying tails in the picosecond temporal range.

As noted above the observed reflection kinetics is dependent on excitation intensity analogously to previous experiments on GaAs samples[4]. The firsthand model explains the increased polarization (reflection) decay rate through additional dephasing of excitons due to increased exciton-exciton collisions. The same explanation was used earlier for transient reflection[4] as well as for degenerate four-wave-mixing experiments[11] on GaAs. Although the numerical fit of the experimental data is not as good as in the low intensity limit (Fig.2), it yields some averaged dephasing rates, which are plotted against incident laser power in Fig. 3. As one readily sees, a linear dependence $\Gamma' = \Gamma + \gamma \cdot I$ is observed, with $\Gamma = 1.5$ cm^{-1} and $\gamma = 4.6$ cm^{-1}/mW. The average incident intensity of 1 mW/$2.84 \cdot 10^{-4}$cm^2 corresponds to the initial concentration of excitons n=$1.3 \cdot 10^{18}$cm^{-3}, where we have taken the absorption depth $\ell = 10^{-4}$cm and the spot size $2.84 \cdot 10^{-4} cm^2$, which gives the exciton-exciton collision efficiency $\gamma' = 3.5 \cdot 10^{-18}$cm^2($\Gamma' = \Gamma + \gamma' \cdot n$). The linear dependence of Γ' on exciton density supports the exciton-exciton collision model and we note that the collision efficiency factor γ' is by a factor of 4

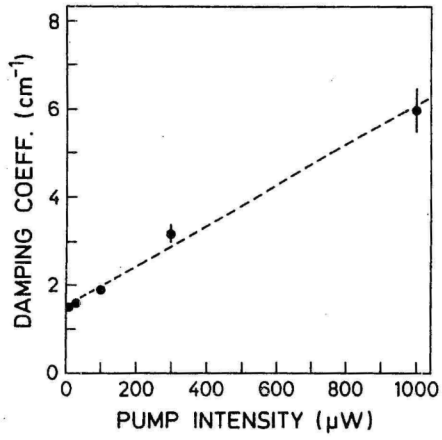

3. Dependence of the phenomenological damping coefficient Γ' on incident laser power.

larger than in the case of GaAs[9]. The reason for the higher dephasing efficiency of exciton-exciton collisions in InP is not yet clear.

4. Conclusion

First, time-resolved resonant reflection from InP crystals reveals distinct material dependent temporal features, secondly, the numerical modeling of the experimental data proceeding from the dielectric permeability function gives us the phenomenological damping constant (homogeneous linewidth) $\Gamma = 1.6$ cm^{-1} of excitons and the value $M=0.2m_e$ for the effective mass of excitons, thirdly, the exciton-exciton collision efficiency is characterized by $\gamma' = 3.5 \cdot 10^{-15}$cm^2.

Finally, let us make a remark concerning terminology. Treating transient phenomena at reflection, we prefer to use "transient reflection" to denote linear resonant reflection of light pulses and "transient reflectivity" to denote transients which arise due to a nonlinear modification of the reflectivity itself and which are usually analyzed in pump-probe experiments to study the ultrafast dynamics of nonequilibrium phenomena[12].

5. Acknowledgement

Thanks are due to H.J. Queisser who suggested InP for the transient reflection measurements as well as H. Scholz for supplying the high-quality samples.

References

1. D. Elert, *Ann. Phys. Ser. 5* **7**, 65 (1930).
2. G.P. Agrawal, J.L. Birman, D.N. Pattanayakand and A. Puri, *Phys. Rev. B* **25**, 2715 (1982).
3. J. Aaviksoo, J. Lippmaa and J. Kuhl, *J. Opt. Soc. Am.* **B5**, 1631 (1988).
4. J. Aaviksoo and J. Kuhl, *IEEE J. Quant. Electr.*, in print.
5. F. Evangelisti, J.U. Fischbach and A. Frova, *Phys. Rev. B* **9**, 1516 (1974).
6. I. Broser, M. Rosenzweig, R. Broser, M. Richard and E. Birkicht, *phys.stat.sol.(b)*, **90**, 77 (1978).
7. W.J. Turner, W.E. Reese and G.D. Pettit, *Phys. Rev.* **136**, A1467 (1964).
8. D.D.Sell, S.E.Stokowski, R.Dingle and J.V. DiLorenzo, *Phys.Rev. B* **7**,4568 (1973).
9. Landolt-Börnstein, New Series, Vol. 22, ed. O. Madelung, Springer Verlag Berlin-Heidelberg (1987).
10. K. Lösch, Thesis, Stuttgart 1977.
11. L. Schultheis, J. Kuhl, A. Honold and C.W. Tu, *Phys. Rev. Lett.* **57**, 1635 (1986).
12. See e.g. "Semiconductors Probed by Ultrafast Laser Spectroscopy "Vol. 1 and 2, ed. R.R.Alfano, Academic Press , Inc. New York (1984).

II

J. Aaviksoo, J. Kuhl, I. Reimand,
"Time resolved resonant reflection of light",
Laser Optics of Condensed Matter, vol. 2,
Plenum New York, pp. 61-69 (1991).

TIME-RESOLVED RESONANT REFLECTION OF LIGHT

J. Aaviksoo[1], J. Kuhl[2], and I. Reimand[1]

[1] Institute of Physics, Estonian Academy of Sciences
Riia 142, 202400 Tartu, Estonia, USSR

[2] Max-Planck Institut für Festkörperforschung
Heisenbergstrasse 1, 7000 Stuttgart 80, WEST GERMANY

1. INTRODUCTION

Light reflected from a dielectric interface shows distinct spectral features near material resonances. Proceeding from the Fresnel formula this spectrum can be related to the dielectric function ϵ and has been widely used to study the corresponding material parameters. The frequency dependence of the reflection coefficent implies that transients should be observed in reflection if light pulses are incident on the interface. In the general case, we can consider a light pulse $E_I(t)$ incident on a semi-infinite dielectric medium, characterized by a dielectric function $\epsilon(\omega,k)$, under angle α, and split into a reflected pulse $E_R(t)$ and a transmitted pulse $E_T(t,z)$ (Fig. 1). The problem of transient reflection is in relating the temporal properties of the reflected pulse to the material parameters of the medium and lacks an analytic solution in the general case. Let us note that these transients appear in a linear reflection process and are treated apart from nonlinear cases where ϵ itself is modified by a strong (additional) incident field. We prefer to call the latter case transient reflectivity and to use the term transient reflection to denote linear response.

Transient reflection was first analyzed by Elert[1] almost 60 years ago. He considered a truncated nonresonant monochromatic wave incident on a semi-infinite local medium and showed that transients arise at the leading edge of the reflected field. The characteristic time-scale of the transients was comparable to the period of the light wave. Later, Birman et al.[2,3] analyzed transient reflection from nonlocal media near

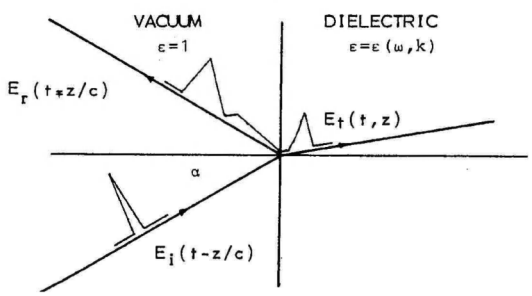

Fig. 1. The transient reflection scheme.

Laser Optics of Condensed Matter, Vol. 2
Edited by E. Garmire *et al.*, Plenum Press, New York, 1991

exciton-polariton resonances. It was shown that transients are associated with the leading and trailing edges of the truncated incident field and have a characteristic duration of ~ 0.1 ps under certain circumstances. Spatial dispersion was shown to enhance the transients, and the manifestation of additional boundary conditions (ABC) was treated. In a recent paper[4] we have considered analytical incident pulses to check the experimental observability of transients in transmission and reflection. A numerical analysis predicted the appearance of extended (over tens of picoseconds) pulse tails in the case of Gaussian incident pulses reflected from a GaAs crystal surface near the exciton resonance.

In the present paper we give a more detailed theoretical analysis of the transient reflection problem, and present the corresponding experimental results for GaAs[5], InP[6], and CdSe. We have focused our attention on the underlying physical mechanisms and tried to relate material parameters to the observed transients.

2. THEORY

The linear reflection problem can be treated by the Fourier analysis method -- the reflected light pulse $E_R(t,z=0)$ is the Fourier transform of the product of the incident pulse spectrum $E_I(\omega)$ and the reflection coefficient $r(\omega)$

$$E_R(t,z=0) = \int E_I(\omega)\cdot r(\omega)\cdot e^{-i\omega t}d\omega. \tag{1}$$

The reflection coefficient $r(\omega)$ can be determined proceeding from the dielectric function $\epsilon(\omega,k)$, which for a classical nonlocal medium is

$$\epsilon(\omega,k) = \epsilon_o + \frac{4\pi\alpha\omega_o^2}{\omega_o^2-\omega^2-i\omega\Gamma+(h\omega_o/m)k^2} \tag{2}$$

In the above formula ϵ_o is the background dielectric constant due to higher lying resonances, ω_o is the transverse exciton frequency, $4\pi\alpha$ is the polarizability of the resonance, m is the exciton effective mass, and Γ is a phenomenological damping constant. It can be shown[7], that Eq. (2) can also be obtained as a special case of the quantum theory. In the following we proceed entirely from these two formulas.

The reflected pulse can also be calculated as a convolution of the incident pulse with the response function of the reflecting surface r(t). The latter is the Fourier transform of the reflection amplitude $r(\omega)$, and is equal to the reflected pulse if the incident pulse is infinitely short ($E_I(t) \sim \delta(t)$).

In order to calculate the reflection coefficient for a nonlocal medium one needs to solve the ABC problem, which we do, following Pekar[8], by assuming that the polarization vanishes at the crystal surface. Additionally, dead layer effects must be considered in the case of excitons in semiconductor crystals[9]. In our theoretical analysis we have avoided this problem by setting the angle of incidence α equal to the Brewster angle $\alpha = \arctan\sqrt{\epsilon_o}$. By this means the dead layer does not contribute to reflection and can be neglected. Furthermore, reflection due to higher lying resonances vanishes altogether and only the resonant contribution to the reflection amplitude is preserved. This makes the interpretation of the results more transparent. Under these conditions the reflection coefficient is

$$r(\omega) = \frac{1-n^*(\omega)}{1+n^*(\omega)}, \tag{3}$$

where $n^*(\omega)$ is the effective index of refraction, which can be calculated from Eq. (2) with the help of the formulas given in Ref. 10.

To get an idea of the reflection kinetics we have calculated the reflected pulse shapes ($|E_R(t)|^2$, see Fig. 2) by using the parameters of a GaAs crystal (ϵ_o=12.6, ω_o = 1.2221.5 cm^{-1}, and $4\pi\alpha = 10^{-3}$ (11)). The incident Gaussian pulse has a FWHM of 1.2 ps and its spectrum covers the resonant reflection region, i.e. it is short enough to introduce no distortions to the transient response under study. It is clearly seen that the reflected pulses have significant tails extending over tens of picoseconds depending on the damping and the effective mass of the excitons. Three other observations are of importance. First, increasing the damping parameter Γ also increases the decay of the reflected pulse and leads to an almost exponential decay for large Γ. Second, for negligible damping increasing the spatial dispersion (decreasing the effective mass m^*) also shortens the reflected pulse. And third, even for no damping and spatial dispersion the reflected pulse decays (in an oscillatory manner).

a. Radiative decay. If $m^* = \infty$ and $\Gamma = 0$ the surface polarization decays only due to the coherent reemission of the excitation in the form of reflected and refracted pulses. This process is characterized by the polarizability $4\pi\alpha$ of the resonance. It can be shown analytically that the first moment of the reflection curve is inversely proportional to the LT-splitting of the resonance

$$\tau = \Delta_{LT}^{-1} = (2\pi\alpha\omega_o/\epsilon_o)^{-1} \quad . \tag{4}$$

From the numerical analysis we got the following equality $\tau(ps) = 10.12 \cdot \Delta_{LT}^{-1}(cm^{-1})$. For GaAs this yields τ = 127 ps in accordance with the curves in Fig. 2.

b Dephasing. This process is characterized by the phenomenological damping constant Γ. If we put $m^* = \infty$ and let $\Delta_{LT}/\Gamma \to 0$ we get for the Brewster angle of incidence an analytical solution (4)

$$r(\omega) = \frac{n_o - n}{n_o + n} = \frac{\pi\alpha\omega_o}{\epsilon_o} \cdot \frac{1}{\omega_o - \omega - i\Gamma/2} \quad , \tag{5}$$

i.e. in this limiting case the reflection response is an exponential with a decay constant $\Gamma/2$ corresponding to a decay time $\tau = 1/\Gamma$ of the reflected pulse.

c. Spatial dispersion. If we put $\Gamma = 0$ and let $\alpha \to 0$ the reflected pulse exhibits a non-exponentially decaying tail with the first moment τ proportional to the effective mass of the excitons. The numerical modeling yields the following proportionality factor (for GaAs parameters) $\tau(ps) = 32.5 \cdot m^*$ (free electron masses). The observed decay in this case is clearly related to exciton propagation -- the calculated time τ is crudely equal to λ/π divided by the group velocity of the exciton normal to the crystal surface

$$\tau = \lambda/\pi v_g = \frac{m^* c^2 (1+\epsilon_o)^{1/2}}{h\omega_o^2 \epsilon_o} \quad . \tag{6}$$

So, transient reflection can be related to certain decay mechanisms of the surface polarization in these limiting cases. We have modelled the decay also for more complicated intermediate situations, where only one of the decay mechanisms can be neglected. The results are depicted in Figs. 3, 4, and 5, where the first moment of the reflection response τ is plotted as a function of $\tau(\Delta_{LT},\Gamma)$ for $m^* = \infty$, $\tau(m^*,\Delta_{LT})$ for $\Gamma = 0$, and $\tau(m^*,\Gamma)$ for $\Delta_{LT} \to 0$. Together with the direct numerical data we have

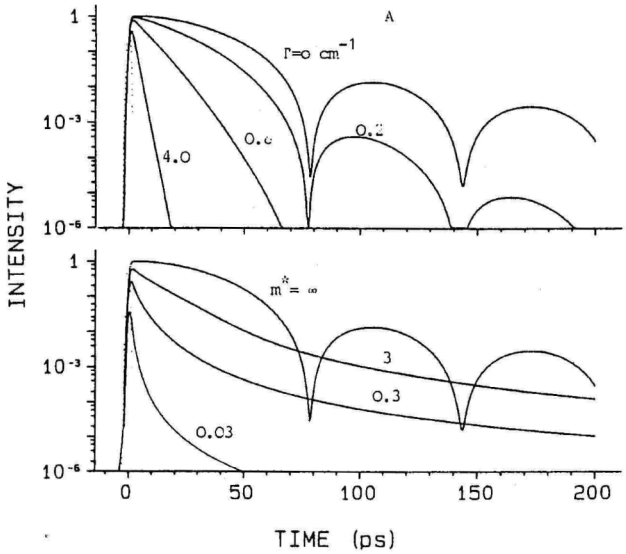

Fig. 2. Transient reflection from a GaAs crystal under Brewster angle. A: Dependenence on $m^* = \infty$. B: Dependence on exciton effective mass m^* for $\Gamma = 0$. The incident pulse is depicted at zero delay by dashed curve.

plotted the τ values calculated from the following phenomenological formula

$$\tau^{-1} = (\Delta_{LT}/10.12) + \Gamma + (0.031/m^*), \qquad (7)$$

which relies on the assumption that the three decay mechanisms are independent. We can see that the deviation of the direct numerical data from the estimates according to (7) is less than 20% for Figs. 3 and 4, indicating that the corresponding decay channels are almost independent of each other. In Fig. 5 the deviation is larger (≈50%) in the intermediate region of parameters, where both damping and spatial dispersion contribute to the decay. This may be understood by noticing that increasing Γ also modifies the dispersion curve of polaritons and influences (enhances) polarization propagation thereby. The increase of group velocity with an increase of damping has been observed experimentally in Ref. 12. Based on our numerical anaysis we draw the following conclusions. Transient reflection manifests the polarization decay process in the reflecting surface layer. Three decay channels can be distinguished --exponential decay due to polarization damping, characterized by the damping parameter Γ, oscillatory decay due to reemission of light, characterized by the value of the LT-splitting of the resonance, and non-exponential ("convex") decay due to polarization propagation, characterized by the effective mass of the excitons. These three decay channels are almost independent and can be summarized by the phenomenological formula (7).

These results can be compared to the results presented in Refs. 2,3,12. The general predictions of the two approaches coincide -- transients appear as decaying tails of abrupt features of the incident pulse. For common semiconductors these tails may extend over several picoseconds making their experimental observation feasible, in contrast to the first treatment of transient nonresonant reflection[1]. However, two principal differences are also evident. An enhancement of the

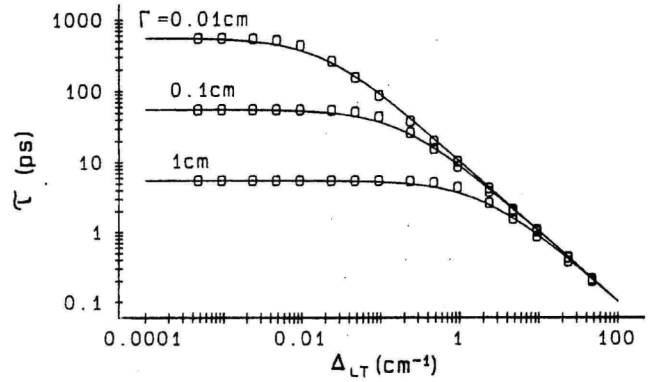

Fig. 3. Decay constants of transient reflection dependent on the LT-splitting and damping parameter $\Gamma(m^* = \infty)$.

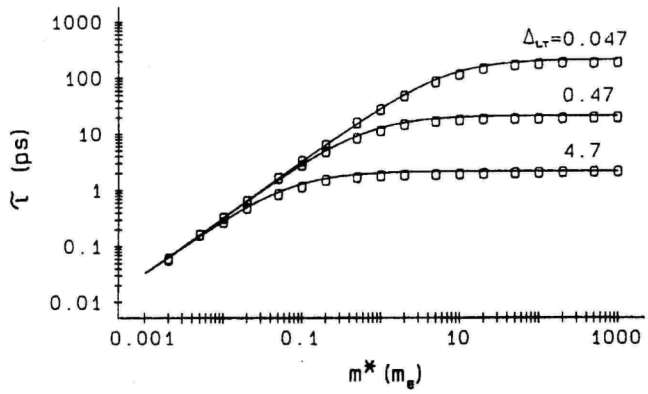

Fig. 4. Decay constants of transient reflection dependent on the effective mass of excitons and LT-splitting ($\Gamma = 0$).

transients is claimed to take place if spatial dispersion is included[2], while we observe a distinct reduction of the transients due to the introduction of a new decay mechanism. Second, a crossover from an exponential to a slow inverse power law is predicted at longer times in Ref. 2. Our analysis, on the contrary, predicts that non-exponential (inverse power law?) decay can be observed at early times if spatial dispersion is the main cause of the surface polarization decay. However, at long enough times exponential decay due to dephasing must still prevail.

Further theoretical analysis as well as experiments should elucidate the reasons for these discrepancies.

3. EXPERIMENTS

3.1. Experimental

The experimental set-up was based on synchronously pumped dye lasers. The reflected pulses were analysed by measuring their cross-correlation functions with the incident pulses using a synchronous detection technique. The laser beam was focused onto the samples to a $\simeq$ 0.1mm spot by an f = 250 mm lens. All the measurements were carried out in an immersion cryostat below the λ-point of liquid helium ($T \simeq 2K$).

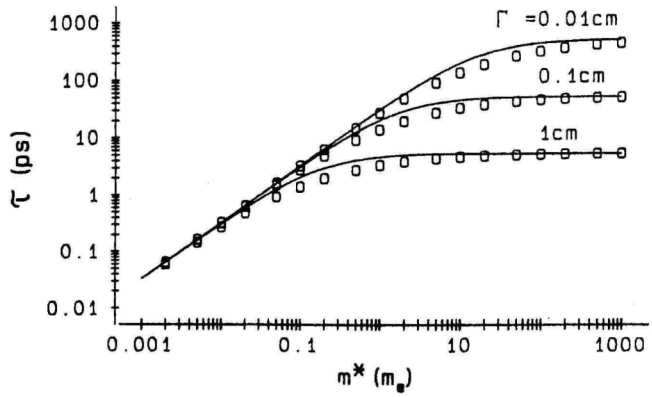

Fig. 5. Decay constants of transient reflection dependent on the effective mass of excitons and damping ($\Delta_{LT} \to 0$).

3.2. GaAs[5]

The expitaxial GaAs samples (R560) showed a characteristic reflection dip near the exciton frequency[11]. Time resolution of the reflected pulse (see Fig. 6), measured at normal incidence and low excitation densities reveals a long non-exponential tail, which starts at about a 1% intensity level and can be detected over 30 ps beyond the pulse maximum. The long term decay time of the tail was 5.4 ps as depicted by the solid line. This general shape of the reflected pulse profile can be divided into a nonresonant contribution, which follows the exciting pulse, and resonant reflection, which is responsible for the delayed tail. We have tried to model the observed decay theoretically by making use of the two sets of material parameters which were used to fit the steady-state reflection spectrum[11], and the results are also given in Fig. 6. Strong overestimation (three times) of the long term intensity of the pulse tail is evident, i.e. the fast initial decay of the resonant contribution is not reproduced by both models. Comparing the two models we see that the model with no spatial dispersion predicts a "concave" nature of the exponential decay, which is not observed experimentally and cannot be altered by varying the parameters of the model. The inclusion of spatial dispersion predicts a "convex" shape of the nonexponential tail and we therefore prefer it as the more appropriate one to describe the observed transients. The fit of the experimental curve can be considerably improved by slightly increasing the damping parameter. We note that the fast initial decay not reproduced by any of the models, may result from additional damping processes near the crystal surface, which has been suggested earlier[14]. The strong dependence of the transients on incident intensity is evidently caused by increased damping due to the induced exciton-exciton collisions. Let us add that the long term decay time of 5.4 ps is reasonably close to the estimate of 3.8 ps from (7).

3.3. InP [6]

The expitaxial InP samples revealed a characteristic excitonic reflection dip at 11441.7 cm^{-1} in accordance with earlier reflection measurements[15]. The results of time resolved reflection measurements are presented in Fig. 7. The measured CCF show clearly that the reflected pulses are delayed and have tails which extend several picoseconds beyond the exciting pulses. The other apparent feature is the dependence of the pulse shape and delay on the incident light intensity. We have modelled the experimental curves numerically (inserting the following

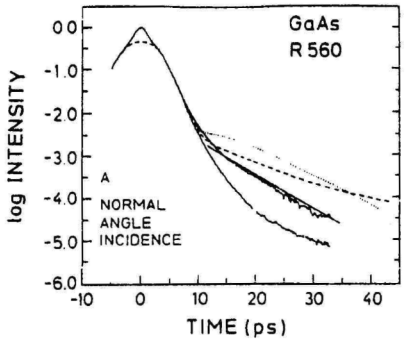

Fig. 6. Experimental cross-correlation functions of the reflected pulses with incident pulses (solid lines, weak excitation - upper curve, strong excitation - lower curve). Dotted line - theoretical fit neglecting spatial dispersion. Dashed line - theoretical fit including spatial dispersion. The slope of 5.4 ps is given by the straight line.

parameters for InP $\epsilon_o = 12.1$, $\omega_o = 11441\ cm^{-1}$, and $4\pi\alpha = 2.3 \cdot 10^{-3}$[15]. The damping constant Γ and the effective mass of the excitons m^* were varied in the curve fitting procedure. The fitting procedure yielded two important results: 1) no reasonable fit could be obtained neglecting spatial dispersion, whereas the inclusion of spatial dispersion provided a good fit over three orders of magnitude of the reflection decay, and 2) at higher excitation intensities the decay curves could be modelled by increasing the dephasing rate, however, the fit was clearly worse than in the low intensity limit. The best fitting parameters were $\Gamma = 1.5\ cm^{-1}$ and $m^* = 0.2\ m_o$.

3.4. CdSe

The transient reflection of vapor grown thin platelets of CdSe was studied near the lowest exciton resonance at $\omega_o = 14729\ cm^{-1}$. The crystals exhibited well pronounced steady-state reflection and polariton emission spectra. The corresponding time resolved normal angle incidence reflection curve is presented in Fig. 8. The incident laser pulse had an autocorrelation FWHM of 650 fs. The reflected pulse includes an ultrafast response at zero delay, which is caused by the nonresident background reflection, and a long non-exponential tail, beginning at about the 30% level, which is related to the resonant excitonic polarization. We can estimate the first moment of the resonant component of the reflected pulse making use of (7) and inserting the following material parameters for CdSe ($\epsilon_o = 8$, $\Delta_{LT} = 1.3...0.5$ meV and $\Gamma = 0.05$ meV[16]). We get $\tau \approx 1$ ps, which is close to the estimate $\tau = 1.2$ ps given in Fig. 8. We may notice that in this case the radiative process contributes significantly to the observed decay, and spatial dispersion seems to be responsible for the strongly nonexponential nature of the decay. A more detailed numerical fit and experiments at the Brewster angle of incidence are needed to yield unambiguous material parameters from this transient reflection measurement.

4. CONCLUSIONS

We have analyzed transient resonant reflection of light pulses and related it to the decay of resonant polarization induced by the incident pulse in the surface layer. Three almost independent decay mechanisms have been distinguished: 1) radiative decay, 2) polarization damping, and

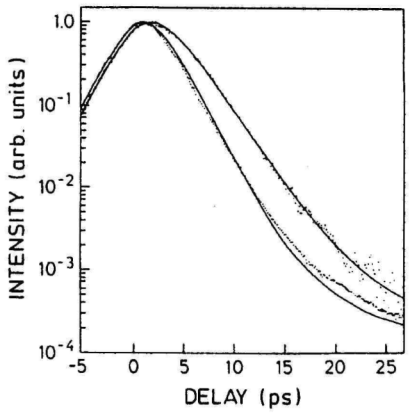

Fig. 7. Logarithmic plot of experimental cross-correlation functions of the reflected pulses (dotted) and theoretical fits to the data (continuous line) at two excitation intensities (incident laser power 30 μW - upper, and 1000-μW lower curves) for InP under Brewster angle incidence.

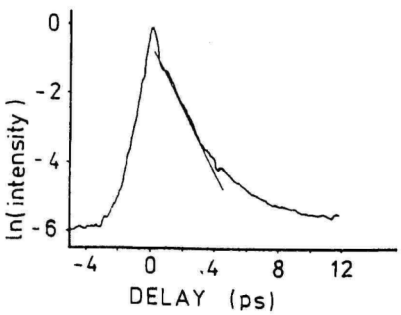

Fig. 8. Logarithmic plot of the experimental cross-correlation function of the reflected pulse from a CdSe crystal atr normal incidence. The slope of 1.2 ps is indicated by the straight line.

3) propagation of the polarization into the crystal. We have reported on the first experimental observations of the transient reflection effect in GaAs, InP, and CdSe. The experimental results can be described by numerical models as well as by general predictions of the theoretical analysis. Material parameters could be determined from the fit of the data in the case of InP.

ACKNOWLEDGMENTS

Thanks are due to E. Bauser, H. Scholz, and P. Lavallard who kindly supplied the samples. One of us (J.A.) thanks the A. von Humboldt Stiftung for the Fellowship to carry out the experiments.

REFERENCES

1. D. Elert, A.. Phys. Ser. 5, 7, 65 (1930).
2. G. P. Agrawal, J. L. Birman, D. N. Pattanayak, A. Puri, Phys. Rev. B25, 2715 (1982).
3. S. V. Branis, K. Arya, J. L. Birman, Phys. Rev. B39, 8371 (1989).
4. J. Aaviksoo, J. Lippmaa, J. Kuhl, J. Opt. Soc. Am. B5, 1631 (1988).
5. J. Aaviksoo, J. Kuhl, IEEE J. Quant. Electr. QE-25, (1989).
6. J. Aaviksoo, J. Kuhl, I. Reimand, Solid State Commun. 71, (1989).
7. W. C. Tait, Phys. Rev. B5, 648 (1972).
8. S. I. Pekar, Sov. Phys. JETP 6, 785 (1958).
9. J. J. Hopfield, D. G. Thomas, Phys. Rev. 132, 563 (1963).
10. S. A. Permogorov, A. V. Selkin, V. V. Travnikov, Sov. Phys. Solid State 15, 1215 (1973).
11. D. D. Sell, S. E. Stokowski, R. Dingle, J. V. DiLorenzo, Phys. Rev. B7, 4568 (1973).
12. J. Aaviksoo, J. Lippmaa, A. Freiberg, A. Anijalg, Izv. AN SSSR. Ser. Fiz. 48, 550 (1984).
13. S. V. Branis, J. L. Birman, in: Laser Optics of Condensed Matter (Plenum Press, New York, 1988) p. 303.
14. L. Schultheis, J. Lagois, Phys. Rev. B29, 6784 (1982).
15. F. Evangelisti, J. U. Fishbach, A. Frova, Phys. Rev. B9, 1516 (1974).
16. T. Itoh, P. Lavallard, J. Reydellet, C. Benoit a la Guillaume, Solid State Commun. 37, 925 (1981).

III

Я. Ю. Аавиксоо, И. Я. Рейманд, В. В. Россин, В. В. Травников,
“Кинетика образования и энергетической релаксации
экситонов в GaAs”,
Письма в ЖЭТФ, том 53, вып. 7, стр. 377, (1991).

Письма в ЖЭТФ, том 53, вып. 7, стр. 377 - 381 10 апреля 1991 г.

КИНЕТИКА ОБРАЗОВАНИЯ И ЭНЕРГЕТИЧЕСКОЙ РЕЛАКСАЦИИ ЭКСИТОНОВ В GaAs

Я.Ю.Аавикссо, И.Я.Рейманд, В.В.Россин, В.В.Травников

Институт физики АН ЭССР
202400, Тарту Физико-технический институт им. А.Ф.Иоффе АН СССР
194021, Ленинград

Поступила в редакцию 11 марта 1991 г.

При исследовании кинетики поляритонной люминесценции GaAs обнаружена задержка импульса излучения, связанная с релаксацией электронов и экситонов по энергии. Показано, что энергетическая релаксация замедляется с уменьшением концентрации мелких примесей.

При гелиевых температурах основное экситонное состояние является конечным этапом энергетической релаксации возбужденного кристалла. В данной работе использовался наиболее прямой способ исследования этой энергетической релаксации путем изучения кинетики экситонной люминесценции при импульсном возбуждении в различные энергетические состояния.

Люминесценция возбуждалась лазером на красителе стирил-9 с накачкой криптоновым лазером с синхронизацией мод. Длительность импульса возбуждения была 5 пс период следования импульсов - 240 нс, полуширина аппаратной функции системы регистрации - 300 пс. Спектральная ширина линии возбуждения $\sim 0{,}7$ мэВ и спектральное разрешение $\sim 0{,}1$ мэВ позволяли четко фиксировать как энергию возбуждения, так и энергию люминесценции. Исследовались чистые эпитаксиальные слои GaAs с различными концентрациями остаточных примесей и типом проводимости. По оценкам концентрация мелких доноров в самом чистом образце Г13 составляла величину $\sim 10^{12}$ см$^{-3}$ [1]. Стационарный спектр этого образца отличается интенсивной линией поляритонной люминесценции, сравнимой по интенсивности с линиями излучения связанных экситонов [2].

На рис. 1 показаны спектры и кинетика экситонной люминесценции различных образцов при температуре $T = 1{,}7$ К. Импульсы люминесценции регистрировались на энергиях, обозначенных стрелками *1*, *2* и соответствующих излучению из состояний нижней и верхней поляритонной ветвей. Во всех образцах наблюдается увеличение времени нарастания импульса люминесценции при уменьшении энергии излучающих поляритонов. На рис. 2*а* показана зависимость времени задержки максимума импульса люминесценции Δt_{max} от энергии излучения. Эта зависимость отражает эффект "бутылочного горла" для поляритонов, возникающий за счет замедления энергетической релаксации поляритонов вблизи экситонного резонанса [3]. Ранее о кинетике релаксации поляритонов сообщалось в работах [4-6], выполненных на кристаллах CdS. В отличие от указанных работ в нашем случае эффект "бутылочного горла" проявлялся в увеличении времени нарастания, а время затухания составляло величину $\tau_d \sim 4 \div 5$ нс (образец Г13) и слабо зависело от энергии люминесценции. Заметим, что указанная величина τ_d превышает полученное в работе [7] значение "излучательного" времени жизни экситона.

Слабая зависимость времени нарастания от энергии экситонной люминесценции GaAs наблюдалась в [8], где она связывалась с диффузией поляритонов из объема к поверхности. Для выяснения роли диффузии мы

исследовали временное затухание излучения, возникающего при аннигиляции поляритонов из области резонанса с одновременным испусканием *LO*-фонона. Коэффициент поглощения для такого излучения очень маленький, а групповая скорость велика, поэтому пространственное распределение поляритонов не может оказывать влияния на временную кинетику излучения. Существенного отличия в кинетике люминесценции поляритонов из области резонанса и из соответствующих точек *LO*-фононного повторения обнаружено не было. Это позволяет сделать вывод о том, что диффузия не оказывает заметного влияния на наблюдаемую задержку импульсов резонансной поляритонной люминесценции.

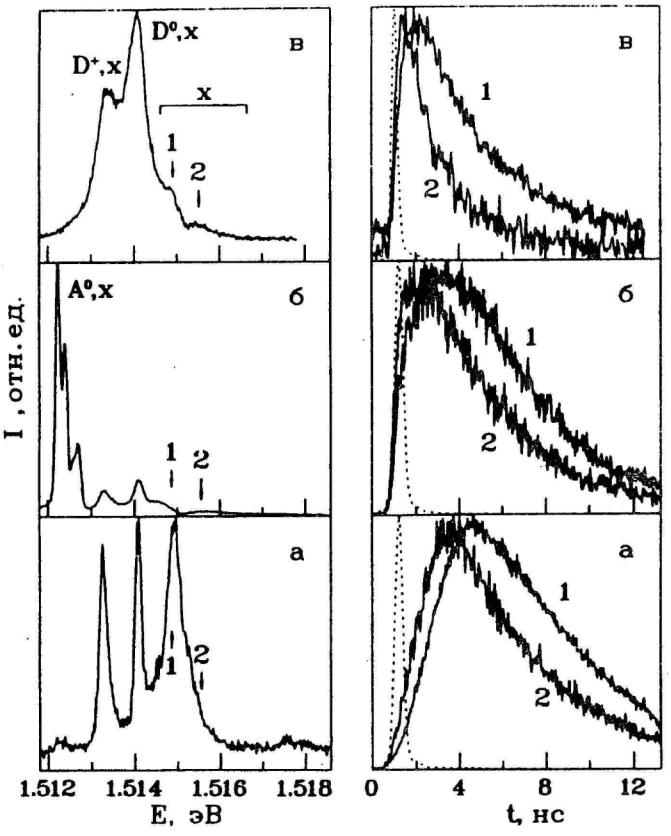

Рис. 1. Спектры (слева) и кинетика (справа) люминесценции различных образцов GaAs: *а* - Г13($N_D \sim 10^{12}$ см$^{-3}$); *б* - Y1(p-GaAs, $N_A \sim 10^{14}$ см$^{-3}$); *в* - K88(n-GaAs, $N_D \sim 10^{14}$ см$^{-3}$); энергия возбуждения - 1,554 эВ; пунктир - импульс лазера; кривые *1* и *2* соответствуют импульсам излучения из энергетических состояний нижней и верхней поляритонных ветвей отмеченных на спектрах стрелками *1* и *2*

Задержка импульса экситонной люминесценции при межзонном возбуждении наблюдалась в GaAs ранее [9], однако ее величина была на порядок меньше, чем в настоящей работе. В GaAs основным каналом образования экситонов при возбуждении полупроводника светом с энергией больше ширины запрещенной зоны является связывание холодных носителей заряда в экситоны [10]. Поэтому

задержка может быть вызвана как энергетической релаксацией возбужденных носителей заряда (такая возможность отмечалась в [9]), так и их связыванием в экситоны.

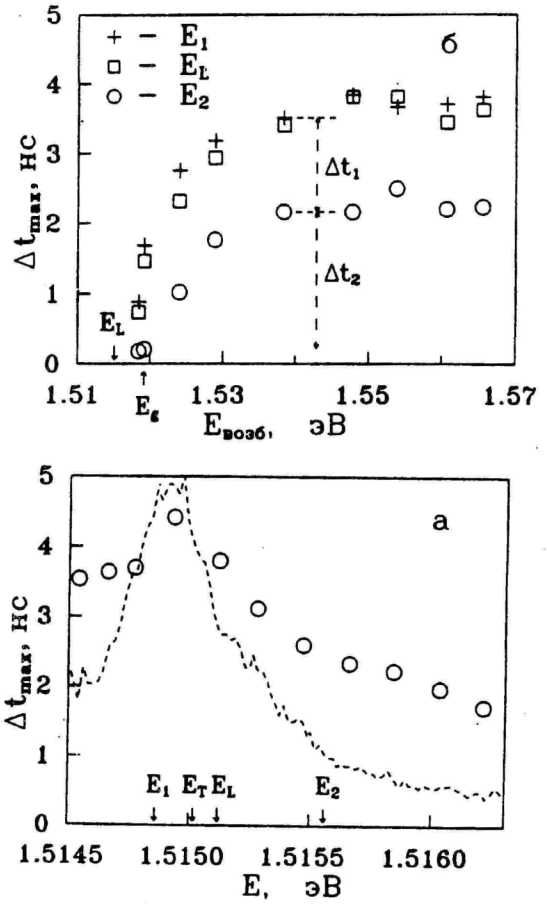

Рис. 2. Зависимость задержки максимума импульса излучения от энергии исследуемой точки в спектре люминесценции (*а*, энергия возбуждения - 1,554 эВ, пунктир - спектр поляритонной люминесценции) и от энергии возбуждения (*б*, для трех точек спектра люминесценции, отмеченных на рис. *а*); E_T и E_L - энергии дна зон поперечного и продольного экситонов, соответственно. Образец Г13

Время нарастания импульса поляритонной люминесценции существенным образом зависит от энергии возбуждения (рис. 3). Из рис. 2*б* видно, что существуют две составляющие задержки максимума люминесценции. Первая почти не зависит от энергии возбуждения и связана с релаксацией экситонов по энергии (характерная величина $\Delta t_1 \sim 1{,}5$ нс). Вторая составляющая Δt_2 возрастает (примерно на 2 нс) для всех энергий люминесценции при увеличении энергии возбуждения выше ширины запрещенной зоны E_g и отражает релаксацию электронов по энергии. В то же время значения Δt_{max} для импульса люминесценции поляритонов верхней ветви при возбуждении в край зоны и в возбужденное состояние экситона $n = 2$ (экспериментальные точки, соответствующие двум минимальным значениям энергии возбуждения

на рис. 2*б*) почти не отличаются, что свидетельствует о незначительности вклада процесса непосредственного образования экситона в задержку импульса поляритонной люминесценции.

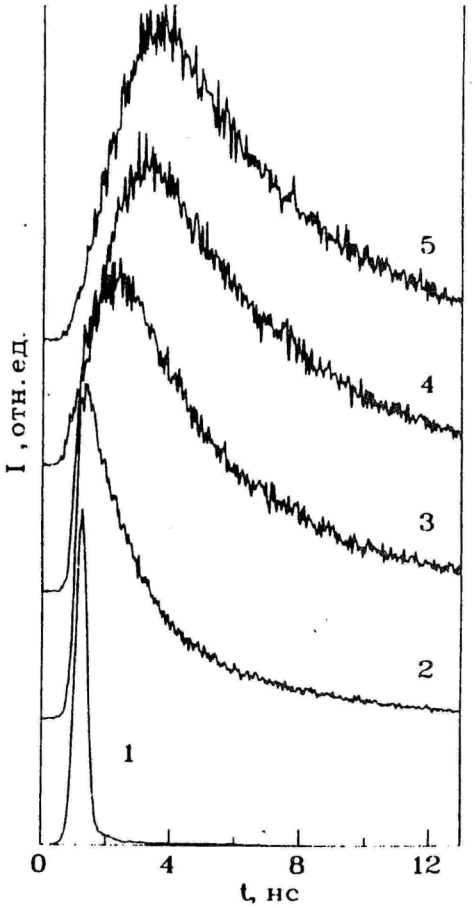

Рис. 3. Кинетика люминесценции из состояний верхней поляритонной ветви (энергия люминесценции 1,5156 эВ) при различных энергиях возбуждения: *2* - 1,520 эВ; *3* - 1,524 эВ; *4* - 1,538 эВ; *5* - 1,554 эВ; *1* - импульс лазера. Образец Г13

Как видно из рис. 1 время нарастания импульса поляритонной люминесценции меняется от образца к образцу. В сверхчистом материале основным механизмом энергетической релаксации электронов с энергией меньше энергии оптического фонона является релаксация на акустических фононах, которая ввиду малой эффективной массы электронов в GaAs весьма медленна (по оценкам [11] для температуры электронов $T_e = 10$K скорость их энергетической релаксации на акустических фононах в GaAs составляет величину $S = 0{,}1$ мэВ/нс). С увеличением концентрации мелких примесей наблюдается существенное уменьшение времени задержки максимума импульса поляритонной люминесценции. Это свидетельствует об ускорении энергетической релаксации электронов, например, вследствие неупругого рассеяния на примесях. Отметим, что в образце *n*-типа (рис. 1*в*) время нарастания люминесценции существенно меньше, чем в образце *p*-типа со сравнимой кон-

центрацией мелких примесей (рис. 1*б*). Это естественно, так как наибольший вклад в энергетическую релаксацию электронов следует ожидать от процессов неупругого рассеяния на мелких донорах.

Литература

1. Голубев В.Г., Жиляев Ю.В., Иванов-Омский В.И. и др. ФТП, 1987, 21, 1771.
2. Жиляев Ю.В., Маркарян Г.Р., Россин В.В. и др. ФТТ, 1986, 28, 2688.
3. Toyozawa J. Suppl. Progr. Theor. Phys., 1959, 12, 111.
4. Wiesner P., Heim U. Phys. Rev. B, 1975, 11, 3071.
5. Askary F., Yu P.Y. Phys. Rev. B, 1983, 28, 6165.
6. Аавиксоо Я.Ю., Липпмаа Я.Э., Фрейберг А.М., Савихин С.Ф. ФТТ, 1989, 31, 203.
7. 't Hooft G.W., van der Poel W.A.J.A., Molenkamp L.W., Foxon C.T. Phys. Rev. B, 1987, 35, 8281.
8. Steiner T., Thewalt M.L.W., Koteles E.S., Salerno J.P. Phys. Rev. B., 1986, 34, 1006.
9. Weisbuch C. Solid St. Electr., 1978, 21, 179.
10. Höger R., Göbel E.O., Kuhl J. et al. J. Phys. C, 1984, 17, L905.
11. Ulbrich R. Phys. Rev. B, 1973, 8, 5719.

IV

I. Reimand, J. Aaviksoo,
"Surface polarization dynamics revealed by time-resolved
resonant reflection of light",
Opt. Commun., vol. 86, no. 2, p. 142, (1991).

Optics Communications 86 (1991) 142–146
North-Holland

OPTICS
COMMUNICATIONS

Surface polarization dynamics revealed by time-resolved resonant reflection of light

I. Reimand and J. Aaviksoo
Institute of Physics, Estonian Academy of Sciences, Riia 142, 202400 Tartu, Estonia

Received 5 March 1991

We have analysed the temporal response function of a reflecting surface near an exciton resonance. The reflected pulse is shown to contain an ultrafast component due to the nonresonant polarization, approximated by ϵ_0, and a transient response, which follows the decay of the resonant polarization induced by the incident pulse. Three quasi-independent mechanisms are shown to contribute to this decay: (i) polarization dephasing, (ii) reradiation, and (iii) polarization propagation. A phenomenological model is proposed to calculate the characteristic decay constant from the material parameters.

1. Introduction

Light reflected from a dielectric interface shows distinct spectral features near material resonances. The frequency dependence of the reflection coefficient, in its turn, implies that transients should be observed in reflection if light pulses are incident on the surface. The problem of transient reflection lies in relating the temporal properties of the reflected pulse $E_R(t)$ to the dielectric function $\epsilon(\omega, k)$ of the medium and the geometry of the experiment, as well as elucidating the underlying physical processes.

Transient reflection was first analysed by Elert [1]. He considered a truncated nonresonant monochromatic wave incident normally on a semi-infinite medium, modelled by a set of Lorentz oscillators, and showed that transients arise at the front edge of the reflected field. The characteristic time-scale of the transients was less than the period of the incident light wave and corresponded to the eigenfrequency of the bound electrons. Under simplifying assumptions, an analytical solution for the reflected wave $E_R(t)$ was given in the form of a Bessel function. The problem has been extensively revisited by Birman et al. [2–4], who extended the analysis to resonant nonlocal media. It was shown, that in the case of exciton resonances in GaAs and CdS, transients in resonant reflection may extend several picoseconds beyond the trailing edge of the truncated wave. Quantitative differences due to various ABCs were found. In ref. [2] the reflection response was separated into local and nonlocal parts within the limit of weak spatial dispersion. No closed form analytical expression exists for $E_R(t)$ in a general case.

Recently, time-resolved reflection experiments were carried out on GaAs and InP crystals [5–7]. The reflected pulses were delayed and had a slowly decaying tail, which extended tens of picoseconds beyond the pulse maximum. In case of InP it was possible to fit the experimental curves with a straightforward numerical calculation of the transient reflection effect and to determine the underlying exciton resonance parameters.

In the present paper, we have carried out a theoretical analysis of the transient reflection problem in order to relate the observed transients in reflection to underlying physical mechanisms and trying to evaluate the role of different decay channels of the surface polarization. Numerical calculations have been carried out to check the applicability of a simple phenomenological approach developed in the present paper.

2. Theory

The linear reflection problem can easily be treated by the Fourier analysis method; the reflected light

pulse $E_R(t, z=0)$ is a Fourier transform of the product of the incident pulse spectrum $E_I(\omega)$ and the reflection coefficient $r(\omega)$

$$E_R(t, z=0) = \frac{1}{2\pi}\int E_I(\omega)\, r(\omega)\exp(-i\omega t)\, d\omega . \quad (1)$$

In the following, we are going to analyze the properties of the reflection response $r(t)$, which corresponds to the reflected pulse if the incident pulse is infinitely short ($E_I(t)=\delta(t)$ i.e. $E_I(\omega)=E_0=\text{const}$):

$$r(t)=\frac{1}{2\pi}\int r(\omega)\exp(-i\omega t)\, d\omega . \quad (2)$$

The reflected pulse $E_R(t, z=0)$ for an arbitrary incident pulse can then be found by convoluting $r(t)$ and $E_I(t, z=0)$.

The reflection coefficient $r(\omega)$ can be calculated proceeding from the dielectric function $\epsilon(\omega, k)$ and making use of the appropriate boundary conditions. In the following we have put

$$\epsilon(\omega, k)=\epsilon_0+\frac{4\pi\alpha\omega_0^2}{\omega_0^2-\omega^2-i\omega\Gamma+\hbar\omega_0 k^2/m^*}, \quad (3)$$

which accounts for the actual resonance at ω_0 with a polarizability $4\pi\alpha$, the dephasing rate Γ, and the effective mass m^*. The influence of higher-lying material resonances is included through ϵ_0. This model dielectric function is generally accepted to describe resonances in nonlocal dielectric media (e.g. excitons in GaAs, CdS, etc.) [8,3].

In the general case of oblique incidence three waves (two transverse and one longitudinal) are excited in a nonlocal medium [9]. The explicit expression for $r(\omega)$ has been calculated for Pekar ABC [9,10], but due to its complexity it is not reproduced here. Throughout this paper equations from tables 1 and 2 of ref. [10] (for πz orientation) have been used for computations of $r(\omega)$.

For an infinitely short incident pulse one has to take into account all the resonances of the crystal in their explicit resonant terms, i.e. (3) cannot be used due to the term ϵ_0. Therefore, let us first elucidate the contribution of higher-lying resonances (ϵ_0) to the reflection response in the simpliest case of normal angle incidence and by putting

$$\epsilon_0(\omega)=1+\frac{4\pi\alpha'\omega_0'^2}{\omega_0'^2-\omega^2}, \quad (4)$$

where higher-lying resonances are replaced with a single resonance at ω_0' ($\omega_0' \gg \omega_0$). Analogously with ref. [1], we have

$$r(t)=\frac{1}{2\pi}\int\frac{1-n(\omega)}{1+n(\omega)}\exp(-i\omega t)\, d\omega$$
$$=2i\cos[(\omega_0'+\Delta_{LT}'/2)t]\, t^{-1}J_1(\Delta_{LT}' t/2) . \quad (5)$$

J_1 is the first-order Bessel function and $\Delta_{LT}'=2\pi\alpha'\omega_0'$ the LT-splitting of the resonance at ω_0'. The envelope function (with respect to ω_0') of this response reveals a maximum at $t=0$ ($r(0)=i\Delta_{LT}$) with a width $\delta t\simeq\Delta_{LT}'^{-1}$, and an oscillatory decaying tail. If we further consider incident pulses of finite duration $\Delta T\gg\delta\simeq\Delta_{LT}'^{-1}$ and near resonances at $\omega_0\ll\omega_0'$, $r(t)$ converges to $\delta(t)$ in the limiting process $\omega_0'\to\infty$ and, correspondingly, $\epsilon_0(\omega)\to\epsilon_0=1+4\pi\alpha'$. In other words, nonresonant polarization terms cause an ultrafast $\delta(t)$-shaped response in reflection, which is accounted for by the ϵ_0-term in (3).

From (3) we see that $r(\omega)$ does not vanish for $\omega\gg\omega_0$, but approaches a constant value r_0, which depends on the angle of incidence φ and equals $r_0=(1-\sqrt{\epsilon_0})/(1+\sqrt{\epsilon_0})$ for $\varphi=0$. If we put $R(\omega)=r(\omega)-r_0$, we get

$$r(t)=\int R(\omega)\exp(-i\omega t)\, d\omega+r_0\delta(t) , \quad (6)$$

i.e. the transient response contains besides the $\delta(t)$-term a resonant component, which depends on the exciton resonance parameters $4\pi\alpha$, Γ and m^*.

Let us now proceed by analysing the dependence of the reflection response on the resonance parameters. In the following analysis (as well as in the experiments carried out so far) the ultrafast nonresonant response has been suppressed by choosing the angle of incidence φ so that $r_0=0$. This corresponds to the Brewster geometry with respect to ϵ_0, i.e. $\varphi=\arctan(\sqrt{\epsilon_0})$. In the latter case only the resonant polarization induces a reflected field and the observed reflection kinetics can be more easily interpreted.

In order to find out the elementary physical processes responsible for the transients in reflection, let

us analyse first three limiting cases, each of which clearly demonstrates a specific decay mechanism:

1. Dephasing of the polarization due to $\Gamma \neq 0$ ($4\pi\alpha \to 0$, $m^* \to \infty$, $\varphi = \varphi_B$). Within this limit an analytical solution can be reached [5]. One has

$$r(\omega) = \frac{\Delta_{LT}}{4} \frac{\epsilon_0 - 1}{\epsilon_0} (\omega_0 - \omega - i\Gamma/2)^{-1},$$

(for $\epsilon_0 \gg 1$ this coincides with formula (13) in ref. [5]) and, correspondingly,

$$r(t) = i \frac{\Delta_{LT}}{4} \frac{\epsilon_0 - 1}{\epsilon_0} \exp(-\Gamma t/2) \exp(-i\omega_0 t). \quad (7)$$

This purely exponential response, depicted in fig. 1a, decays with a time constant

$$\bar{\tau}_\Gamma = \Gamma^{-1}, \quad (8)$$

which is determined by the damping rate Γ of the material polarization. In other words, in this limit the reflected pulse "reflects" the polarization decay due to the dephasing of the material excitations.

2. Radiative decay of the polarization due to $4\pi\alpha \neq 0$ ($m^* \to \infty$, $\Gamma = 0$, and $\varphi = \varphi_B$). For normal angle of incidence and $\epsilon_0 = 1$ we end up with (5), (where ω' must be changed with ω), i.e. an oscillatory decay in the form of the Bessel function. The oscillation period equals the inverse LT-splitting Δ_{LT}, which determines the width of the band gap with $|r(\omega)| \equiv 1$. For arbitrary ϵ_0 and φ no closed form expression can be obtained for $r(t)$, however, the decay shows always the same oscillatory features. The time scale of the decay can be characterized by a time constant found as the first momentum of $|r(t)|^2$,

$$\bar{\tau} = \frac{\int |r(t)|^2 t \, dt}{\int |r(t)|^2 \, dt}. \quad (9)$$

A numerical calculation yields for the InP crystal ($\epsilon_0 = 12.1$)

$$\bar{\tau}_\Delta \text{ (ps)} = 20.9 \Delta_{LT}^{-1} \text{ (cm}^{-1}\text{)}. \quad (10)$$

The proportionality constant varies between 15 and 23 in the region from $\epsilon_0 = 1$ to $\epsilon_0 = 15$. Hence, exciton-photon coupling itself also damps the surface polarization due to coherent reradiation of photons in the form of reflected and refracted pulses. The increasing of $\bar{\tau}$ for higher ϵ_0 indicates to a reduction of the radiative decay at higher nonresonant polarizabilities. The characteristic reflection kinetics in the

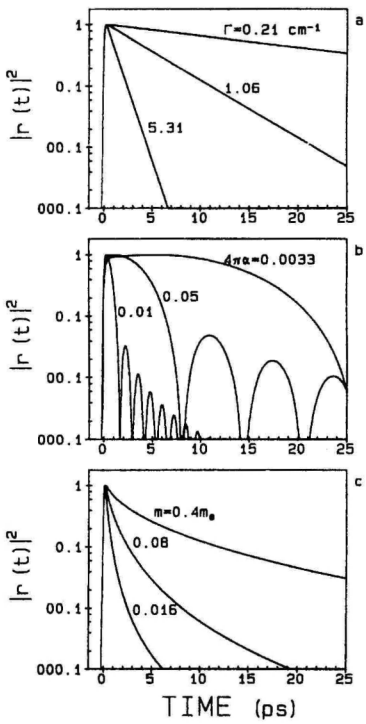

Fig. 1. Characteristic decay curves of the reflection response in three limiting cases: (a) polarization dephasing ($m^* \to \infty$, $4\pi\alpha \to 0$), (b) radiative decay ($m^* \to \infty$, $\Gamma = 0$), and (c) polarization propagation ($\Gamma = 0$, $4\pi\alpha \to 0$) for $\epsilon_0 = 12.1$, $\omega_0 = 11441$ cm^{-1}, and $\varphi = \varphi_B$.

case of purely radiative decay is depicted in fig. 1b.

3. Spatial dispersion of the polarization due to $m^* \neq \infty$ ($\Gamma = 0$, $4\pi\alpha \to 0$ and $\varphi = \varphi_B$). A set of computed response functions in dependence on m^* is depicted in fig. 1c. The response is decaying non-exponentially and the first momentum $\bar{\tau}$ is proportional to the effective mass of excitons. The proportionality factor depends weakly on ϵ_0 and for $\epsilon_0 = 12.1$

$$\bar{\tau}_m \text{ (ps)} = 30.3 m^* \text{ (free electron masses)}. \quad (11)$$

The observed kinetics in this case is clearly related to exciton propagation. We can make an estimate of $\bar{\tau}$ from the following argumentation. The incident

light pulse excites excitons with the wavevector $k_0=\omega_0 c^{-1}/\sqrt{\epsilon_0}$, which propagate away from the surface at the group velocity v_g. The propagation time, $t=(\lambda/\pi)/v_g\cos(\varphi')$, where φ' is the refraction angle, yields

$$t=\frac{m^*c^2\sqrt{1+\epsilon_0}}{\hbar\omega_0^2\epsilon_0}\approx 50\ \text{ps}\ m^*\ (\text{ps})\,, \tag{12}$$

which is in good correspondence with the numerical result (11), ($\epsilon_0=12.1$, $\omega_0=11441\ \text{cm}^{-1}$). The present limit applies if the damping rate Γ and the LT-splitting Δ_{LT} are less than the kinetic energy of excitons at exact resonance $\omega_{kin}=\hbar\epsilon_0\omega_0^2/2m^*c^2$. Birman et al. [4] have assumed $\omega_{kin}<\Delta_{LT}$ (or $\beta\gg\delta$ in their notation) and therefore the spatial dispersion effect appears only as correction to the local resonance model.

4. If these limits do not apply, the reflection response is a complicated interplay of all three decay mechanisms. In general, they are not independent. However, we suggest that they can be regarded quasi-independent as far as the first moment $\bar{\tau}$ of the response computed proceeding from (2 and 3) is concerned. In other words, we propose a phenomenological formula, which related $\bar{\tau}$ to three material parameters, Δ_{LT}, Γ and m^*, of the reflecting medium:

$$\bar{\tau}^{-1}\ (\text{ps})=\frac{\delta_{LT}\ (\text{cm}^{-1})}{20.9}+\Gamma+\frac{1}{30.3m^*(m_e)}\,. \tag{13}$$

We checked the model numerically for intermediate situations where only one of the decay mechanisms can be neglected. The results are depicted in figs. 2a, 2b and 2c as $\bar{\tau}(m^*, \Gamma)$ for $4\pi\alpha\to 0$, $\bar{\tau}(m^*, 4\pi\alpha)$ for $\Gamma=0$, and $\bar{\tau}(4\pi\alpha, \Gamma)$ for $m^*\to\infty$. Solid lines are computed from (13). The deviation of the direct numerical data from the estimates according to (13) is less than 20% for figs. 2b and 2c, which indicates that the corresponding decay channels are almost independent of each other. In fig. 2a, the deviation in the intermediate region of parameters is somewhat larger ($\approx 50\%$). In this region both damping and spatial dispersion contribute to the decay. This may be understood by noting that an increased Γ modifies also the dispersion curve of polaritons and influences (enhances) therefore the polarization decay propagation. The increasing of the group velocity of

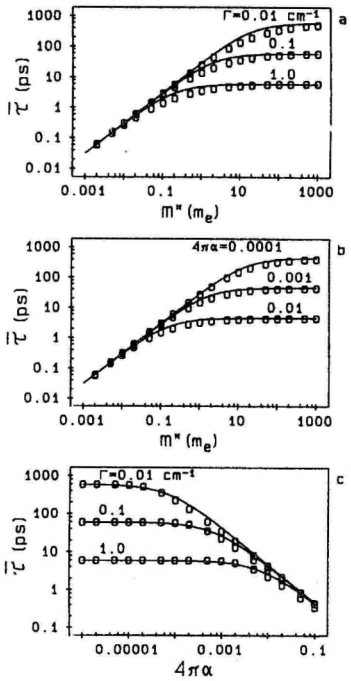

Fig. 2. Dependence of the computed decay time $\bar{\tau}$ of the reflection response on resonance parameters (empty squares) (a) $\bar{\tau}(m^*, \Gamma)$ at $4\pi\alpha\to 0$, (b) $\bar{\tau}(m^*, 4\pi\alpha)$ at $\Gamma=0$, and (c) $\bar{\tau}(4\pi\alpha, \Gamma)$ at $m^*\to\infty$. ($\epsilon_0=12.1$, $\varphi=\varphi_B$). Solid lines correspond to the phenomenological formula (13).

polaritons at higher damping has been observed experimentally in ref. [11].

Let us finish the analysis of the reflection kinetics with the InP crystal (experiment see ref. [7]), and put $4\pi\alpha=0.0023$ [12], $\Gamma=1.5\ \text{cm}^{-1}$ and $m^*=0.2m_e$ [7]. In this case all three decay mechanisms contribute, $\bar{\tau}_\Gamma=3.5$ ps, $\bar{\tau}_\Delta=19$ ps and $\bar{\tau}_m=6.1$ ps, and finally, following (13), $\bar{\tau}=2.0$ ps. The direct numerical computation yields $\bar{\tau}=1.3$ ps and the corresponding reflection response is plotted in fig. 3A together with those due to separate decay mechanisms (B, C, D). The first momentum $\bar{\tau}$ given by the proposed phenomenological model (13) is also shown on curve (A).

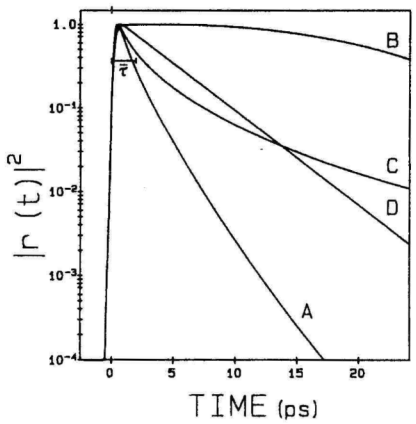

Fig. 3. The calculated reflection response in the case of exciton parameters of InP ($\epsilon_0=12.1$, $\omega_0=11441$ cm^{-1}, $4\pi\alpha=0.0023$, $m^*=0.2\ m_e$, $\Gamma=1.5$ cm^{-1}) (A). The underlying separate responses: (B) radiative decay ($4\pi\alpha=0.0023$, $m^*\to\infty$, $\Gamma=0$), (C) polarization propagation ($4\pi\alpha\to 0$, $m^*=0.2m_e$, $\Gamma=0$), (D) polarization dephasing ($4\pi\alpha\to 0$, $m^*\to\infty$, $\Gamma=1.5$ cm^{-1}). The first momentum $\bar{\tau}$ computed from (13) is shown on curve (A).

3. Conclusion

We have treated the transient reflection problem relating it to the dynamics of resonant polarization in the crystal. It has been shown that nonresonant terms cause an infinitely fast component in the reflection response. The resonant response is influenced by three physical processes: (i) dephasing of the polarization, (ii) radiative decay and (iii) polarization propagation. These processes can be regarded quasi-independent and a simple phenomenological formula gives a fairly good estimate to the duration of the reflection response. By means of numerical modelling we have checked the applicability of this formula and concluded that these processes are only weakly dependent on each other and may be treated separately. The experiments [6,7] have supported the given approach to the transient reflection problem.

Acknowledgements

JA wishes to thank J.L. Birman and S. Branis for a thorough and useful discussion of their results.

References

[1] D. Elert, Ann. Phys. Ser. 5, 7 (1930) 65.
[2] D.N. Pattanayak, G.P. Agrawal and J.L. Birman, Phys. Rev. Lett. 46 (1981) 147;
G.P. Agrawal, J.L. Birman, D.N. Pattanayak and A. Puri, Phys. Rev. B 25 (1982) 2715.
[3] S.V. Branis, K. Arya and J.L. Birman, in: Laser optics of condensed matter, eds. J.L. Birman, H.Z. Cummins and A.A. Kaplyanskii (Plenum Press, NY, 1988) pp. 303–314.
[4] S.V. Branis, K. Arya and J.L. Birman, Phys. Rev. B 39 (1988) 8371.
[5] J. Aaviksoo, J. Lippmaa and J. Kuhl, J. Opt. Soc. Am. B 5 (1988) 1631.
[6] J. Aaviksoo and J. Kuhl, IEEE J. Quant. Electr. QE-25 (1989) 2523.
[7] J. Aaviksoo, J. Kuhl and I. Reimand, Solid State Commun. 72 (1989) 49.
[8] V.M. Agranovich and V.L. Ginzburg, Crystal Optics with Spatial Dispersion and Excitons (Springer, Berlin, 1984) p. 236.
[9] S.A. Permogorov, A.V. Sel'kin and V.V. Travnikov, Sov. Phys. Solid State 15 (1973) 1215.
[10] I. Broser, M. Rosenzweig, R. Broser, M. Richard and E. Birkicht, Phys. Stat. Sol. (b) 90 (1978) 77.
[11] J. Aaviksoo, J. Lippmaa, A. Freiberg and A. Anijalg, Izv. AN SSSR Ser. Fiz. 48 (1984) 550.
[12] F. Evangelisti, J.U. Fischbach and A. Frova, Phys. Rev. B 9 (1974) 1516.

V

Я. Ю. Аавиксоо, И. Я. Рейманд, В. В. Россин, В. В. Травников,
“Гашение экситонной люминесценции горячими электронами в GaAs”,
ФТТ, том 33, вып. 8, стр. 2408, (1991).

УДК 535.343.2

ГАШЕНИЕ ЭКСИТОННОЙ ЛЮМИНЕСЦЕНЦИИ ГОРЯЧИМИ ЭЛЕКТРОНАМИ В GaAs

Я. Ю. Аавиксоо, И. Я. Рейманд, В. В. Россин, В. В. Травников

При исследовании кинетики поляритонной фотолюминесценции в сверхчистых эпитаксиальных слоях GaAs обнаружен эффект гашения люминесценции следующим импульсом фотовозбуждения. Зависимости эффекта от энергии люминесценции, энергии и интенсивности возбуждения указывают на то, что эффект связан с разогревом поляритонов за счет их взаимодействия с горячими электронами, возникающими при фотовозбуждении.

В кристаллах GaAs при фотовозбуждении светом с энергией больше ширины запрещенной зоны рождаются неравновесные носители заряда, которые после энергетической релаксации связываются в экситоны. Этот канал образования экситонов в GaAs является преобладающим [1]. Таким образом, при фотовозбуждении могут одновременно существовать неравновесные носители заряда и экситоны и взаимодействовать между собой. В [2, 3] отмечалось, что экситон-электронное взаимодействие может оказывать влияние на форму спектра поляритонной люминесценции GaAs. В [4] удалось описать форму спектра поляритонной люминесценции при малых интенсивностях возбуждения $I_{возб}$ сверхчистых эпитаксиальных слоев GaAs, учитывая взаимодействие поляритонов с фононами и примесями. В то же время наблюдаемый с увеличением $I_{возб}$ длинноволновый сдвиг максимума излучения из состояний нижней поляритонной ветви в рамках почти упругого рассеяния поляритонов на акустических фононах объяснить невозможно. Предполагалось, что он связан с существенно неупругим экситон-электронным рассеянием. В [5] сообщалось о влиянии магнитного поля на энергетическую функцию распределения поляритонов в GaAs. При этом для объяснения эффекта существенная роль также отводилась экситон-электронному рассеянию. Целью настоящей работы являлось выяснение роли процессов экситон-электронного рассеяния в кинетике нестационарной поляритонной фотолюминесценции GaAs.

Люминесценция возбуждалась перестраиваемым лазером на красителе стирил-9 с накачкой криптоновым лазером с синхронизацией мод. Длительность импульса фотовозбуждения 5 пс, период следования 12.2 нс, полуширина аппаратной функции системы регистрации 300 пс. Спектральная ширина линии возбуждения (~0.7 мэВ) и спектральное разрешение (~0.1 мэВ) позволяли четко фиксировать как энергию возбуждения, так и энергию люминесценции. Образцы представляли собой сверхчистые слои GaAs, изготовленные методом газофазной эпитаксии в хлоридной системе. По оценкам, концентрация мелких примесей в них составляла величину $\sim 10^{12}$ см$^{-3}$ [6]. Стационарный спектр фотолюминесценции этих образцов отличается интенсивной линией поляритонной люминесценции, сравнимой по интенсивности с линиями излучения связанных экситонов [4].

На рис. 1 представлен квазистационарный спектр фотолюминесценции образца GaAs при температуре 1.7 K и интенсивности возбуждения $I_{возб}=2.4$ Вт/см^2 (квазистационарный спектр отличается от обычного ста-

ционарного тем, что представляет собой временно́й интеграл люминесценции при указанном выше импульсном возбуждении). На рис. 2 показаны импульсы поляритонной люминесценции, зарегистрированные в трех характерных точках спектра: энергии максимума поляритонной люминесценции, соответствующей излучению нижней поляритонной ветви (*1*); энергии коротковолнового плеча, соответствующей энергии продольного экситона E_L (*2*); энергии из области излучения верхней поляритонной ветви (*3*). Обращают на себя внимание две характерные особенности импульсов люминесценции: задержка максимума импульса поляритонной люминесценции относительно импульса возбуждения, связанная с энергетической релаксацией носителей заряда [7] и поляритонов [8, 9], и гашение поляритонной люминесценции следующим импульсом возбуждения. Эффект гашения исчезает при приближении энергии возбуждения к краю запрещенной зоны (рис. 2, *б*). Эффект гашения наблюдается также и в кинетике люминесценции связанных экситонов. При этом наиболее ярко он проявляется в кинетике линии (D^0, x)-экситона, связанного на нейтральном доноре.

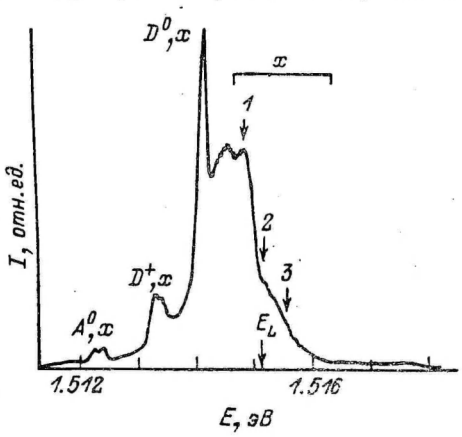

Рис. 1. Квазистационарный спектр фотолюминесценции образца Г13.1. $I_{возб}$=2.4 Вт/см², энергия возбуждения 1.554 эВ.

Как видно из рис. 2, *а*, эффект гашения тем больше, чем меньше энергия люминесценции. Для количественной оценки эффекта гашения можно ввести величину R_d, характеризующую глубину провала импульса люминесценции и равную отношению интенсивности люминесценции в начале импульса возбуждения в момент t_1, когда наблюдается резкое изменение временно́й производной, и в максимуме импульса возбуждения в момент t_2: $R_d=I(t_1)/I(t_2)$ (на рис. 2, *а* значения t_1 и t_2 отмечены стрелками). Значение $R_d < 1$ соответствует возрастанию люминесценции при приходе очередного импульса возбуждения.

На рис. 3 представлена зависимость величины R_d от энергии люминесценции. Видно, что глубина провала максимальна в области экситонного резонанса. Эффект гашения поляритонной люминесценции сильно зависит от интенсивности фотовозбуждения (рис. 4). Максимальное гашение достигается при средних $I_{возб}=\sim 2.4$ Вт/см².

Тот факт, что при малых энергиях люминесценции при приходе очередного импульса возбуждения наблюдается уменьшение интенсивности люминесценции, а при больших энергиях, наоборот, возрастание, позволяет сделать вывод, что происходит разогрев поляритонов. Мы предлагаем следующее возможное объяснение наблюдаемого эффекта. При возбуждении существенно выше края запрещенной зоны рождаются горячие электроны. Экситон-электронное взаимодействие приводит к разогреву поляритонов, т. е. к рассеянию поляритонов, накопившихся в состояниях с малой энергией, в состояния с большой энергией. В результате и наблюдается гашение люминесценции поляритонов с малой энергией, оставшихся от предыдущего импульса возбуждения. При этом максимального эффекта следует ожидать в области максимума энергетической функции распределения поляритонов в районе экситонного резонанса. Разогрев поляритонов приводит и к уменьшению концентрации связанных экситонов из-за того, что вероятность связывания уменьшается с увеличением энергии поляритонов [10]. При возбуждении в край зоны рождаются холодные электроны и разогрева поляритонов не происходит.

Зависимость эффекта гашения поляритонной люминесценции от интенсивности возбуждения также имеет разумное объяснение. Вероятность экситон-электронного рассеяния пропорциональна концентрации электронов n_e. Поэтому при малых интенсивностях возбуждения процессы экситон-электронного рассеяния несущественны и эффект отсутствует. При больших интенсивностях возбуждения эффект не заметен на фоне возрастания интенсивности поляритонной люминесценции за счет образования новых экситонов. Действительно, рассмотрим, чем определяется вре-

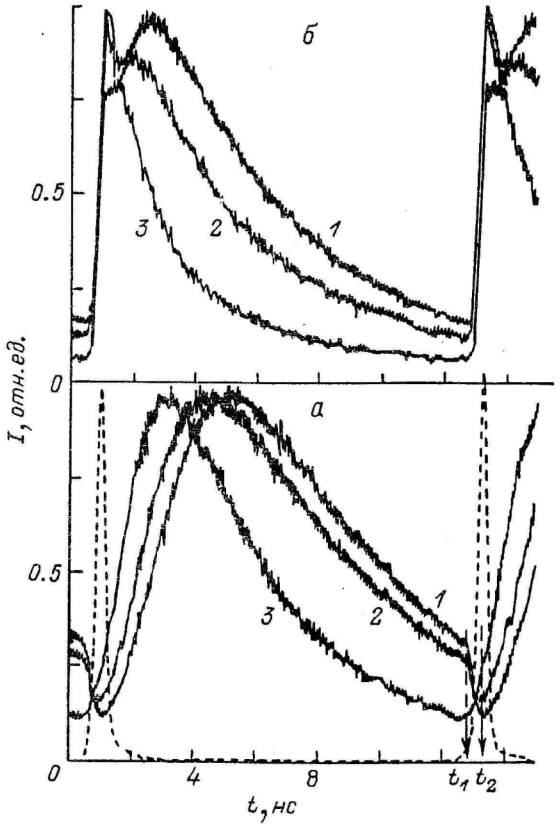

Рис. 2. Кинетика поляритонной люминесценции GaAs.

Энергия возбуждения (эВ): *а* — 1.554, *б* — 1.520, $I_{возб}$=2.4 Вт/см². Пунктир — импульс лазера; цифры у кривых соответствуют точкам спектра рис. 1. Стрелками указаны точки, отношение интенсивностей в которых определяет величину R_d.

менна́я зависимость интенсивности поляритонной люминесценции при приходе очередного импульса возбуждения. Для простоты не будем учитывать экситон-фотонное взаимодействие, которое для качественного рассмотрения несущественно. Предположив максвелловское распределение экситонов по энергии с эффективной температурой T^*, для интенсивности люминесценции на энергии E получим

$$I_E(t) \sim n_x(t) \exp(-E/k_B T^*(t))/T^*(t))^{3/2}, \qquad (1)$$

где n_x — полная концентрация экситонов. Тогда производная по времени интенсивности экситонной люминесценции определяется выражением

$$\frac{dI}{dt} \sim \left(\frac{1}{n_x}\frac{dn_x}{dt} - \frac{3/2 \cdot k_B T^* - E}{k_B T^*}\frac{1}{T^*}\frac{dT^*}{dt}\right) I_E. \qquad (2)$$

Нарастание полной концентрации экситонов во время импульса возбуждения пропорционально квадрату концентрации электронов n_e, а ско-

рость увеличения эффективной температуры экситонов за счет экситон-электронного рассеяния линейно зависит от n_e

$$dn_x/dt \sim n_e^2, \quad dT^*/dt \sim n_e. \tag{3}$$

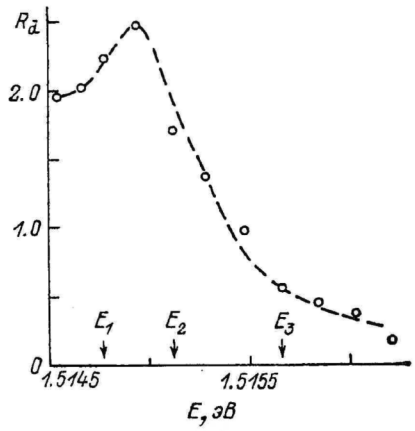

Рис. 3. Зависимость величины R_d от энергии люминесценции.

Энергия возбуждения 1.554 эВ, $I_{возб}$ = =2.4 Вт/см². Стрелками отмечены энергии, указанные на спектре рис. 1.

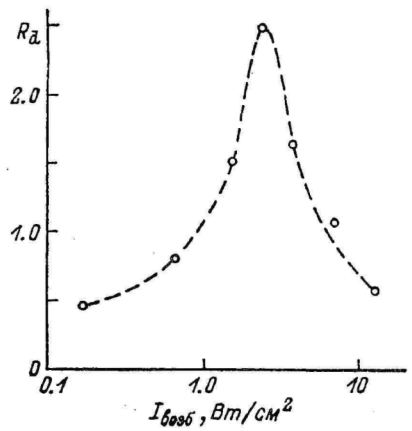

Рис. 4. Зависимость величины R_d от интенсивности возбуждения

Энергия возбуждения 1.554 эВ, энергия люминесценции 1.5149 эВ.

Из выражений (2), (3) видно, что при малых E и не слишком больших интенсивностях возбуждения возможны отрицательные значения временно́й производной интенсивности люминесценции, что соответствует гашению люминесценции импульсом возбуждения. При больших $I_{возб}$ скорость рождения экситонов начинает превышать их скорость разогрева.

Следует отметить, что для возможности наблюдения эффекта существенны два обстоятельства. Во-первых, время затухания поляритонной люминесценции должно быть достаточно большим по сравнению с периодом следования импульсов, чтобы к приходу очередного импульса возбуждения был заметный сигнал люминесценции. Во-вторых, необходима

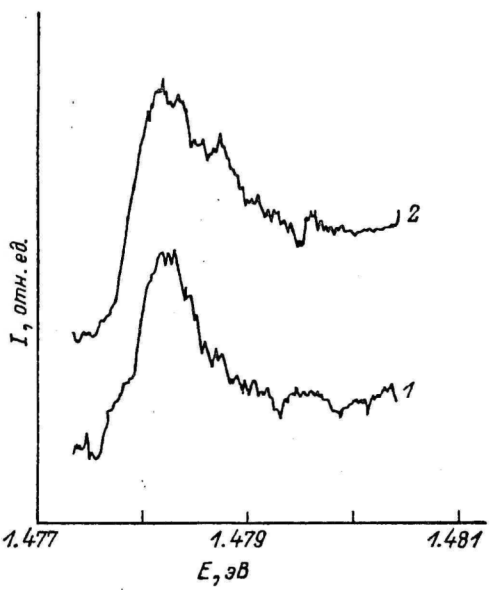

Рис. 5. Спектры излучения экситонов с испусканием LO фонона.

Энергия возбуждения (эВ): 1 — 1.520, 2 — 1.554.

значительная задержка между рождением горячих электронов и образованием новых экситонов. Эти два условия удается выполнить в наших сверхчистых слоях GaAs, в которых время затухания поляритонной люминесценции достигает значений $\tau_d \sim 4 \div 5$ нс, а задержка максимума поляритонной люминесценции относительно импульса лазера составляет величину $\Delta t_{max} \sim 4$ нс.

Экситон-электронное взаимодействие проявляется и в эксперименте по исследованию формы линии фононного повторения квазистационарной поляритонной люминесценции в зависимости от энергии возбуждения. Как видно из рис. 5, с увеличением энергии возбуждения возрастает эффективная температура поляритонов, которая определяет коротковолновый спад фононного повторения. Это прямо указывает на непосредственную связь эффективных температур поляритонов и электронов.

Обращает на себя внимание также, что форма спектра квазистационарной поляритонной люминесценции отличается от стационарной при соответствующей интенсивности возбуждения. В последнем случае в районе энергии продольного экситона наблюдается ярко выраженный провал в спектре, отсутствующий на рис. 1. Дело в том, что в случае импульсного возбуждения временные максимумы концентраций горячих электронов и поляритонов оказываются разнесенными, что обусловливает не слишком сильный разогрев поляритонов за счет взаимодействия с горячими электронами и отражается в отсутствии провала в спектре.

Для эффективного экситон-электронного взаимодействия существенно также совпадение пространственных распределений горячих электронов и поляритонов, дающих вклад в излучение. Из-за невыполнения этого условия при исследовании кинетики люминесценции поляритонов с испусканием *LO* фонона не наблюдается гашения люминесценции при приходе импульса фотовозбуждения. В отличие от резонансной поляритонной люминесценции фононное повторение связано с излучением из всего объема. К моменту прихода очередного импульса фотовозбуждения поляритоны диффундируют в глубь кристалла, где они не могут взаимодействовать с горячими электронами.

Таким образом, показано, что при приходе импульса фотовозбуждения происходит разогрев поляритонов горячими электронами, что проявляется в наблюдаемом эффекте гашения люминесценции в районе экситонного резонанса.

Список литературы

[1] Weisbuch C. // Solid St. Electr. 1978. V. 21. N 1. P. 179—183.
[2] Aoki K., Kinugasa T., Yamamoto K. // Phys. Letters. 1979. V. 72A. N 1. P. 63—66.
[3] Aoki K., Okuyama Y., Kobayvshi T., Yamamoto K. // J. of Phys. C. 1979. V. 12. N 4. P. 647—654.
[4] Жиляев Ю. В., Маркарян Г. Р., Россин В. В., Россина Т. В., Травников В. В. // ФТТ. 1986. Т. 28. № 9. С. 2688—2695.
[5] Жиляев Ю. В., Россин В. В., Россина Т. В., Травников В. В. // ЖЭТФ. 1991. Т. 99. № 4.
[6] Голубев В. Г., Жиляев Ю. В., Иванов-Омский В. И., Маркарян Г. Р., Осутин А. В., Челноков В. Е. // ФТТ. 1987. Т. 21. № 10. С. 1771—1776.
[7] Höger R., Göbel E. O., Kuhl J., Ploog K., Queisser H. J. // J. Phys. C. 1984. V. 17. P. L905—L910.
[8] Toyozawa J. // Suppl. Progr. Theor. Phys. 1959. V. 12. P. 111—140.
[9] Wiesner P., Heim U. // Phys. Rev. B. 1975. V. 11. № 8. P. 3071—3077.
[10] Гросс Е. Ф., Пермогоров С. А., Травников В. В., Селькин А. В. // ФТТ. 1972. Т. 14. № 5. С. 1547—1548.

Физико-технический институт
им. А. Ф. Иоффе АН СССР
Ленинград

Поступило в Редакцию
18 марта 1991 г.

VI

J. Aaviksoo, I. Reimand, V. V. Rossin, V. V. Travnikov,
"Kinetics of free exciton luminescence in GaAs",
Phys. Rev. B, vol. 45, no. 3, p. 1473, (1992).

Kinetics of free-exciton luminescence in GaAs

J. Aaviksoo and I. Reimand
Institute of Physics, 202400, Tartu, Estonia

V. V. Rossin and V. V. Travnikov
A. F. Ioffe Physico-Technical Institute, 194 021, Leningrad, U.S.S.R.

(Received 23 July 1991)

Exciton-polariton photoluminescence kinetics under short-pulse excitation in nominally undoped GaAs has been investigated. A delayed onset revealing the energy relaxation of electrons and polaritons has been observed. In an ultrapure sample ($N_D \sim 10^{12}$ cm^{-3}) the maximum luminescence is reached after a considerable delay of 4 ns. Energy relaxation speeds up with an increase in impurity concentration and depends on the type of conductivity. At a high repetition rate, the next excitation pulse causes fast quenching of polariton luminescence in the vicinity of exciton resonance because of heating of excitons by photoexcited hot electrons.

At low temperatures excitons constitute the final state in energy relaxation of the photoexcited crystal. In GaAs the main channel of exciton formation after excitation above the energy gap E_g is binding of thermalized electrons and holes.[1] Various processes are involved in exciton kinetics: energy relaxation of the photoexcited charge carriers, electron-hole binding, energy relaxation and trapping of free excitons, spatial diffusion, etc., and also polariton effects.[2,3] A direct way to determine the contribution of the mentioned processes is to study the time behavior of free-exciton luminescence at different luminescence energies after pulse excitation at variable photon energy. In previous papers devoted to free-exciton luminescence kinetics in GaAs most attention was paid to the luminescence decay[4] and time-resolved spectra.[2] We have focused on the luminescence onset as in Ref. 5; however, better spectral resolution and variation of the excitation energy were obtained and ultrahigh-purity samples were used.

Luminescence was excited by a synchronously pumped mode-locked Styryl-9 dye laser. Optical pulse duration was $\Delta t_p = 5$ ps, and cavity dumping rates $f = 82$ and 4.1 MHz were used. The average excitation power density $I_{av} \sim 1$ W/cm^2. Photoluminescence was measured at $T = 1.7$ K by a time-correlated photon-counting system with a time resolution of 300 ps (FWHM). The spectral linewidth of excitation (~ 0.7 meV) and spectral resolution (~ 0.1 meV) permitted tunable excitation and luminescence energies. The samples were pure epitaxial layers grown by vapor phase epitaxy in a chloride system with various residual impurity concentration and conductivity types. In the purest sample G13 (Refs. 6 and 7) shallow-donor concentration was estimated to be $\sim 10^{12}$ cm^{-3},[6] whereas reference samples with $N_D \approx 10^{14}$ cm^{-3} and $N_A \approx 10^{14}$ cm^{-3} were also measured. A characteristic of the low-temperature photoluminescence spectrum of the ultrapure sample obtained under cw excitation is a distinct exciton-polariton line, with an intensity comparable to the bound-exciton lines usually dominant in the spectrum.[7]

Time-integrated luminescence spectra and the corresponding luminescence time behavior of different samples are depicted in Fig. 1. The latter were measured at energies denoted by arrows 1,2 and correspond to the emission from lower and upper polariton branches. In all samples a slowing of the onset with decreasing polariton luminescence energy is observed. The dependence of the delay time of the pulse maximum Δt_{max} on the luminescence en-

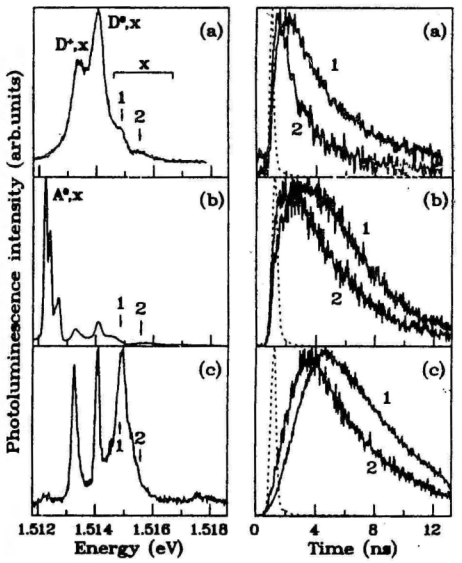

FIG. 1. Time-integrated photoluminescence spectra (on the left) and corresponding time behavior (on the right) of different GaAs samples. (a) n^0-GaAs, $N_D \sim 10^{14}$ cm^{-3}. (b) Y1, p^0-GaAs, $N_A \sim 10^{14}$ cm^{-3}. (c) Sample G13, $N_D \sim 10^{12}$ cm^{-3}. The dashed line represents the excitation pulse. Excitation energy is 1.554 eV. Traces 1 and 2 correspond to the luminescence energies denoted by arrows on the spectra.

ergy of sample G13 is shown in Fig. 2(a). This dependence reveals the effect of a polariton bottleneck due to a reduced energy relaxation rate in the vicinity of the exciton resonance.[8] Unlike the results concerning the polariton bottleneck in CdS,[9-11] the decay time here weakly depends on the luminescence energy. In ultrapure sample G13 this decay time reaches the value of 4–5 ns. It is worth noting that this value exceeds the radiative exciton lifetime in GaAs obtained by 't Hooft *et al.*[4] A weak dependence of the luminescence onset on the exciton luminescence energy in GaAs was observed by Steiner *et al.*[2] and attributed to energy-dependent diffusion of polaritons from the bulk to the surface. To determine the contribution of the polariton diffusion to the observed delayed onset of the polariton luminescence we measured the temporal evolution of the exciton luminescence accompanied with LO-phonon emission. Because of the small absorption coefficient and high group velocity, spatial distribution of polaritons should not affect the time behavior of this emission. No essential difference in the onset of the luminescence at the exciton resonance and corresponding energies of the LO-phonon replica was found in sample G13. This fact rules out the contribution of the polariton diffusion to the observed delayed onset of luminescence.

The luminescence onset essentially depends on the excitation energy, so that Δt_{max} is increased (approximately by the value 2 ns) with increasing excitation energy above the band gap for all luminescence energies [Fig. 2(b)]. It is natural to attribute this part of the delay time to the energy relaxation of electrons. At the same time we could not resolve the process of exciton formation from cold electrons and holes since the values of the delay time are practically the same for the excitation at the band edge and $n=2$ excited state of the free exciton [experimental points corresponding to two smallest values of excitation energy in Fig. 2(b)].

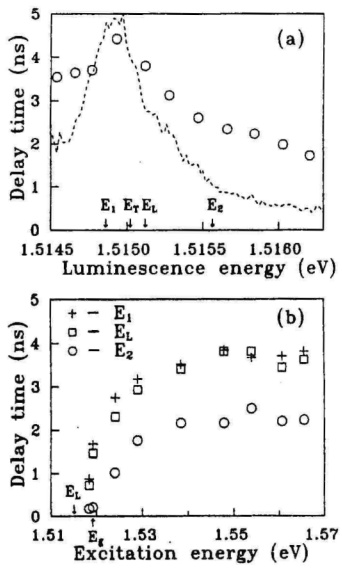

FIG. 2. The dependence of the luminescence maximum time delay on (a) the luminescence energy and (b) excitation energy for sample G13. (a) Excitation energy is 1.554 eV; the dashed line represents the polariton luminescence spectrum. (b) Luminescence energies correspond to those denoted in (a). E_L and E_T are longitudinal and transverse exciton energies, respectively.

As it is seen in Fig. 1, the onset of the polariton luminescence depends on impurity concentration. It is usually assumed[5] that the energy relaxation of electrons in GaAs with energy less than the energy of optical phonon is governed by the emission of acoustical phonons. This process, however, is rather slow because of the small value of the electron effective mass (according to calculations carried out by Ulbrich[12] the energy relaxation rate via emission of acoustical phonons for the electron temperature $T_e=10$ K is determined to be $S\sim 0.1$ meV/ns). The observed impurity concentration dependence in our experiments clearly points to the role of extrinsic processes in the electron energy relaxation. The noticeable decrease in Δt_{max} and the appearance of a fast initial rise with increasing impurity concentration is caused by an enhancement of the electron energy relaxation rate due to inelastic impurity scattering. Furthermore, in the *n*-type sample [Fig. 1(a)] the luminescence onset is considerably faster than in *p*-type sample [Fig. 1(b)], with a comparable total impurity concentration. This appears reasonable, since inelastic scattering by neutral donors is more probable because of the smaller binding energy.

All the experiments described above were performed at a low repetition rate of excitation pulses $f=4.1$ MHz. At $f=82$ MHz the polariton luminescence signal of the ultrapure GaAs sample does not decay completely during the time interval between two successive excitation pulses $\Delta t=12.2$ ns. In this case we observed interaction of newly created excitations with those left from the preceding pulse. Figure 3 presents the luminescence kinetics of sample G13 at different energies, E_1, E_L, and E_2 (see also Fig. 2). It is seen in Fig. 3(b) that at luminescence energies in the vicinity of the exciton resonance the next excitation pulse causes a fast luminescence quenching. This effect disappears when the excitation energy approaches the band gap [Fig. 3(a)]. Luminescence quenching is also observed in the bound-exciton luminescence kinetics, especially in the case of (D^0,x) line (exciton bound to neutral donor).

The magnitude of the dip in the luminescence kinetics is the greatest in the vicinity of the exciton resonance. At the same time at higher luminescence energies the expected rise of the luminescence intensity after the excitation pulse is observed. We propose the following explanation of the observed phenomenon. Photoexcitation with photon energy well above the band gap leads to creation of hot electrons. Exciton-electron interaction causes scattering of the polaritons accumulated in the states with small energies to the states with higher energies. Due to this heating effect the thermalized population of excitons around E_T is reduced, which is reflected in the luminescence kinetics. The greatest effect should be expected at

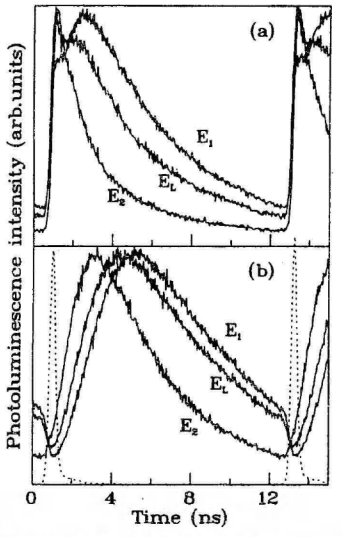

FIG. 3. Time behavior of the polariton luminescence of sample G13 at a high repetition rate. Excitation energy is (a) 1.520 eV, equal to the energy gap and (b) 1.554 eV. The dashed lines represent the excitation pulses. Traces are measured at the luminescence energies denoted in Fig. 2(a).

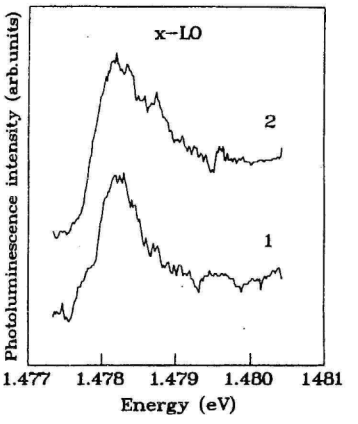

FIG. 4. Time-integrated LO-phonon replica of exciton emission of sample G13. Curves 1 and 2 correspond to excitation energies 1.520 and 1.554 eV, respectively.

the energy of the maximum of the polariton distribution function in the vicinity of the exciton resonance. Polariton heating also causes a decrease in bound-exciton concentration, because the exciton trapping probability decreases with increasing polariton energy.[13] In the case of excitation close to the band edge cold electrons are created and polaritons are not heated.

The proposed interpretation requires a dependence on the excitation density. Such a dependence really exists. The magnitude of the dip in the luminescence kinetics is a function of excitation density with a maximum at the average density ~ 2.5 W/cm^2. A decrease in the magnitude of the dip at lower excitation density is natural due to a reduced rate of exciton-electron scattering. At higher excitation densities the effect is not observed because of an increase in the electron energy relaxation rate (due to the same processes of exciton-electron interaction) and a concurrent fast increase in exciton population.

Exciton-electron interaction was already considered to influence the polariton luminescence line shape under cw excitation.[14,15] The importance of exciton-electron scattering to exciton dephasing at comparable, moderate excitation level was shown by Schultheis *et al.*[16] Exciton-electron interaction also was revealed in our study of the line shape of the time-integrated phonon replica of the polariton luminescence at different excitation energies. As it is shown in Fig. 4 the effective polariton temperature determined from the high-energy tail of the phonon replica increases with an increase in excitation energy. This result directly indicates the close relation between electron and exciton temperatures.

It is important to note that efficient exciton-electron interaction implies coincidence of excitons and electrons in time and space. Under pulse excitation concentration maxima of excitons and hot electrons are separated in time. This is the reason why the dip, usually observed at longitudinal exciton energy in the polariton luminescence spectrum under cw excitation,[7] is absent in the ultrapure sample even at rather high excitation densities. Due to spatial separation of excitons and electrons luminescence quenching by the next excitation pulse is not observed in the kinetics of LO-phonon replica of exciton emission. Unlike the resonance polariton luminescence its LO-phonon replica originates from the bulk. During the time between two succeeding excitation pulses polariton spatial distribution shifts inside the crystal due to diffusion, while hot electrons are created at the surface.

In conclusion, we have shown that the maximum of polariton luminescence from high-purity GaAs is reached after a considerable delay (up to 4 ns) from the excitation pulse. This delay is caused by the energy relaxation of the photoexcited electrons and slow thermalization of excitons around a polariton bottleneck. The energy relaxation rate in samples with higher impurity concentration is increased due to inelastic impurity scattering. The electron-exciton interaction provides another channel of electron cooling and is evidenced by a quenching of the polariton luminescence by the next excitation pulse.

[1]C. Weisbuch, Solid State Electron. **21**, 179 (1978).
[2]T. Steiner, M. L. W. Thewalt, E. S. Koteles, and J. P. Salerno, Phys. Rev. B **34**, 1006 (1986).
[3]W. J. Rappel, L. F. Feiner, and M. F. H. Schuurmans, Phys. Rev. B **38**, 7874 (1988).
[4]G. W. 't Hooft, W. A. J. A. van der Poel, L. W. Molencamp, and C. T. Foxon, Phys. Rev. B **35**, 8281 (1987).
[5]R. Höger, E. O. Göbel, J. Kuhl, K. Ploog, and H. J. Queisser, J. Phys. C **17**, L905 (1984).
[6]V. G. Golubev, Yu. V. Zhilyaev, V. I. Ivanov-Omskii, G. R. Markaryan, A. V. Osutin, and V. E. Chelnokov, Fiz. Tekh. Poluprovodn. **21**, 1771 (1987) [Sov. Phys. Semicond. **21**, 1074 (1987)].
[7]Yu. V. Zhilyaev, G. R. Markaryan, V. V. Rossin, T. V. Rossina, and V. V. Travnikov, Fiz. Tverd. Tela (Leningrad) **28**, 2688 (1986) [Sov. Phys. Solid State **28**, 1506 (1986)].
[8]Y. Toyozawa, Progr. Theor. Phys. Suppl. **12**, 111 (1959).
[9]P. Wiesner and U. Heim, Phys. Rev. B **11**, 3071 (1975).
[10]F. Askary and P. Y. Yu, Phys. Rev. B **28**, 6165 (1983).
[11]Ya. Yu. Aaviksoo, Ya. E. Lippmaa, A. M. Freiberg, and S. F. Savikhin, Fiz. Tverd. Tela (Leningrad) **31**, 203 (1989) [Sov. Phys. Solid State **31**, 462 (1989)].
[12]R. Ulbrich, Phys. Rev. B **8**, 5719 (1973).
[13]E. F. Gross, S. A. Permogorov, V. V. Travnikov, and A. V. Sel'kin, Fiz. Tverd. Tela (Leningrad) **14**, 1547 (1972) [Sov. Phys. Solid State **14**, 1331 (1972)].
[14]K. Aoki, T. Kinugasa, and K. Yamamoto, Phys. Lett. **72A**, 63 (1979).
[15]K. Aoki, Y. Okuyama, T. Kobayashi, and K. Yamamoto, J. Phys. C **12**, 647 (1979).
[16]L. Schultheis, J. Kuhl, A. Honold, and C. W. Tu, Phys. Rev. Lett. **57**, 1635 (1986).

VII

J. Aaviksoo, I. Reimand, V. Rossin, V. Travnikov,
"Kinetics of free exciton formation and relaxation in GaAs",
J. Lumin., vol. 53, p. 423, (1992).

Journal of Luminescence 53 (1992) 423–426
North-Holland

JOURNAL OF
LUMINESCENCE

Kinetics of exciton formation and relaxation in GaAs

J. Aaviksoo [a], I. Reimand [a], V.V. Rossin [b] and V.V. Travnikov [b]

[a] *Institute of Physics, EE 2400 Tartu, Estonia*
[b] *A.F. Ioffe Physico-Technical Institute, 194021, Leningrad, Russia*

Exciton–polariton photoluminescence kinetics under short-pulse excitation in nominally undoped GaAs has been investigated. A delayed onset revealing energy relaxation of electrons and polaritons has been observed. Energy relaxation speeds up with an increase in impurity concentration and depends on the type of conductivity. At high repetition rate the next excitation pulse causes a fast quenching of polariton luminescence in the vicinity of exciton resonance due to heating of excitons by photoexcited hot electrons.

At low temperatures excitons constitute the final state in energy relaxation of the photoexcited crystal. In GaAs the main channel of exciton formation after excitation above the energy gap E_g is binding of thermalised electrons and holes [1]. Various processes are involved in exciton kinetics: energy relaxation of the photoexcited charge carriers, electron–hole binding, energy relaxation and trapping of free excitons, spatial diffusion, etc. We also have to take into account polariton effects [2]. A direct way to determine the contribution of the mentioned processes is to study the time behaviour of free exciton luminescence at different luminescence energies after pulse excitation at variable photon energy. We have focussed on the luminescence onset as in ref. [3], however, a better spectral resolution and variation of excitation energy were applied and ultrahigh purity samples were used.

Luminescence was excited by a synchronously pumped modelocked Styryl 9 dye-laser. Optical pulse duration was $\Delta t_p = 5$ ps, cavity dumping rates $f = 82$ MHz and 4.1 MHz were used. The average excitation power density $I_{av} \approx 1$ W/cm^2. Photoluminescence was measured at $T = 1.7$ K by a time-correlated photon-counting system with a time resolution of 300 ps (FWHM). Spectral line width of excitation (~ 0.7 meV) and spectral resolution (~ 0.1 meV) allowed to tune excitation and luminescence energies. The samples were pure epitaxial layers grown by vapor phase epitaxy in chloride system with various residual impurity concentration and conductivity type. In the purest sample G13 shallow donor concentration was estimated to be $N_D \approx 10^{12}$ cm^{-3}, whereas reference samples with $N_D \approx 10^{14}$ cm^{-3} and $N_A \approx 10^{14}$ cm^{-3} were also measured. Characteristic to the low-temperature photoluminescence spectrum of the ultra pure sample obtained under cw-excitation is a distinct exciton–polariton line, with an intensity comparable to bound exciton lines usually dominating in the spectrum [4].

Time-integrated luminescence spectra and corresponding luminescence time behaviour of different samples are depicted in fig. 1. The latter were measured at energies denoted by arrows 1, 2 and correspond to the emission from the lower and upper polariton branches. In all samples a slowing of the onset with decreasing polariton luminescence energy is observed. The dependence of the delay time of the pulse maximum Δt_{max} on the luminescence energy of the sample G13 is shown in fig. 2(a). This dependence reveals the effect of polariton bottleneck due to reduced energy relaxation rate in the vicinity of the exciton resonance [5]. Unlike the results con-

Correspondence to: Dr. J. Aaviksoo, Institute of Physics, Riia 142, EE 2400 Tartu, Estonia.

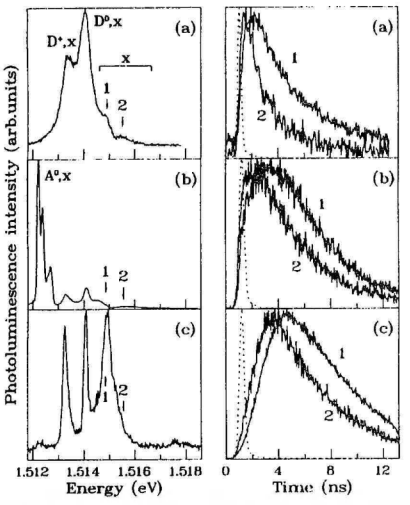

Fig. 1. Time-integrated photoluminescence spectra (on the left) and corresponding time behaviour (on the right) of different GaAs samples. (a) K88, $N_D \approx 10^{14}$ cm^{-3}, (b) Y1, p-GaAs, $N_A \approx 10^{14}$ cm^{-3}. (c) G13, $N_D \approx 10^{12}$ cm^{-3}. The dashed line represents the excitation pulse. Excitation energy is 1.554 eV. Traces 1 and 2 correspond to the luminescence energies denoted by arrows on the spectra.

cerning polariton bottleneck in CdS [6–8], the decay time weakly depends on the luminescence energy. A weak dependence of the luminescence onset on the exciton luminescence energy in GaAs was observed by Steiner et al. [2] and attributed to energy-dependent diffusion of polaritons from the bulk to the surface. To determine the contribution of the polariton diffusion to the observed delayed onset of the polariton luminescence we measured temporal evolution of the exciton luminescence accompanied with LO-phonon emission. Because of the small absorption coefficient and high group velocity, spatial distribution of polaritons should not affect the time behaviour of this emission. No essential difference in the onset of the luminescence at the exciton resonance and corresponding energies of the LO-phonon replica was found in the sample G13. This fact rules out the contribution of the polariton diffusion to the observed delayed onset of luminescence.

The luminescence onset essentially depends on the excitation energy, so that Δt_{max} is increased (approximately by the value of 2 ns) with increasing excitation energy above the band gap for all luminescence energies (fig. 2(b)). It is natural to attribute this part of the delay time to the energy relaxation of electrons. At the same time we could not resolve the process of exciton formation from cold electrons and holes since the values of the delay time are practically the same for the excitation at the band edge and $n = 2$ excited state of the free exciton (experimental points corresponding to two smallest values of excitation energy in fig. 2(b)).

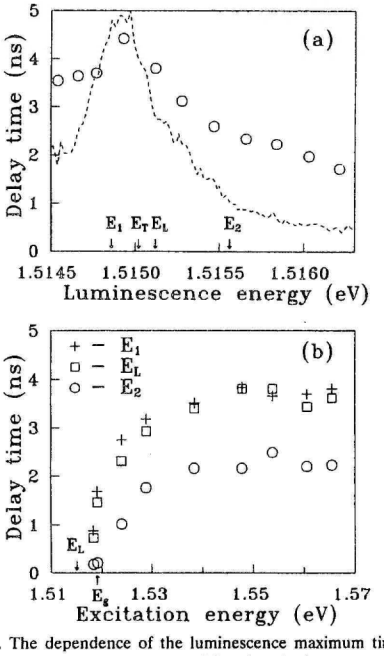

Fig. 2. The dependence of the luminescence maximum time delay on the luminescence energy (a) and excitation energy (b) for the sample G13. (a) excitation energy is 1.554 eV, dashed line represents the polariton luminescence spectrum. (b) luminescence energies correspond to those denoted in (a). E_L and E_T are longitudinal and transverse exciton energies, respectively.

As it is seen in fig. 1 the onset of the polariton luminescence depends on impurity concentration. It is usually assumed [3] that the energy relaxation of electrons in GaAs with energy less than the energy of optical phonon is governed by emission of acoustical phonons. This process, however, is rather slow because of the small value of electron effective mass (according to calculations carried out by Ulbrich [9] the energy relaxation rate via emission of acoustical phonons for electron temperature $T_e = 10$ K is determined to be $S \approx 0.1$ meV/ns). The observed impurity concentration dependence in our experiments clearly points to the role of extrinsic processes in the electron energy relaxation. Essential decrease in Δt_{max} and the appearance of a fast initial rise with increasing impurity concentration is caused by an enhancement of the electron energy relaxation rate due to inelastic impurity scattering. Further, in n-type sample (fig. 1(a)) the luminescence onset is considerably faster than in p-type sample (fig. 1(b)), with comparable total impurity concentration. It appears reasonable since inelastic scattering by neutral donors is more probable because of smaller binding energy.

All above described experiments were performed at low repetition rate of excitation pulses $f = 4.1$ MHz. At $f = 82$ MHz polariton luminescence signal of ultra pure GaAs sample does not decay completely during the time interval between two successive excitation pulses $\Delta t = 12.2$ ns. In this case we observed interaction of newly created excitations with those left from the preceding pulse. Figure 3 presents the luminescence kinetics of sample G13 at different energies E_1, E_L, E_2 (see also fig. 2). It is seen in fig. 3(b) that at luminescence energies in the vicinity of exciton resonance the next excitation pulse causes a fast luminescence quenching. This effect disappears when the excitation energy approaches the band gap (fig. 3(a)). The magnitude of the dip in the luminescence kinetics is the greatest in the vicinity of exciton resonance. At the same time at higher luminescence energies the expected rise of luminescence intensity after excitation pulse is observed.

We propose the following explanation of the observed phenomenon. Photoexcitation with photon energy well above the band gap leads to creation of hot electrons. Exciton–electron interaction causes scattering of the polaritons accumulated in the states with small energies to the states with higher energies. Due to this heating effect the thermalised population of excitons around E_T is reduced, which is reflected in the luminescence kinetics. The greatest effect should be expected at the energy of the maximum of the polariton distribution function in the vicinity of exciton resonance.

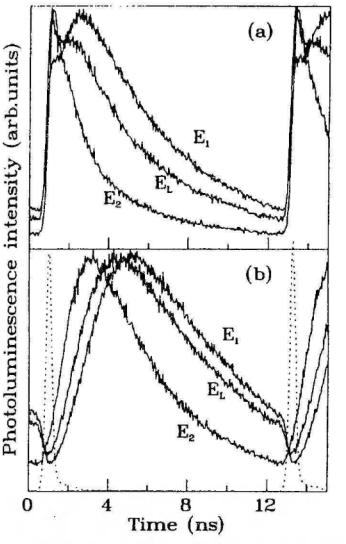

Fig. 3. Time behaviour of the polariton luminescence of the sample G13 at high repetition rate. Excitation energy is 1.520 eV, equal to the energy gap (a) and 1.554 eV (b). The dashed lines represent the excitation pulses. Traces are measured at luminescence energies denoted in fig. 2(a).

In conclusion, we have shown that the maximum of polariton luminescence from high purity GaAs is reached after a considerable delay (up to 4 ns) from the excitation pulse. This delay is caused by energy relaxation of the photoexcited electrons and slow thermalisation of excitons around polariton bottleneck. Energy relaxation rate in samples with higher impurity concentration is increased due to inelastic impurity scatter-

ing. Electron–exciton interaction causes a quenching of the polariton luminescence by the next excitation pulse.

References

[1] C. Weisbuch, Solid State Electron. 21 (1978) 179.
[2] T. Steiner, M.L.W. Thewalt, E.S. Koteles and J.P. Salerno, Phys. Rev. B 34 (1986) 1006.
[3] R. Höger, E.O. Göbel, J. Kuhl, K. Ploog and H.J. Queisser, J. Phys. C 17 (1984) L905.
[4] Yu.V. Zhilyaev, G.R. Markaryan, V.V. Rossin, T.V. Rossina and V.V. Travnikov, Sov. Phys. Solid State 28 (1986) 1506.
[5] Y. Toyozawa, Progr. Theor. Phys. Suppl. 12 (1959) 111.
[6] P. Wiesner and U. Heim, Phys. Rev. B 11 (1975) 3071.
[7] F. Askary and P.Y. Yu, Phys. Rev. B 28 (1983) 6165.
[8] Ya.Yu. Aaviksoo, Ya.E. Lippmaa, A.M. Freiberg and S.F. Savikhin, Sov. Phys. Solid State 31 (1989) 462.
[9] R. Ulbrich, Phys. Rev. B 8 (1973) 5719.

VIII

D. Varding, I. Reimand, G. Zimmerer,
"Time-resolved luminescence of exciton-polaritons in solid xenon",
Physica Status Solidi B, vol. 185, no. 1, p.301, (1994).

phys. stat. sol. (b) **185**, 301 (1994)

Subject classification: 71.35 and 78.55, 71.36; S5.2

II. Institut für Experimentalphysik der Universität Hamburg[1]) *(a) and Institute of Experimental Physics and Technology, Tartu University*[2]) *(b)*

Time-Resolved Luminescence of Exciton-Polaritons in Solid Xenon

By

D. VARDING (a), I. REIMAND (b), and G. ZIMMERER (a)

The decay of excitons in solid Xe is investigated with time and spectrally resolved luminescence as a function of temperature and photon energy of excitation. The luminescence of free excitons exceeds the self-trapped exciton luminescence by a factor of 50 (peak-to-peak). The FE-decay curves yield a non-exponential behaviour. They can be reproduced with Monte-Carlo simulations of the exciton-polariton transport to the sample/vacuum interface, taking into account phonon scattering and trapping. A new upper limit for the intrinsic self-trapping rate in the lower $10^7\ s^{-1}$ range and a surprisingly large experimental value for the scattering length (≈ 100 nm at $T = 5$ K) are deduced. It is indispensable to discuss the decay of excitons in solid Xe in terms of the exciton-polariton model.

1. Introduction

The onset of optical absorption of solid xenon in the vacuum ultraviolet spectral range is governed by excitations consisting of a hole in the p-type valence band (total angular momentum $j = 3/2$) and an electron in the s-type conduction band [1]. Whereas the energetic positions of the higher members of the $\Gamma(3/2)$ exciton series are reasonably well described by the Wannier formula, $E_n = E_g - B/n^2$ (band gap energy $E_g = 9.33$ eV, binding energy $B = 1.02$ eV; n is the main quantum number), the energy of the strongest line, $n = 1$, deviates considerably from the Wannier formula. This is a consequence of the small exciton radius [1]. The $n = 1$ exciton has a large oscillator strength ($F = 0.16$ [2]) which causes a large longitudinal–transverse splitting of the order of 100 [2] to 170 meV [3]. Then it is indispensable to take into account explicitly the exciton-polariton nature of the excitation. This has been amply demonstrated by, e.g. Kink and Selg [3], who calculated reflectivity spectra and the spectral shape of excitonic luminescence within the framework of exciton-polariton theory, and by Fugol et al. [2] who treated the transmission of solid xenon and spatial dispersion effects.

The radiative decay of the $n = 1$ exciton of solid xenon displays some peculiarities. It consists of a rather narrow line which stems from exciton-polaritons in the bottleneck region of the dispersion curve (so-called free-exciton line (FE line) at 8.359 eV), and broad, strongly Stokes-shifted bands originating from trapped excitons indicating a strong coupling with the lattice [1]. The bands are ascribed to the radiative decay of intrinsically trapped excitons or to excitons trapped on defects in a molecular-type configuration (self-trapped exciton, STE) [4 to 6].

[1]) Luruper Chaussee 149, D-22761 Hamburg, Federal Republic of Germany.
[2]) Tähe 4, EE-2400 Tartu, Estonia.

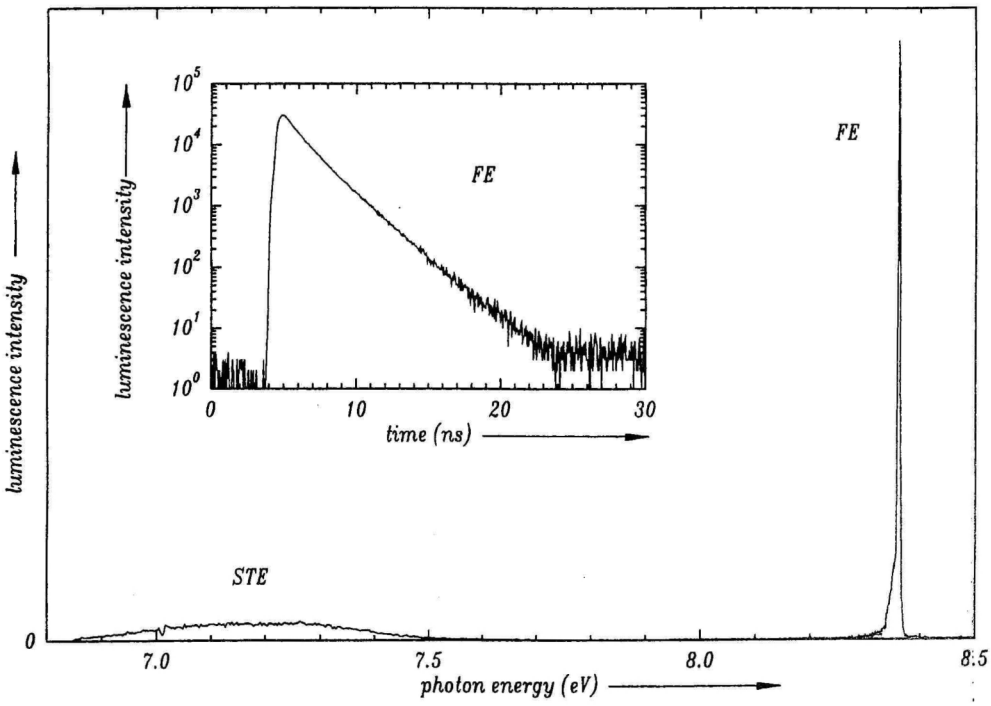

Fig. 1. Luminescence of solid Xe at $T = 4.7$ K, excited with synchrotron radiation (photon energy 8.86 eV). The inset shows a time-resolved spectrum of the FE line at 8.359 eV. The spectral resolution intervals are given in the text

The strength of the FE line in the luminescence spectra sensitively depends on sample quality [6]. In earlier investigations, the FE line was only a faint contribution to luminescence [1]. However, contradictory to all the results before, Varding et al. [6] recently proved that the FE line can exceed the STE band by a factor of 50, the ratio of the wavelength-integrated luminescence intensities, I_{FE}/I_{STE} being of the order of unity. A typical luminescence spectrum of solid xenon of [6] is reproduced in Fig. 1. The most dominant feature is the narrow FE line at 8.359 eV and the STE bands around 7.2 eV are only weakly indicated.

The strength of the FE line enabled the first precise time-resolved measurements. As an example, in the inset of Fig. 1, the decay curve of the FE line is included. Note, the huge dynamical range of about five orders of magnitude, exceeding the dynamical range in earlier measurements [7] by about a factor of 100. The most interesting observation is the non-exponential behaviour of the decay curve. As will be shown below, the details of the decay curves depend on the photon energy of the primary excitation as well as on the temperature of the sample.

The most important information hidden in the decay curves is the trapping probability of excitons due to exciton–phonon interaction. In a crude approximation, Varding et al. [6] tried to deduce this information with a model which did not take into account the exciton-polariton nature of the excitation. The decay of excitons created somewhere in the crystal was described by a trapping probability and a radiative decay rate. The non-exponential nature of the decay curves was ascribed to a superposition of the dynamical

behaviour of hot and thermalized excitons. In the present paper, a more refined model will be proposed. It explicitly takes into account the exciton-polariton nature of the excitation. In other words, the decay of the $n = 1$ exciton consists of three steps, (i) population of the bottleneck region of the exciton-polariton dispersion curve, (ii) transport of the exciton-polariton to the surface, and (iii) transmission from the crystal to the vacuum.

In Section 2, the essential experimental details will be sketched. Experimental results which were not included in [6], will be presented in Section 3 which also contains the description of the theoretical model and a comparison between experiment and theory. Finally, in Section 4, the parameters deduced will be analysed.

2. Experiment

The experiments were performed at the SUPERLUMI station [8] of the Hamburger Synchrotronstrahlungslabor HASYLAB at DESY. The main parameters of the experiment are (i) selective photon excitation ($8\,\text{eV} \leqq h\nu \leqq 20\,\text{eV}$) with $\lambda/\Delta\lambda \leqq 10^4$, (ii) spectral analysis of luminescence in a wide spectral range ($1\,\text{eV} \leqq h\nu \leqq 20\,\text{eV}$) with $\lambda/\Delta\lambda \leqq 10^4$, and (iii) time resolution from the sub-ns to the ms range. All results to be presented were obtained with a resolution interval $\Delta\lambda = 0.25$ nm in excitation. Luminescence analysis was performed with a high-resolution 1 m VUV monochromator. In combination with a position-sensitive detector, the resolution interval $\Delta\lambda = 0.8$ nm was used. For the time-resolved measurements (decay curves), a medium-resolution high-flux VUV monochromator was used. The resolution interval then was $\Delta\lambda = 1.5$ nm. The basis of time resolution is the pulsed nature of synchrotron radiation. At the storage ring DORIS in Hamburg, the light pulses have a FWHM of 130 ps. The convolution of the temporal behaviour of the excitation pulse, the response of the detector, and of the electronics used was 0.4 ns.

The crucial part of the experiment was sample preparation. With the set-up described in [9], samples were grown under nearly thermal equilibrium conditions at $T = 118$ K. The growing rate was $\approx 10^3$ nm/min, the preparation time was up to 24 h. In this way, bulk, clear samples were obtained with a thickness up to a few mm. The background pressure in the sample chamber was in the 10^{-8} Pa range.

3. Experimental Results and Monte-Carlo Simulations

3.1 Experimental results

Whereas in [6] results have been presented only for $T = 4.7$ K, one of the additional aspects in the present paper is the temperature dependence of the FE luminescence of solid xenon. In Fig. 2, at set of FE-luminescence spectra measured at different temperatures is given. The photon energy of excitation was 8.86 eV which is well below the energy of $n = 2$ excitons (9.07 eV [1]). The upper limit of T (60 K) arises from the vapour pressure of the sample (sublimation temperature ≈ 65 K). The spectra were measured for increasing and decreasing temperature because annealing can lead to irreversible changes if the spectra stem from defect-rich samples. The data of Fig. 2 amply demonstrate that the samples obtained with the preparation method described exhibit reproducible results. The peak positions (accuracy ± 5 meV) are in agreement with [2]. The intensity scale (given in arbitrary units) is the same for all curves. Up to ≈ 50 K, the wavelength-integrated intensities are nearly independent of temperature. Only above 50 K, a decrease is found. This behaviour

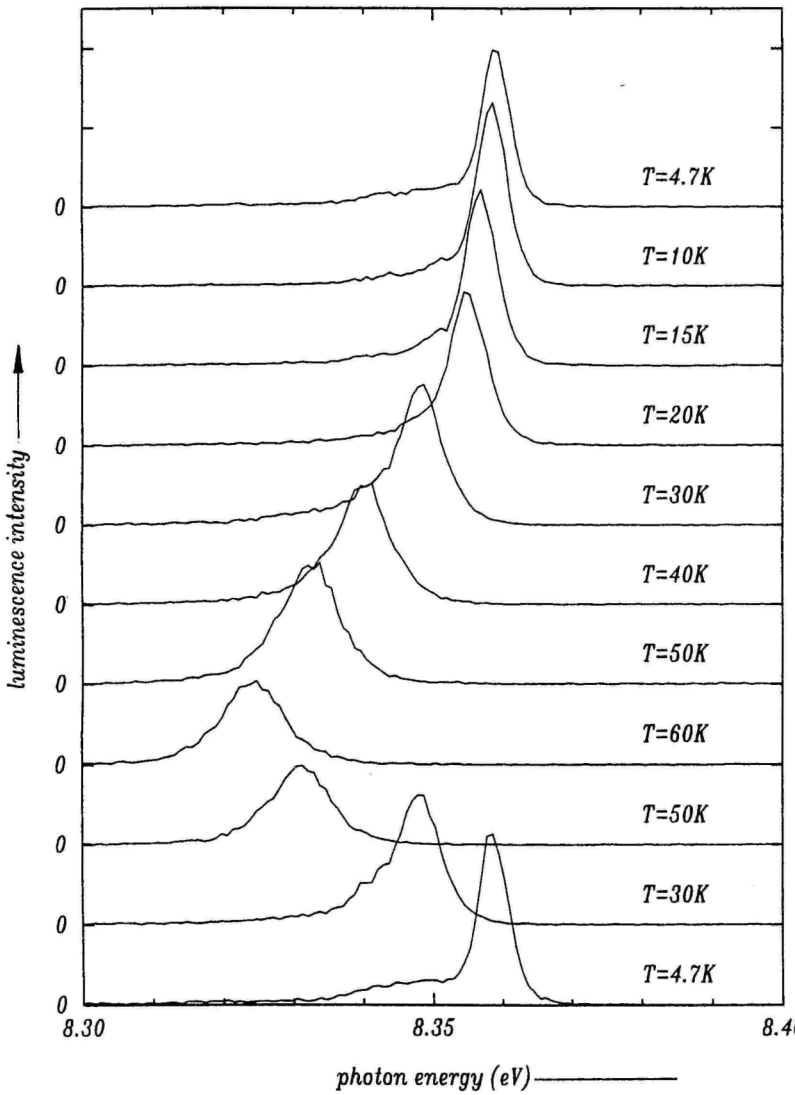

Fig. 2. FE luminescence of solid Xe for different temperatures. Photon energy of excitation 8.86 eV. Spectra were taken for increasing and decreasing temperature to demonstrate that annealing effects can be neglected

is shown in Fig. 3. It is in agreement with [3]. Fig. 3 also includes the wavelength-integrated intensities of all molecular-type STE contributions. At low temperatures, there exist two bands peaking at 7.05 and 7.25 eV, and around 50 K, an additional band at 7.6 eV appears [4 to 6]. It is not the purpose of the present paper to discuss the various aspects of the STE bands in solid xenon. In the context of the present paper it is necessary to show that the increase of STE luminescence above 50 K cannot be explained by a decrease of FE luminescence alone, but the total luminescence intensity increases. This is a clear proof

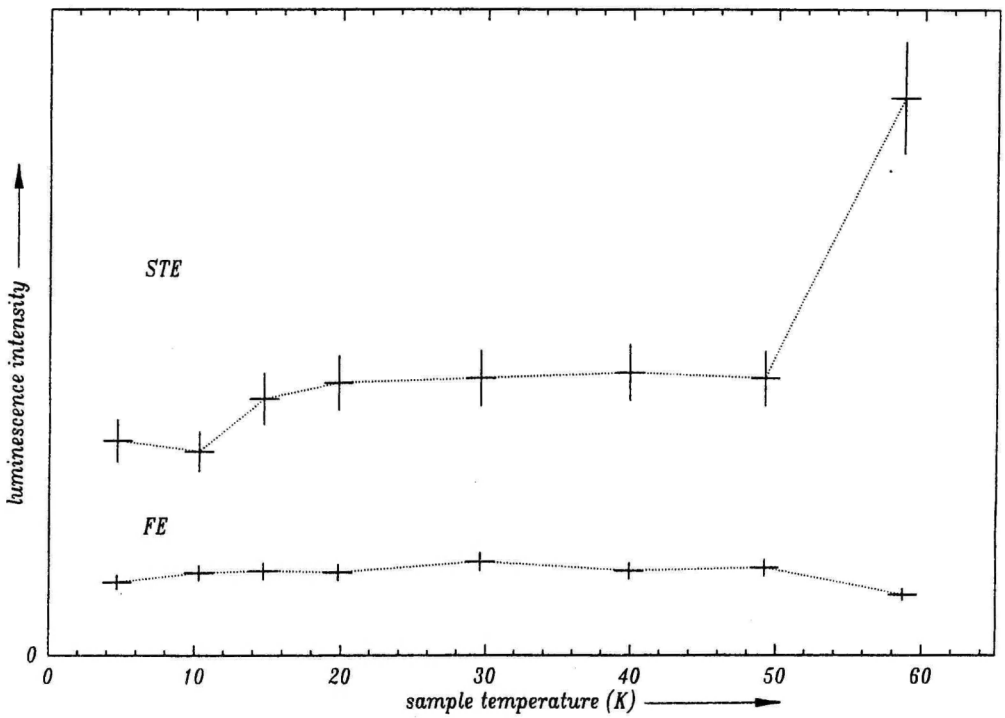

Fig. 3. Wavelength-integrated luminescence intensities of the FE line and of the STE bands of solid Xe, including the so-called "7.6 eV band" which is responsible for the strong increase above $T = 50$ K

that the quantum efficiency at low temperatures is well below unity, indicating non-radiative decay of the FE in competition with formation of STEs. The non-radiative processes seem to be correlated with thermoluminescence [10].

In Fig. 4, decay curves of the FE luminescence are presented. The photon energy of excitation was fixed to $h\nu = 8.86$ eV. The temperature varied between 4.7 and 60 K. Contrary to what we expect, the decay is slowed down with increasing temperature up to ≈ 50 K. Only above this temperature, the decay speeds up. This behaviour is in disagreement with the early results of [7]. Note, however, the results of [7] were obtained with samples condensed onto the substrate far away from thermal equilibrium conditions. The preliminary results of Kloiber [11] on samples grown under nearly thermal equilibrium conditions, however, at lower temperature than in the present work, yielded qualitatively the same result. The unexpected result has been carefully checked with different samples.

In Fig. 5, FE-decay curves are presented for fixed temperature (4.7 K). Here, the photon energy of excitation is varied between 8.86 and 10.33 eV. Below the band-gap energy, $E_g = 9.33$ eV, excitons of the $\Gamma(3/2)$ series are created. Above 9.33 eV, the situation is not so clear because the continuum (free electron–hole pairs) of the $\Gamma(3/2)$ series overlaps with the $\Gamma(1/2)$ exciton series. Starting from 8.86 eV, with increasing photon energy of excitation, the non-exponential decay behaviour gets more and more pronounced. Above 9.3 eV, the overall decay is slowed down, and with further increasing photon energy of excitation, a cascade-like temporal behaviour develops additionally to a spike-type luminescence signal which displays the apparatus function. These results clearly show that samples prepared

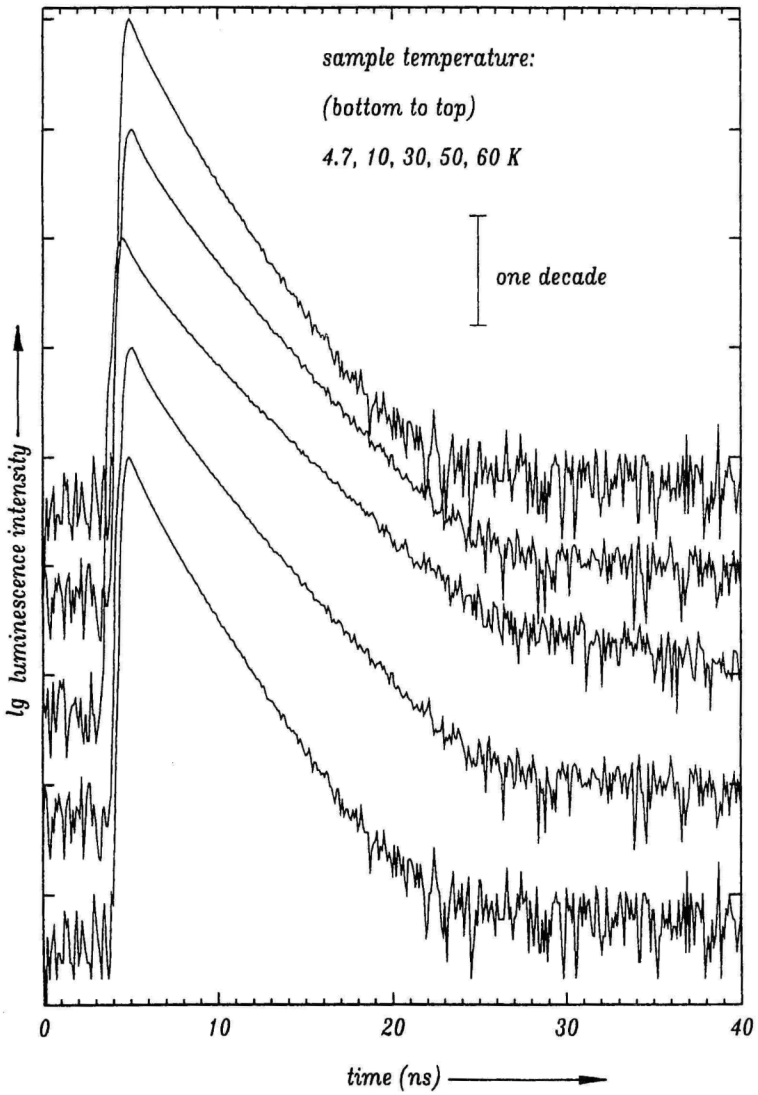

Fig. 4. Time-resolved spectra (decay curves) of the FE line of solid Xe, measured for different temperatures. Photon energy of excitation 8.86 eV. The temperatures are given in the figure

with the method described allow for a time-resolved investigation of the recombination of free electrons and holes. They will not be discussed in this paper because the evaluation is under way now.

3.2 Theoretical model

As already pointed out in the introduction, the temporal behaviour of the FE luminescence is described in a three-step model. The model is sketched in Fig. 6. In the first step (1 in Fig. 6a) it is assumed that the exciton-polaritons reach thermal quasi-equilibrium in the

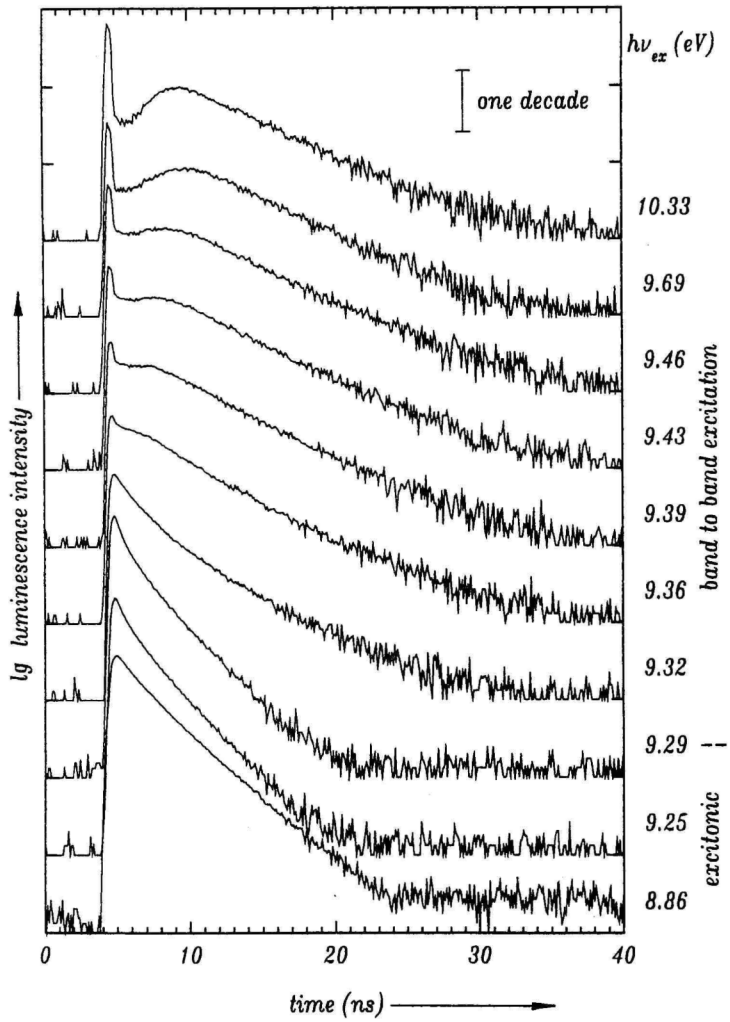

Fig. 5. Time-resolved spectra (decay curves) of the FE luminescence of solid Xe, measured at different photon energies of excitation. The values are given at each curve. $T = 4.7$ K

bottleneck of the dispersion curve. This assumption is justified except within a small part of the time interval under investigation, namely $\approx$ the first 100 ps out of ≈ 50 ns. The second step is the transport of the bottleneck exciton-polaritons (2 in Fig. 6b). The transport character of the exciton-polariton decay has already been pointed out by Toyozawa [12] and was experimentally verified in, e.g., [13]. The third step ("radiative decay") includes two possibilities, (i) inelastic phonon scattering from the bottleneck to the photon-like part of the dispersion curve (3 in Fig. 6a), and (ii) transmission of bottleneck exciton-polaritons at the sample/vacuum interface into the vacuum (3′ in Fig. 6b). The phonon-scattering process causes phonon sidebands of FE luminescence and can be pronounced in systems with optical phonons like alkali halides [14] or in molecular crystals with their intramolecular modes [13]. In solid xenon, no optical phonons exist. Inelastic scattering from

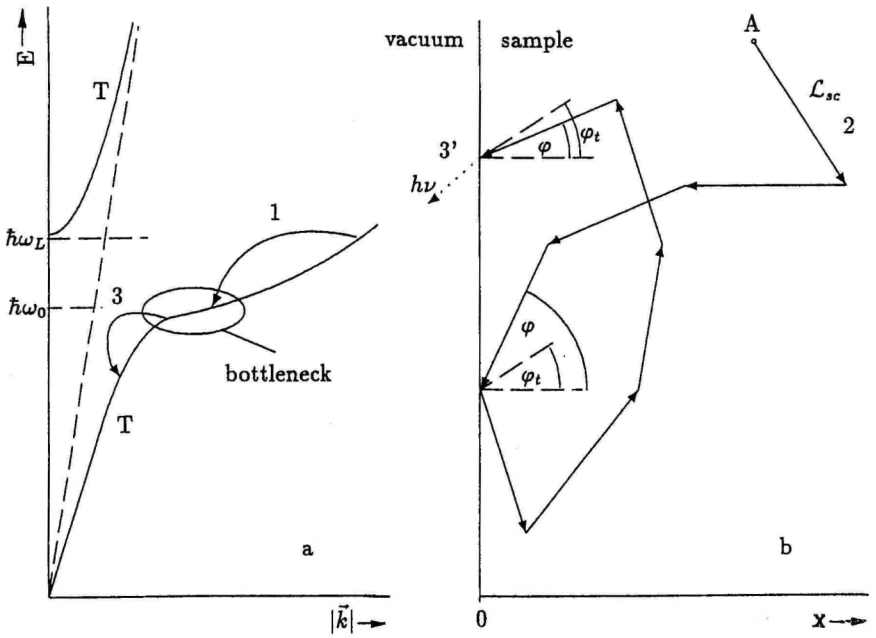

Fig. 6. a) Schematic dispersion curves and model of the population and the radiative decay of exciton-polaritons of solid Xe inside the solid; b) schematic model for the transport of exciton-polaritons to the sample/vacuum interface and transmission into the vacuum. For details see text

the bottleneck to the photon-like branch of the dispersion curve requires multiphonon scattering on acoustic phonons because the combination of small changes in the wave vector but a sufficient change in energy is not possible in a single scattering event. Indeed, the FE-luminescence spectra presented in this paper yield nearly no sideband emission. Consequently, this type of decay can be neglected. The third step then is due to the transmission of bottleneck exciton-polaritons into vacuum (Fig. 6b). This step is complicated by the fact that the reflectivity at the interface has to be taken into account as well as total reflection of exciton-polaritons which reach the surface at an angle of incidence, φ, which is larger than the angle of total reflection, φ_t. It is not straightforward how to proceed because of the problem of the additional boundary conditions for exciton-polaritons.

In the calculations, the transport was simulated with Monte Carlo methods. At time zero, a bottleneck exciton-polariton was created at a certain depth, x, below the surface (A in Fig. 6b). The x-axis is perpendicular to the sample/vacuum interface. Then, the particle starts moving with group velocity, v_g, into an arbitrary direction. As a rough estimate of the group velocity, we took an average value, $v_g = (3kT/m_{ex})^{1/2}$ with $m_{ex} = m_e^* + m_h^*$ (sum of the effective masses of the electron and hole). After a scattering length, $\mathcal{L}_{sc}$, the direction was changed arbitrarily. Trapping and non-radiative loss processes like defect formation were taken into account in the following way. The probability for an exciton-polariton to survive its motion along a scattering length was taken as $\exp(-\Gamma\mathcal{L}_{sc}/v_g)$. Here, $\Gamma = \Gamma_{ST} + \Gamma_{nr}$ is the sum of the self-trapping rate, Γ_{ST}, and a yet not specified non-radiative decay rate, Γ_{nr}. Concerning reflection at the interface for $\varphi < \varphi_t$, we took $R = 0.3$, measured by Kink et al. [3] at the photon energy of the FE luminescence for normal incidence. The further motion of reflected exciton-polaritons, including those which were totally reflected,

was included in the simulations. The whole calculation has been repeated about 10^6 to 10^7 times for a semi-infinite sample (note, the actual thickness was in the mm range). The damping of the exciting light along the x-axis according to Beer's law was taken into account as a weight function for the individual events. Values of the absorption coefficient, α, were taken from [15, 16]. All exciton-polaritons decaying in this way at the crystal surface were registrated including their time-correlation to time zero (excitation process). The time-resolution interval in the calculations was 40 ps. In this way, decay curves of FE luminescence were constructed.

3.3 Comparison between experimental results and simulations

Before presenting the results of the model calculations, the various parameters entering the calculation must be discussed. It was not tried to deduce the variety of parameters from fits of the experimental curves, but as much as possible parameters were taken from the literature. The effective masses of the electron and hole constituting the exciton were taken from [1]. Then, at $T = 4.7$ K, the value for the group velocity is $v_g = 9.2 \times 10^3$ m/s. The scattering length was taken from Fugol [17] in the following way. Fugol deduced $\mathscr{L}_{sc} = 46.4$ nm for $T = 10$ K. Assuming scattering on acoustic phonons (scattering probability $\propto T^{3/2}$), the 10 K value can be scaled to 4.7 K (98.7 nm). We have to note that Fugol used the term "diffusion length" for the scattering length [17]. From the formulae in [17], however, the meaning of the respective quantity is beyond doubt. As will be shown below, one of the crucial parameters is the refractive index. In the exciton-polariton model with exciton mass being less than infinite, two polariton waves are propagating in the crystal with the same wave vector and with the same polarization. Consequently, two refractive indices are needed, one for each (transverse) mode. Adopting Pekar's additional boundary condition [18], one can introduce an effective refractive index [3]. Values for this effective refractive index have been calculated from the reflectivity value via $R = [(1 - n)/(1 + n)]^2$. The only parameter then remaining open is the rate $\Gamma = \Gamma_{ST} + \Gamma_{nr}$.

In Fig. 7, results of the simulations are shown. The lower set of curves was calculated for an excitation energy $h\nu = 8.86$ eV. The penetration depth of the exciting light is here rather large. The absorption coefficient has a value of $\alpha = 10^4\ \mathrm{cm}^{-1}$. The dashed curve was calculated for comparison purposes with $\Gamma = 0$ (no trapping, no non-radiative losses inside the crystal). The full line was obtained with $\Gamma = 4.5 \times 10^8\ \mathrm{s}^{-1}$. All simulations were convoluted with the apparatus function (convolution of the shape of excitation pulses, detector response, and electronic response, FWHM 0.4 ns). The agreement between the full curve and the measurement (dots) over a dynamical range of five orders of magnitude is remarkable. The upper set of curves corresponds to a much smaller penetration depth of exciting radiation. The photon energy of excitation was $h\nu_{ex} = 9.1$ eV, absorption coefficient $\alpha = 3 \times 10^5\ \mathrm{cm}^{-1}$. Again, the dashed curve was calculated for comparison purposes with $\Gamma = 0$. Apart from the value of the absorption coefficient, all parameters remained unchanged. Nevertheless, the agreement between experiment and calculation is remarkable as well. The influence of penetration depth is weak at longer times. It is dramatic in the short-time region. The curve with the small penetration depth exhibits a strong spike which is nearly perfectly reproduced by the model calculation. The spike mainly stems from those exciton polaritons excited within $x \leqq \mathscr{L}_{sc}$ having a chance to reach the surface with one step, whereas the motion of particles from deeper parts of the sample is more diffusive-like, contributing to the decay curve at longer times. The agreement between simulation and

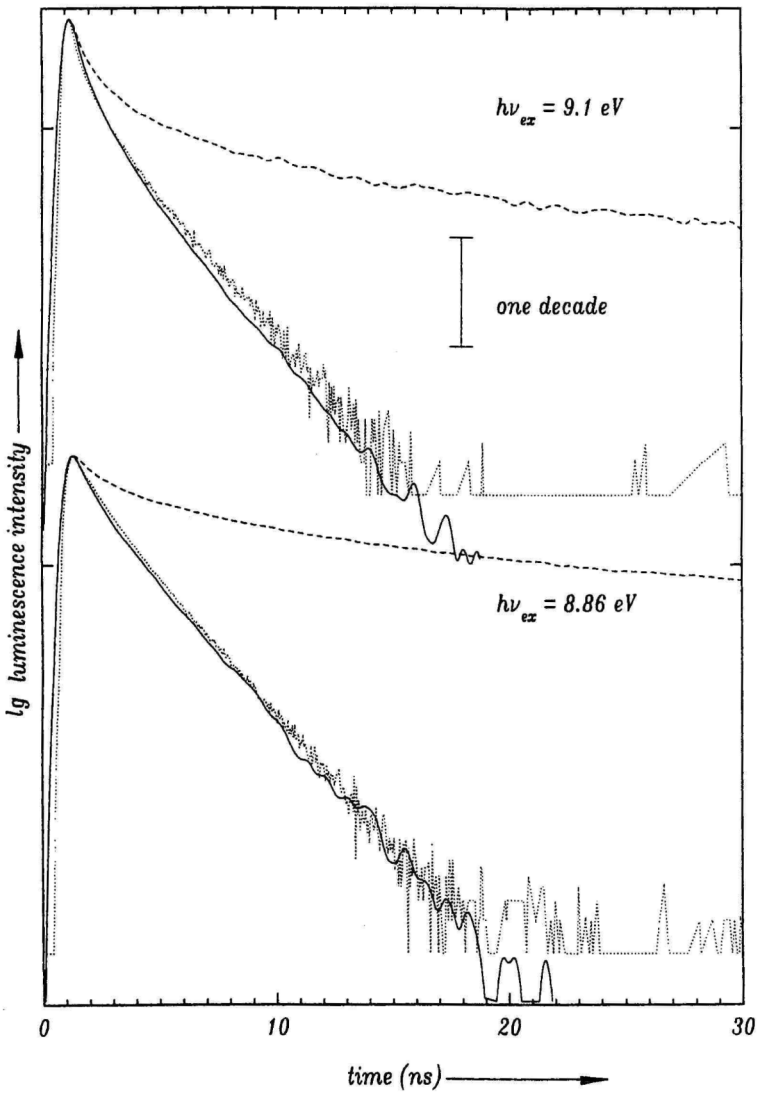

Fig. 7. Monte-Carlo simulations of the FE-luminescence decay of solid xenon neglecting any trapping (dashed curves) and including trapping (solid curves). The dots represent the respective measurements (T = 4.7 K). The photon energy of excitation for the lower set of curves was 8.86 eV (absorption constant 10^4 cm^{-1}). For the upper set of curves, the photon energy of excitation was 9.1 eV (absorption constant 3×10^5 cm^{-1})

measurement for curves obtained with dramatically different penetration depths of exciting radiation is a strong support of the applicability of the model in spite of its simplifications.

The scattering rate of the bottleneck exciton-polaritons can be deduced from the scattering length and the group velocity, $\Gamma_{sc} = v_g/\mathscr{L}_{sc}$. At T = 4.7 K, we obtain $\Gamma_{sc} = 9.3 \times 10^{10}$ s^{-1}. In other words, $\Gamma_{sc} \gg \Gamma$. Under these conditions, the survival probability of a particle along a scattering length could be written as $(1 - \Gamma\mathscr{L}_{sc}/v_g)$. Nevertheless, we took the expression

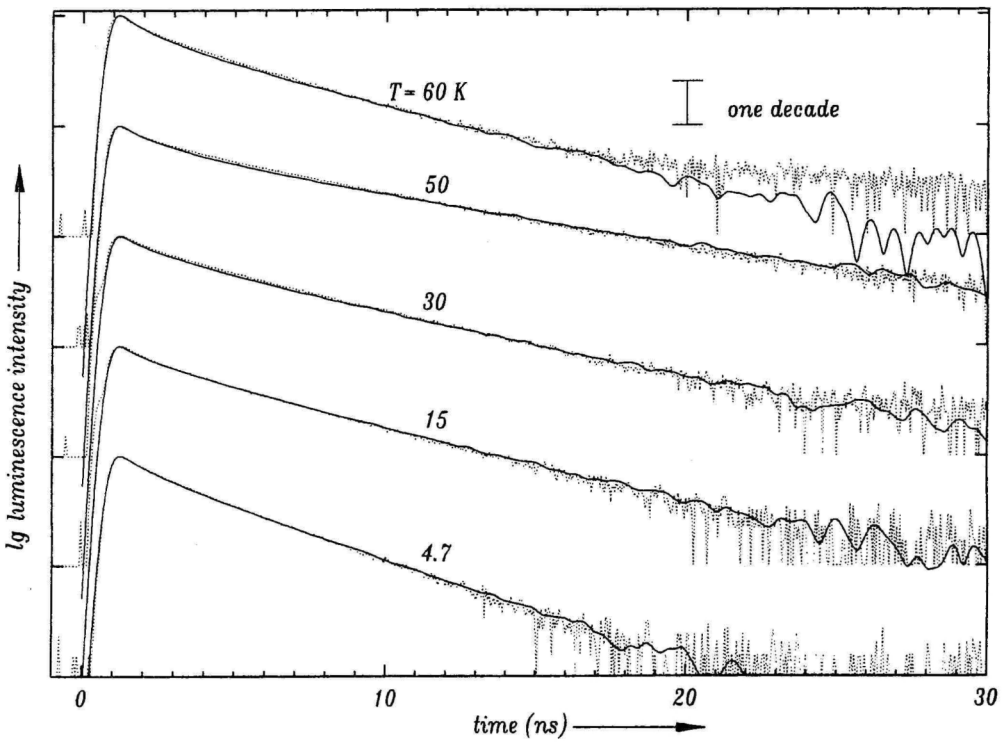

Fig. 8. Simulations (full lines) of FE-decay curves from solid Xe, measured at different temperatures. For details see text

given in Section 3.2 because then the model can also be applied to samples with a much larger trapping rate.

Now we want to discuss the temperature dependence of the decay curves. First of all, we tried to simulate them in the following way. All parameters were taken from the simulation of the $T = 4.7$ K curves (Fig. 7) with two exceptions. The scattering length and the group velocity were calculated from the $T = 4.7$ K values assuming scattering on acoustic phonons.

Table 1

FE-trapping rates Γ of solid Xe for different temperatures deduced from simulations of the decay curves. The self-trapping rates Γ_{ST} were obtained with (2). $\Gamma_{ST,intr}$ has to be regarded as an upper limit of the intrinsic self-trapping rate. For details, see text

T (K)	Γ (10^8 s^{-1})	Γ_{ST} (10^8 s^{-1})	$\Gamma_{ST,intr}$ (10^8 s^{-1})
5	4.5	1.6	≈ 0.5
10	3.4	1.3	
15	3.1	1.8	
20	2.9	2.0	
30	2.6	1.9	
40	2.3	2.2	
50	1.9	2.0	
60	3.2	4.5	

With $\Gamma_{sc} \propto T^{3/2}$ and $v_g \propto T^{1/2}$, $\mathscr{L}_{sc} \propto T^{-1}$. As a clear result, it turned out that the temperature dependence cannot be simulated in this way. The decay at longer times is insensitive to these changes but very sensitive to the values of $\Gamma = \Gamma_{ST} + \Gamma_{nr}$. The experimental curves are fairly well reproduced, taking Γ as a parameter. It is then of minor importance whether the group velocity and the scattering length are fixed to their values at $T = 4.7$ K or not. In the fits shown in Fig. 8, both quantities were adjusted to their values at the respective temperature. Moreover, slight adjustments of the refractive index were necessary for a quantitative simulation of the short-time part of the decay curves. The agreement between the fits and the measured curves is very good. The Γ-values deduced from the fits are collected in Table 1.

4. Discussion

4.1 Self-trapping rate and scattering length at low temperature

Concerning the dynamical behaviour of excitons in solid xenon, two of the quantities involved in the simulations are of special interest, $\Gamma = \Gamma_{ST} + \Gamma_{nr}$, and $\mathscr{L}_{sc}$. Γ mainly determines the decay at longer times. The value is rather insensitive to changes of the other parameters. The contrary is true for $\mathscr{L}_{sc}$ which is mainly involved in the spike at short times showing up for small penetration depths of exciting radiation. The spike depends on the choice of the refractive index, too. Therefore, it is necessary to discuss the interplay

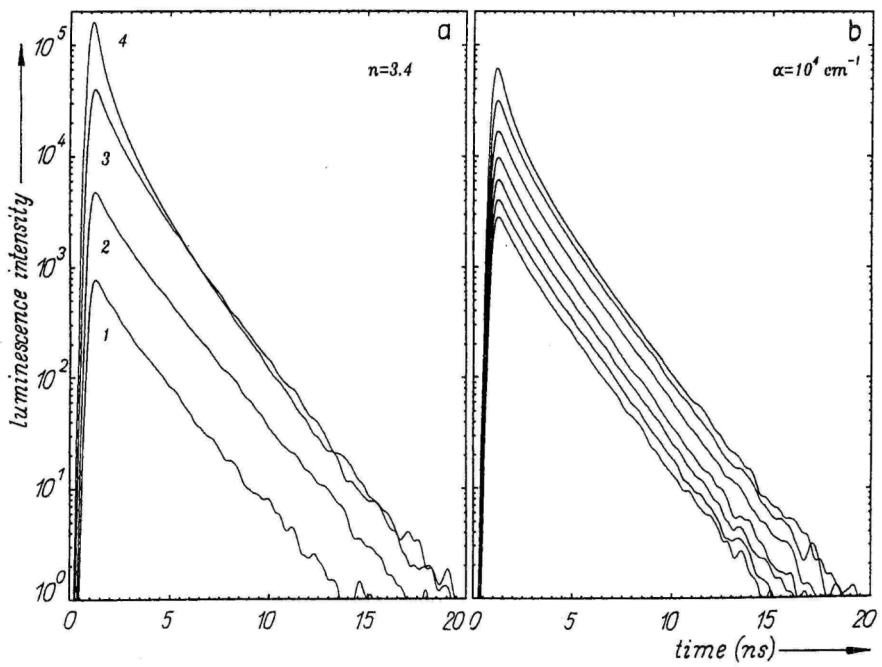

Fig. 9. Monte-Carlo simulations of the FE-luminescence decay of solid Xe at $T = 5$ K for fixed values of the scattering length $\mathscr{L}_{sc}$ (92.8 nm at 5 K) and for the trapping rate Γ (4.5×10^8 s^{-1}). In a) the refractive index was fixed ($n = 3.4$) and the absorption coefficient was varied: (1) $\alpha = 10^2$, (2) 10^3, (3) 10^4, (4) 10^6 cm^{-1}. In b) the absorption coefficient was kept fixed ($\alpha = 10^4$ cm^{-1}) and the refractive index was varied between $n = 2$ (uppermost curve) and $n = 8$ (lowest curve)

between $\mathscr{L}_{sc}$, n_{eff}, and α in more detail. For this purpose, in Fig. 9, two sets of simulations are presented for $T = 5$ K. In Fig. 9b, the effective refractive index was varied, and all the other parameters were kept fixed ($\Gamma = 4.5 \times 10^8\ s^{-1}$, $\mathscr{L}_{sc} = 92.8$ nm at $T = 5$ K, absorption coefficient $\alpha = 10^4\ cm^{-1}$). All the calculated curves have been convoluted with the experimental apparatus function. The larger the refractive index, the more pronounced is the spike. This effect would even be more drastic for a better experimental time resolution and δ-like excitation pulses. Fig. 9a displays the dependence of the spike on the value of α (Γ and $\mathscr{L}_{sc}$ like in Fig. 9b, however, $n_{eff} = 3.4$). Similar trends are observed as in Fig. 9b, the value of α varies by orders of magnitude. A change of α by a factor of 2 which is expected to be an upper limit of the data in [15] would hardly show up in the simulations.

It must be admitted that the strong influence of the value of n_{eff} can be balanced with a different choice of the scattering length. Changing n by $\approx 10\%$ is equivalent to a change of the value of $\mathscr{L}_{sc}$ by a factor of 2. A 10% uncertainty of the refractive index seems to be an upper limit. The value of $\mathscr{L}_{sc}$ has therefore an uncertainty of a factor of 2. In any case, it is beyond doubt that the scattering length is equivalent to some hundred nearest-neighbour distances.

The surprisingly large values of the scattering length pose the question concerning the nature of scattering. Besides scattering on acoustic phonons, we have to take into consideration scattering on impurities and defects. The gas used for preparation of the samples contains about 30 ppm impurities (mainly other rare gases, 10 ppm oxygen, nitrogen, etc.). Then, the average distance of the impurities is considerably smaller than the scattering length. In the simplest case, we could ascribe the scattering length exclusively to impurity scattering ($\mathscr{L}_{sc} \equiv \mathscr{L}_{sc,imp}$). In this case, with

$$\mathscr{L}_{sc,imp} = \frac{1}{n\sigma}, \tag{1}$$

an estimate of the average impurity scattering cross section yields $\sigma \approx 200\ nm^2$, a value which seems to be too high. Fugol [17] also showed that up to rather high impurity concentrations, the scattering length due to scattering on acoustic phonons will be smaller than the impurity-scattering length. In order to get more insight into the problem of impurity scattering, measurements with an improved and controlled sample purity would be most helpful. In the following discussion of the results, impurity scattering is neglected.

Next, we want to deduce the self-trapping rates from the experiment and the simulation. Note, the simulation yields only the sum of the self-trapping rate and a rate of non-radiative effects, $\Gamma = \Gamma_{ST} + \Gamma_{nr}$. Additionally, the simulation yields the relative number of excitations that are transmitted into the vacuum, $N_{FE}/N_0 = a$, and the relative number of excitations that are lost during transport via self-trapping and non-radiative effects (it is tacitly assumed that all self-trapped excitations show up in the respective luminescence bands). From the data presented in Fig. 3, we obtain the time-integrated intensity ratio I_{FE}/I_{STE} ($= b$) as a function of temperature. Then a straightforward calculation yields

$$\Gamma_{ST} = \frac{1}{b}\,\frac{a}{1-a}\,\Gamma. \tag{2}$$

The simulation shown in Fig. 7 yields $a = 0.126$. From Fig. 3 we take $b = 0.35$. The result then is $\Gamma_{ST} = 1.85 \times 10^8\ s^{-1}$. This value must be compared with the corresponding result of [6], $\Gamma_{ST} = 1.5 \times 10^8\ s^{-1}$. Though the model in [6] was very crude, there is excellent agreement concerning the self-trapping rates.

In [6], we compared the measured self-trapping rates with theoretical values published by Schreiber and Kmiecik [19]. Although there is good agreement between theory [19] and experiment, this agreement should be taken with care. Ioselevich and Rashba [20] recently pointed out that it is nearly impossible to calculate the self-trapping rates with sufficient accuracy. According to their theory, the self-trapping rate can be represented by

$$\Gamma_{ST}(T) = \omega B(T) \exp[-S(T)], \tag{3}$$

where $S(T)$ is the temperature-dependent Hamiltonian action. At low temperatures, the pre-factor $B(T)$, the co-called enhancement factor, is given approximately by $(E_b/\omega)^{3/2}$, with E_b being the half width of the exciton band (450 meV [1]), and ω the characteristic phonon frequency. Taking the Debye frequency for ω (Debye energy 5.5 meV [1]) and the experimental value of Γ_{ST}, one then obtains $S \approx 19$ at low temperature. This is an important result because it demonstrates the applicability of the semiclassical theory of Ioselevich and Rashba [20] which is only valid for $S(T) \gg 1$. On the other hand, it also clearly demonstrates that a small uncertainty in S introduces a large uncertainty in the theoretical value of the self-trapping rate. The theoretical uncertainty in S may be of the order of 2 [21], introducing an uncertainty in the theoretical value of Γ_{ST} by many orders of magnitude.

4.2 Temperature dependence of the self-trapping rate

Decay curves of the free-exciton luminescence of solid Xe have been presented for various temperatures in Fig. 4. From the Monte-Carlo simulations (Fig. 8), the trapping rates were deduced (Table 1), and finally, the self-trapping rates were calculated as it was described in Section 4.1. The results for Γ_{ST} are included in Table 1. For $T \leqq 50$ K, the self-trapping rate is slightly increasing with increasing temperature. Above $T = 50$ K, however, it increases dramatically. It turns out that the unexpected decrease of the decay rate with increasing temperature which is obvious from Fig. 4, is not a property of the self-trapping rate itself but of the branching between formation of self-trapped excitons and the formation of long-lived centers, described by Γ_{nr}.

In Fig. 10a, we reproduce a figure of the paper of Schreiber and Kmiecik [19] which displays calculated self-trapping rates of solid Xe as a function of temperature. Different curves are given. The parameter α_{int} at each curve characterizes a different interaction mode of the exciton–lattice system. At low temperatures, the trapping would follow the curve with the highest α_{int}. Additionally, we included the experimental values of Γ_{ST} as crosses. At low temperatures, the agreement concerning the temperature trend is satisfactory (concerning the absolute value, see our remarks in Sections 4.1 and 4.3). At higher temperatures, the theoretical rate increases much stronger than the measured values. In view of the complexity of theory as well as experiment, the overall agreement is satisfactory.

In Fig. 10b, the self-trapping rates are plotted in a linear scale and compared with the theoretical predictions of Ioselevich and Rashba [20]. This comparison is not straightforward. The authors discuss both the temperature dependence of the enhancement factor, $B(T)$, and of the exponent in (3) in the high and low temperature limits. At low temperatures, the exponent approaches a temperature-independent value, whereas at high temperatures, it approaches a value $\propto W/T$ with W being the barrier height (Arrhenius-type behaviour). At low temperatures, the enhancement factor yields a temperature dependence of the form $(1 - 2T/\omega)^{-3/2}$ with ω being the characteristic phonon frequency, whereas at high temperatures, a $T^{3/2}$ behaviour is predicted. For a detailed comparison with the experiment,

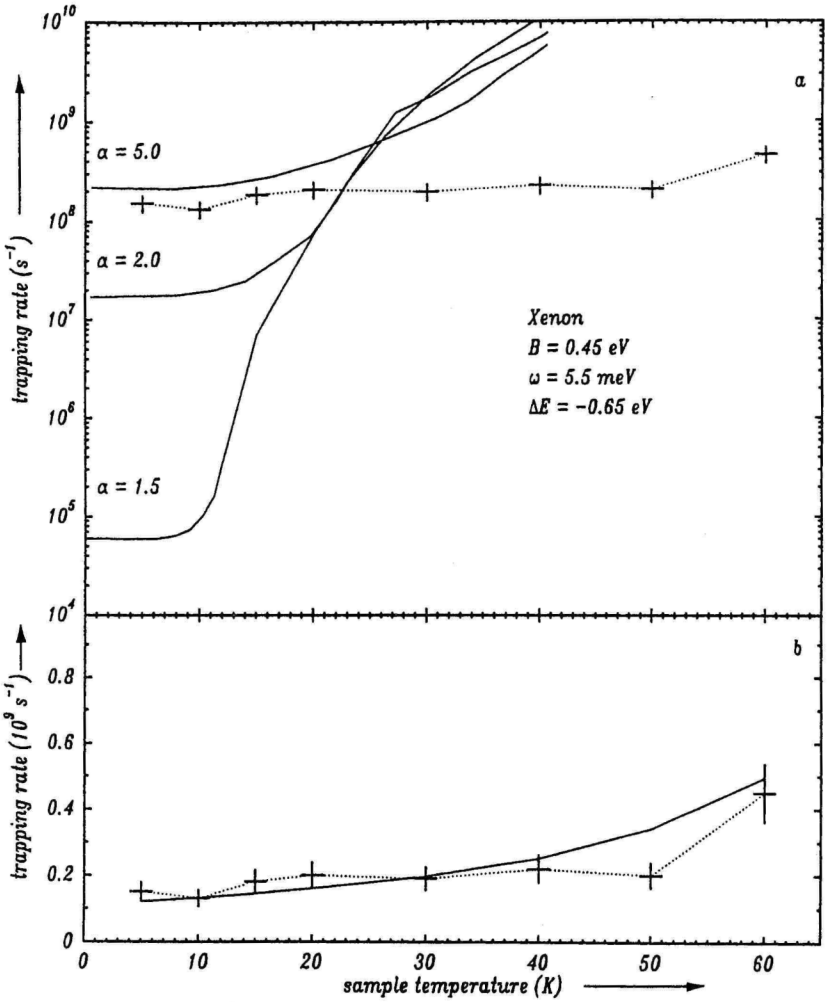

Fig. 10. a) self-trapping rates of free excitons in solid Xe, calculated for different interaction modes as a function of T (reproduced from [19]). The points are results of the present paper (Γ_{ST} from Table 1). b) Comparison between experimental self-trapping rates of free excitons in solid Xe with the theoretical prediction of [20]. For details see text

the limiting cases are not sufficient because we obviously cover the transition from the low temperature to the high temperature regime. Nevertheless, we tried to fit points with the $(1 - 2T/\omega)^{-3/2}$ law (full curve). The fit is satisfactory.

4.3 Non-radiative processes

From the results of Fig. 3 it is well established that the total luminescence intensity of solid Xe increases by nearly a factor of 2 between $T = 50$ and 60 K. This unexpected result has been checked with different samples [22]. In the early paper of Kink et al. [4], an increase around 50 K also shows up (summing up the contributions A and B in their Fig. 4a), however, by far not as pronounced as in our work.

This increase of the total luminescence intensity is a definite proof that non-radiative competing FE-decay processes take place at low temperatures. One of the experimental methods to get more insight into such non-radiative processes is thermoluminescence. Indeed, in the case of solid Kr, thermoluminescence following X-ray excitation has already been observed [23]. Solid Xe, doped with metal atoms, also exhibits X-ray induced thermoluminescence [24]. Preliminary data on nominally pure solid Xe, obtained following primary excitation with the zeroth order of the SUPERLUMI primary monochromator, yield thermoluminescence, too. The various thermoluminescence data underline that the results of the present paper concerning the increase of total luminescence intensity around 50 K make sense. They leave open the question whether excitonic excitation is responsible for thermoluminescence.

Another type of experiment has to be mentioned in this context. Vaness [25] characterized deep electron traps in rare-gas solids including Xe. Preferentially at low temperatures, these traps are populated efficiently following primary selective excitonic excitation. At low temperatures, they are stable for many hours. They were established with photo-electron spectroscopic methods and in laser-stimulated luminescence measurements. The population of such traps following primary excitonic excitation requires the separation of the electron and the hole constituting the exciton which is improbable in the ideal lattice. Two different mechanisms can account for the population of the electron traps, (i) impurity enhanced ionization of the exciton and trapping of the electron at the respective impurity, and (ii) defect-induced separation of the charge carriers. In the latter case, the electron may be trapped at a vacancy.

Our data clearly establish once more that such processes take place and allow for an estimate of the branching ratio between the radiative and the non-radiative FE-decay processes. However, more detailed investigations are needed to establish the microscopic mechanism of the non-radiative processes.

Another type of non-radiative process has to be mentioned here. Although our experiments are carried out in an UHV environment (lower 10^{-8} Pa range), contamination of the surface on a time scale of hours cannot be avoided. Such a surface contamination leads to surface quenching of FE luminescence. As was described in [6], the quenching processes obviously contribute to desorption of the contamination. Therefore, at the illuminated spot of the sample, the FE luminescence persists even on a time scale of days, however, with a reduced intensity. The quenching factor, γ, is of the order of 1/2 (rough estimate). Taking into account this quenching factor requires to replace $b = I_{FE}/I_{STE}$ by $b = \gamma I_{FE}/I_{STE}$. Consequently, (2) has to be replaced by

$$\Gamma_{ST} = \frac{\gamma}{b} \frac{a}{1-a} \Gamma . \tag{4}$$

In others words, neglecting surface quenching means an overestimation of Γ_{ST}. With $\gamma = 1/2$, a more realistic value of the self-trapping rate is found in the upper $10^7\ s^{-1}$ range.

Even this value seems to be too high because at least part of the surface quenching of FE luminescence may be due to surface trapping. In other words, the number N_{STE} in the parameter b is underestimated. The probability of surface trapping is unknown, therefore, this effect cannot be taken into account quantitatively.

Another additional fact that reduces the self-trapping rate has to be mentioned in this context. As was discussed in [6], two contributions to the broad luminescence bands around 7.2 eV exist, a band peaking at 7.05 eV, and a band peaking at 7.25 eV. These bands have

already been observed by different groups [4, 5]. At least one of the bands (the band peaking at 7.05 eV) arises from an exciton trapped at a lattice defect. In our sample, the intensity ratio between both bands is of the order of unity. If we restrict the quantity Γ_{ST} to the formation of the centres which show up in the 7.25 eV band (most probably independent of lattice defects), we finally obtain a value for this "intrinsic self-trapping rate" $\Gamma_{ST,intr} \leqq 5 \times 10^7\ s^{-1}$. This value, which should only be taken as a rough estimate, is included in Table 1. Thus, compared to [6], the more refined evaluation of the FE-decay curves with the transport model yields a significantly lower value of the intrinsic self-trapping rate.

4.4 Scattering length and diffusion length

In several early investigations of the exciton dynamics of evaporated rare-gas films, exciton motion was probed with photoelectron spectroscopy and with luminescence excitation spectroscopy [1, 26]. The motion was characterized with a diffusion length, $L_{diff} = \sqrt{D\tau}$ (D diffusion constant, τ exciton lifetime). The values of L_{diff} of solid Xe which were reported in the early work ranged well below 100 nm. The diffusion length plays an important role not only in the field of energy transfer phenoma, but also, e.g., in the field of electronic sputtering from rare-gas solids [27]. It is therefore indispensable to discuss this quantity in view of the new results of this paper.

The diffusion length can be calculated from the scattering length, replacing D in $L_{diff} = \sqrt{D\tau}$ by $D = \frac{1}{3} v_{ave} \mathscr{L}_{sc}$, and taking the group velocity for v_{ave}. In doing so, we obtain for solid Xe at $T = 5$ K at value $L_{diff} = 816$ nm which is an order of magnitude larger than the values reported so far. It is interesting to note, however, that a similar value has been reported for solid Kr recently [28]. The Kr value was deduced from well annealed samples. It thus turns out that this quantity sensitively depends on sample preparation.

5. Concluding Remarks

In the present paper, decay curves of the FE luminescence of solid Xe following primary selective pulsed photoexcitation have been reported. The non-exponential FE decay was interpreted in terms of a model for exciton-polariton transport to the sample/vacuum interface, including phonon scattering and trapping. The decay curves were successfully reproduced with Monte-Carlo simulations of the transport process. A new value for an upper limit of the self-trapping rate in the lower $10^7\ s^{-1}$ range was deduced. This value is about five orders of magnitude smaller than the values obtained from early investigations of the exciton dynamics in solid Xe [1, 26]. Similarly, new values for the scattering length and diffusion length of excitons in solid Xe, exceeding the early results [1, 26] by an order of magnitude, were established. The new experimental values of the scattering length are in surprisingly good agreement with calculated values [17]. The new results are valid for samples obtained from the gas phase at elevated temperatures under nearly thermal equilibrium conditions, whereas the early results were obtained from thin films condensed onto a substrate at low temperatures. It thus turns out that the exciton dynamics are an extremely sensitive probe of the sample quality. Interestingly enough, FE luminescence is already used to analyze the quality of, e.g., chemical vapour deposited diamonds [29].

Acknowledgements

One of the authors (I.R.) would like to thank for a stipend within the exchange programme between the Universities of Hamburg and Tartu. Comments of H. Nishimura (Osaka),

R. Kink (Tartu), and M. Selg (Tartu) on the results published in [6] were very helpful. Financial support from the Bundesministerium für Forschung und Technologie of the Federal Republic of Germany under grants No. 05 405 AXB 6 TP7 and No. 05 5GUAYI TP2 is gratefully acknowledged.

References

[1] G. ZIMMERER, in: Excited-State Spectroscopy in Solids, Ed. U. M. GRASSANO and N. TERZI, North-Holland Publ. Co., Amsterdam 1987 (p. 37).
[2] I. YA. FUGOL, O. N. GRIGORASHCHENKO, and E. V. SAVCHENKO, phys. stat. sol. (b) **111**, 397 (1982).
[3] R. KINK and M. SELG, phys. stat. sol. (b) **96**, 101 (1979).
[4] R. KINK, A. LÔHMUS, and M. SELG, phys. stat. sol. (b) **107**, 479 (1981).
[5] I. YA. FUGOL, A. N. OGURTSOV, O. N. GRIGORASHCHENKO, and E. V. SAVCHENKO, Soviet J. low-Temp. Phys. **18**, 27 (1992).
[6] D. VARDING, J. BECKER, L. FRANKENSTEIN, B. PETERS, M. RUNNE, A. SCHRÖDER, and G. ZIMMERER, Low-Temp. Phys. **19**, 427 (1993).
[7] E. ROICK, R. GAETHKE, G. ZIMMERER, and P. GÜRTLER, Solid State Commun. **47**, 333 (1983).
[8] G. ZIMMERER, Nuclear Instrum. and Methods **A308**, 178 (1991).
[9] W. LAASCH, H. HAGEDORN, T. KLOIBER, and G. ZIMMERER, phys. stat. sol. (b) **158**, 753 (1990).
[10] M. HUFNAGEL, J. BECKER, M. RUNNE, A. SCHRÖDER, D. THOMAS, D. VARDING, und G. ZIMMERER, Ann. Rep. 1993, HASYLAB at DESY, Jan. 1994 (p. 195).
[11] T. KLOIBER, PhD Thesis, The University of Hamburg, 1989; Internal Rep. DESY-HASYLAB 89-09, September 1989.
[12] Y. TOYOZAWA, Progr. theor. Phys. (Kyoto), Suppl. **12**, 111 (1959).
[13] H. NISHIMURA, T. YAMAOKA, K. HATTORI, A. MATSUI, and K. MIZUNO, J. Phys. Soc. Japan **54**, 4370 (1985).
[14] H. NISHIMURA and T. YAMANO, J. Phys. Soc. Japan **51**, 2947 (1982).
[15] G. BALDINI, Phys. Rev. **128**, 1562 (1962).
[16] V. SAILE, Appl. Optics **19**, 4115 (1980).
[17] I. YA. FUGOL, Adv. Phys. **37**, 1 (1988).
[18] S. I. PEKAR, Zh. eksper. teor. Fiz. **33**, 1022 (1957).
[19] M. SCHREIBER and H.-J. KMIECIK, in: Dynamical Processes in Codensed Molecular Systems, Ed. A. BLUMEN, J. KLAFTER, and D. HAARER, World Scientific Publ. Co., Singapore 1990 (p. 225). M. SCHREIBER and H.-J. KMIECIK, J. Lum. **45**, 282 (1990).
[20] A. S. IOSELEVICH and E. I. RASHBA, in: Quantum Tunneling in Condensed Media, Ed. YU. KAGAN and A. J. LEGGETT, Elsevier Sci. Publ. B.V., Amsterdam 1992 (p. 347).
[21] E. I. RASHBA, private communication.
[22] M. HUFNAGEL, Diploma Work, University of Hamburg 1994, in preparation.
[23] M. KIRM and H. NIEDRAIS, J. Lum. **60/61**, 611 (1994).
[24] K. GÖTTSCHE, Diploma Work, The University of Marburg 1993.
[25] T. VANESS, PhD Thesis, The University of Hamburg, 1990; Internal Rep. DESY-HASYLAB 90-04, November 1990.
[26] N. SCHWENTNER, E.-E. KOCH, and J. JORTNER, Electronic Excitations in Condensed Rare Gases, Springer Tracts mod. Phys., Vol. **107**, Springer 1985.
[27] R. E. JOHNSON and J. SCHOU, in: Fundamental Processes in Sputtering of Atoms and Molecules (SPUT 92), Ed. P. SIGMUND, Matematisk-fysiske Modelelser, Vol. **43**, Munksgaard, Copenhagen 1993.
[28] B. HERKERT, A. SCHRIMPF, K. GÖTTSCHE, T. BORNEMANN, R. BRÜNING, and H.-J. STÖCKMANN, J. Lum. **60/61**, 768 (1994).
[29] H. KAWARADA, T. TSUTSUMI, H. HIRAYAMA, and A. YAMAGUCHI, Appl. Phys. Letters **64**, 451 (1994).

(Received May 30, 1994)

Я. Ю. Аавиксоо, И. Я. Рейманд, В. В. Россин, В. В. Травников,
“Влияние экситон-электронного взаимодействия
на кинетику экситонной люминесценсии”,
ФТТ, т. 36, № 5, стр. 1470, (1994).

УДК 535.343.2

ВЛИЯНИЕ ЭКСИТОН-ЭЛЕКТРОННОГО ВЗАИМОДЕЙСТВИЯ НА КИНЕТИКУ ЭКСИТОННОЙ ЛЮМИНЕСЦЕНЦИИ

Я.Аавиксоо, И.Рейманд, В.В.Россин, В.В.Травников

Исследован эффект динамического гашения люминесценции сверхчистых эпитаксиальных слоев GaAs следующим импульсом фотовозбуждения. Для объяснения эффекта предложена модель, основанная на взаимодействии экситонов с горячими фотовозбужденными электронами. Выполнен расчет динамики экситонов и электронов после короткого импульса фотовозбуждения с учетом экситон-электронного взаимодействия. Результаты расчета согласуются с экспериментально обнаруженными зависимостями эффекта гашения от энергии возбуждающего кванта света и интенсивности возбуждения.

При фотовозбуждении полупроводника светом с энергией больше ширины запрещенной зоны рождаются неравновесные носители заряда, которые при низких температурах после энергетической релаксации связываются в экситоны. Экситонная и электронная подсистемы могут взаимодействовать между собой. При больших интенсивностях возбуждения это взаимодействие может приводить к экранированию экситонов [1,2]. При не слишком больших интенсивностях возбуждения экситон-электронное взаимодействие может приводить к рассеянию экситонов и электронов по своим зонам и существенно влиять на процессы энергетической релаксации. Вероятность взаимодействия экситона с электронами ω_{e-x} можно оценить по формуле [3]

$$\omega_{e-x} = 20\hbar a_x n_e / m_e, \qquad (1)$$

где a_x — боровский радиус экситона, n_e и m_e — концентрация и эффективная масса электронов. Видно, что эффективность взаимодействия возрастает с увеличением боровского радиуса экситона и уменьшением эффективной массы электрона. В этом смысле подходящим полупроводниковым материалом, в котором должно ярко проявляться экситон-электронное взаимодействие, представляется GaAs, в котором $a_x = 140$ К, $m_e = 0.06m_0$, и в то же время экситон при низких температурах стабилен и наблюдается в спектрах фотолюминесценции [4].

В работах [1,5,6] отмечалось, что экситон-электронное взаимодействие может оказывать влияние на форму спектра стационарной экситонной люминесценции GaAs. Исследования спектров экситонной люминесценции GaAs в зависимости от энергии фотовозбуждения и

магнитного поля [7] позволили получить прямые доказательства влияния экситон-электронного взаимодействия на функцию энергетического распределения экситонов. Определение времени фазовой когерентности экситонов методом четырехволнового смешивания при межзонной подсветке показало эффективное рассеяние экситонов свободными электронами [8]. Тем не менее прямое наблюдение экситон-электронного рассеяния в экспериментах по кинетике люминесценции при импульсном фотовозбуждении представляет определенные трудности. Дело в том, что в нестационарном эксперименте экситоны и электроны оказываются разделенными по времени, так как экситоны образуются после энергетической релаксации фотовозбужденных электронов. Лишь в сверхчистом GaAs, в котором время затухания экситонной люминесценции сравнимо с периодом следования импульсов фотовозбуждения, удалось наблюдать взаимодействие фотовозбужденых электронов с экситонами, оставшимися от предыдущего импульса [9,10]. При этом наблюдался эффект динамического гашения экситонного излучения горячими электронами.

Целью настоящей работы являлось теоретическое описание динамики экситонов и электронов после короткого импульса фотовозбуждения с учетом экситон-электронного взаимодействия для объяснения экспериментальных особенностей эффекта динамического гашения экситонной люминесценции сверхчистого GaAs.

1. Эксперимент

Люминесценция возбуждалась перестраиваемым лазером на красителе стирил-9 с накачкой криптоновым лазером с синхронизацией мод. Длительность импульса фотовозбуждения 5 ps, период следования 12.2 ns, полуширина аппаратной функции системы регистрации 300 ps. Спектральная ширина линии возбуждения 0.7 meV. Люминесценция регистрировалась методом время-кореллированного счета фотонов с временным разрешением 300 ps и спектральным разрешением $\sim$ 0.1 meV при температуре 1.7 K. Образцы представляли собой сверхчистые слои GaAs, изготовленные методом газофазной эпитаксии в хлоридной системе. По оценкам, концентрация мелких примесей в них составляла $\sim 10^{12}\,\mathrm{cm}^{-3}$ [11].

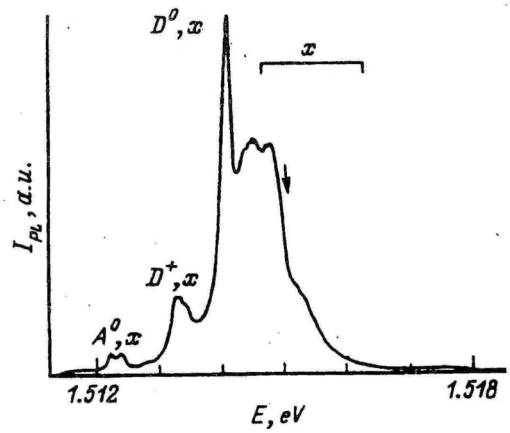

Рис. 1. Спектр фотолюминесценции образца GaAs.
I_{ex} = 2.4 W/cm^2, энергия возбуждения 1.554 eV.

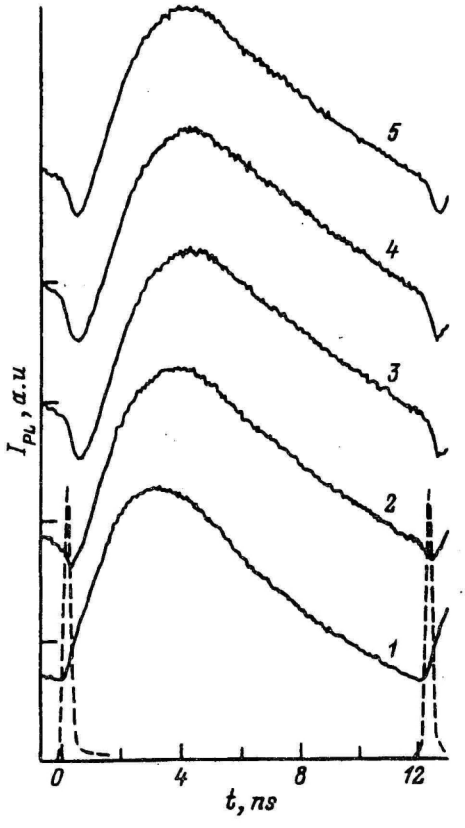

Рис. 2. Кинетика экситонной люминесценции GaAs при различных энергиях возбуждения.
1 — 1.525, *2* — 1.532, *3* — 1.539, *4* — 1.554, *5* — 1.565 eV. Интенсивность возбуждения 2.4 W/cm^2. Пунктир — импульс лазера.

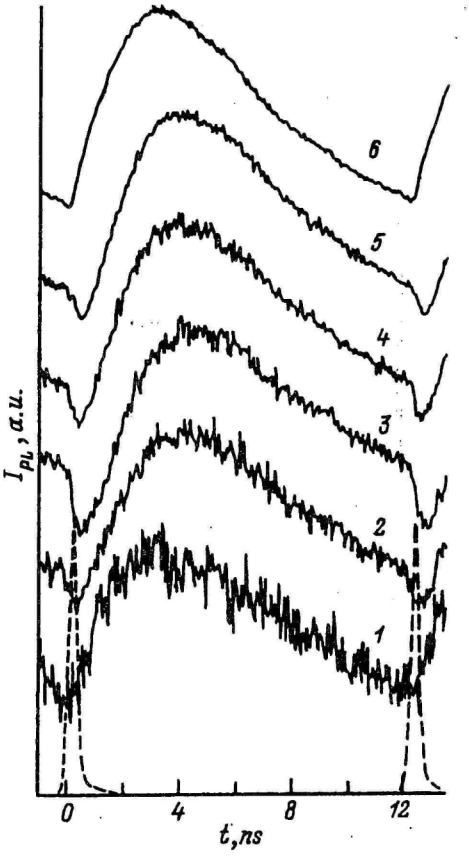

Рис. 3. Кинетика экситонной люминесценции GaAs при различных энергиях возбуждения.
1 — 0.6, *2* — 1.5, *3* — 2.4, *4* — 3.8, *5* — 7.0, *6* — 12.7 W/cm^2. Энергия возбуждения 1.554 eV. Пунктир — импульс лазера.

На рис. 1 представлен спектр фотолюминесценции образца GaAs при интенсивности возбуждения $I_{ex} = 2.4$ W/cm^2. Наблюдается интенсивное излучение свободных экситонов (полоса x). На рис. 2 показаны импульсы экситонной люминесценции, зарегистрированные в области излучения свободных экситонов на энергии, отмеченной стрелкой на рис. 1, при разных значениях энергии возбужденного света. Большое время затухания люминесцении $\sim$ 5 ns приводит к тому, что за время между двумя последующии импульсами возбуждения экситонная люминесценция не затухает полностью. При энергиях фотовозбуждения, заметно превышающих ширину запрещенной зоны ($E_g = 1.5192$ eV), приход очередного импульса фотовозбуждения вызывает быстрое уменьшение интенсивности люминесценции (кривые *3–5* на рис. 2). Эффект динамического гашения экситонной люминесценции исчезает при приближении энергии возбуждения к краю запрещенной зоны GaAs (кривая *1*). В работе [9] мы предложили следу-

ющее объяснение наблюдаемого эффекта. При возбуждении существенно выше края запрещенной зоны рождаются горячие электроны. Экситон-электронное взаимодействие приводит к разогреву экситонов, т.е. к их рассеянию из области резонанса, в результате чего и наблюдается гашение люминесценции экситонов. При возбуждении в край зоны рождаются холодные электроны и разогрева экситонов не происходит. Эффект уменьшается и в случае, когда энергия фотовозбужденных электронов слегка превышает энергию оптического фотона (кривая *5* на рис. 2).

Предложенная модель предполагает сильную зависимость от интенсивности фотовозбуждения, так как величина экситон-электронного взаимодействия зависит от концентрации электронов и экситонов. Эффект динамического гашения экситонной люминесценции действительно сильно зависит от интенсивности фотовозбуждения (рис. 3). Однако зависимость эта немонотонна. Максимальная величина гашения достигается при средних интенсивностях возбуждения ($\sim 2.4\,\mathrm{W/cm^2}$). На первый взгляд это противоречит предложенной модели. Результаты расчета, представленные в следующем разделе, позволяют устранить кажущееся противоречие.

2. Теория

Для расчета временно́й зависимости экситонного излучения рассмотрим динамику экситонов и электронов после импульса фотовозбуждения. При фотовозбуждении выше края зоны рождаются горячие электроны и дырки. Задача состоит в том, чтобы проследить за процессами их охлаждения, связывания в экситоны, энергетической релаксации экситонов к области резонанса и излучения фотонов. Ввиду сложности задачи сделаем несколько упрощений. Во-первых, не будем учитывать дырки и их энергетическую релаксацию. Во-вторых, предположим, что экситонная и электронная энергетические функции распределения максвелловские и соответствующие эффективные температуры устанавливаются быстро. Следовательно, задача сводится к вычислению концентраций и эффективных температур электронов и экситонов: n_e, n_x, T_e, T_x. В-третьих, пренебрежем поляритонными эффектами. И наконец, будем рассматривать одномерную задачу, так как диаметр области фотовозбуждения существенно превосходит диффузионные длины.

Рассмотрим нестационарные уравнения непрерывности для концентраций n и плотностей энергии $3/2 \cdot k_{\mathrm{B}} nT$

$$\frac{\partial n_i}{\partial z} = D_i \frac{\partial^2 n_i}{\partial z^2} - R_i + G_i, \tag{2}$$

$$\frac{3}{2} k_{\mathrm{B}} \frac{\partial n_i T_i}{\partial t} = \frac{3}{2} k_{\mathrm{B}} D_i \frac{\partial^2 n_i T_i}{\partial z^2} - S_i + P_i. \tag{3}$$

Здесь индекс i принимает значение e или x для электронов и экситонов соответственно, D_i — коэффициенты диффузии, R_i и G_i — скорости рекомбинации и генерации

$$R_e = \frac{n_e}{\tau_e} + \gamma n_e^2, \quad G_e = g_{\mathrm{ex}}(t)\alpha_{\mathrm{ex}} \exp(-\alpha_{\mathrm{ex}} z), \tag{4}$$

$$R_x = \frac{n_x}{\tau_x}, \quad G_x = \gamma n_e^2, \tag{5}$$

где τ_i — времена жизни электронов и экситонов; γ — коэффициент связывания носителей в экситоны, зависящий от электронной температуры [12]; α_{ex} — коэффициент поглощения возбуждающего света; $g_{\text{ex}}(t)$ — импульс возбуждения. Скорость энергетических потерь S_i и плотность мощности возбуждения P_i определяются следующими выражениями:

$$S_e = n_e \left(\left\langle \frac{dE_e}{dt} \right\rangle_{\text{op}} + \left\langle \frac{dE_e}{dt} \right\rangle_{\text{ac}} + \left\langle \frac{dE_e}{dt} \right\rangle_{\text{pe}} + \left\langle \frac{dE_e}{dt} \right\rangle_{\text{imp}} \right) +$$

$$+ \frac{3}{2} k_{\text{B}} \gamma_{e-x} n_e n_x (T_e - T_x) + \frac{3}{2} k_{\text{B}} T_e R_e, \tag{6}$$

$$P_e = \frac{3}{2} k_{\text{B}} T_{ge} G_e, \tag{7}$$

$$S_x = n_x \left\langle \frac{dE_x}{dt} \right\rangle_{\text{ac}} + \frac{3}{2} k_{\text{B}} T_x R_x, \tag{8}$$

$$P_x = \frac{3}{2} k_{\text{B}} \gamma_{e-x} n_e n_x (T_e - T_x) + \frac{3}{2} k_{\text{B}} T_{gx} G_x. \tag{9}$$

Скорости энергетических потерь складываются из вероятностей рассеяния, усредненных по максвелловскому распределению (индексы «op», «pe», «ac», и «imp» означают процессы рассеяния на оптических фононах, пьезоэлектрического и деформационного рассеяния на акустических фононах, неупругого рассеяния на примесях соответственно), обмена энергией между электронами и экситонами (γ_{e-x} — константа экситон-электронного взаимодействия, см. Приложение) и рекомбинации, уносящей среднюю энергию $3/2 \cdot k_{\text{B}} T_i$. Энергии, передаваемые электронной и экситонной подсистемам внешним возбуждением и в результате процесса образования экситонов, равны $3/2 \cdot k_{\text{B}} T_{ge}$ и $3/2 \cdot k_{\text{B}} T_{gx}$ соответственно.

Исключая n_i из производной по времени в уравнении (3), получим следующие уравнения для температур:

$$\frac{\partial T_e}{\partial t} = \frac{D_e}{n_e} \left(\frac{\partial^2 n_e T_e}{\partial z^2} - T_e \frac{\partial^2 n_e}{\partial z^2} \right) - \frac{2}{3 k_{\text{B}}} \left\langle \frac{dE_e}{dt} \right\rangle - \gamma_{e-x} n_x (T_e - T_x) + \frac{G_e}{n_x} (T_{ge} - T_e), \tag{10}$$

$$\frac{\partial T_x}{\partial t} = \frac{D_x}{n_x} \left(\frac{\partial^2 n_x T_x}{\partial z^2} - T_x \frac{\partial^2 n_x}{\partial z^2} \right) - \frac{2}{3 k_{\text{B}}} \left\langle \frac{dE_x}{dt} \right\rangle + \gamma_{e-x} n_x (T_e - T_x) + \gamma \frac{n_e^2}{n_x} (T_{gx} - T_x). \tag{11}$$

Уравнения (2), (10), (11) должны быть дополнены граничными условиями

$$D_e \frac{\partial n_e}{\partial z} = s_e n_e \Big|_{z=0}, \quad \frac{\partial n_e}{\partial z} = 0 \Big|_{z=l}, \tag{12}$$

$$D_e \frac{\partial T_e}{\partial z} = s_{Te} (T_e - T_L) \Big|_{z=0}, \quad \frac{\partial T_e}{\partial z} = 0 \Big|_{z=l}, \tag{13}$$

$$D_x \frac{\partial n_x}{\partial z} = s_x n_x\Big|_{z=0}, \quad n_x = 0\Big|_{z=l}, \tag{14}$$

$$D_x \frac{\partial T_x}{\partial z} = s_{Tx}(T_x - T_L)\Big|_{z=0}, \quad T_x = T_L\Big|_{z=l}, \tag{15}$$

Здесь s_i и s_{Ti} — скорости поверхностной рекомбинации и поверхностного охлаждения, l — толщина активного слоя, T_L — температура решетки.

Средние скорости энергетических потерь вследствие различных механизмов рассеяния определяются выражениями из [13]

$$\left\langle \frac{dE_e}{dt} \right\rangle_{\text{op}} = (2m_e)^{1/2}(\hbar\omega_{LO})^{3/2}\frac{e^2}{\hbar^2}(\varepsilon_\infty^{-1} - \varepsilon_0^{-1}) \left[\exp\left(-\frac{\hbar\omega_{LO}}{k_{\text{B}}T_e}\right) - \exp\left(-\frac{\hbar\omega_{LO}}{k_{\text{B}}T_L}\right)\right], \tag{16}$$

$$\left\langle \frac{dE_e}{dt} \right\rangle_{\text{pe}} = \frac{32\pi^{1/2}e^2e_{14}^2m_e^{3/2}a(k_{\text{B}}T_e)^{1/2}}{2^{1/2}\hbar^2\varepsilon_0^2\rho}\,\frac{T_e - T_L}{T_e}, \tag{17}$$

$$\left\langle \frac{dE_e}{dt} \right\rangle_{\text{ac}} = \frac{8\cdot 2^{1/2}E_1^2m_e^{5/2}(k_{\text{B}}T_e)^{3/2}}{\pi^{3/2}\hbar^4\rho}\,\frac{T_e - T_L}{T_e}, \tag{18}$$

$$\left\langle \frac{dE_e}{dt} \right\rangle_{\text{imp}} = \frac{\pi^{5/2}N_Da_D^2E_D(k_{\text{B}}T_e)^{1/2}}{(2m_e)^{1/2}} \exp\left(-\frac{E_D}{k_{\text{B}}T_e}\right), \tag{19}$$

где $\hbar\omega_{LO}$ — энергия оптического фонона; ε_∞ и ε_0 — высокочастотная и низкочастотная диэлектрическая проницаемости; e_{14} — константа пьезоэлектрического взаимодействия; a — геометрический фактор ($a = 0.4$); ρ — плотность кристалла; E_1 — деформационный потенциал зоны проводимости; N_D, a_D и E_D — концентрация, боровский радиус и разница энергии возбужденного и основного состояний донора.

Средняя скорость энергетических потерь экситонов определяется выражением [14]

$$\left\langle \frac{dE_x}{dt} \right\rangle = \frac{8\cdot 2^{1/2}E_{\text{cv}}^2M_e^{5/2}(k_{\text{B}}T_x)^{3/2}}{\pi^{3/2}\hbar^4\rho}\,\frac{T_x - T_L}{T_x}, \tag{20}$$

где M — масса экситона, E_{cv} — разница деформационных потенциалов зоны проводимости и валентной зоны. Мы считаем, что для экситонов при низких температурах доминирующим механизмом энергетической релаксации является рассеяние на акустических фононах.

Константу связывания носителей заряда в экситон γ можно определить на основании результатов работы [15], принимая во внимание, что электронная температура отличается от решеточной

$$\gamma = \frac{16\cdot 2^{1/2}m_e^{5/2}E_1^2e^6}{3\pi^{1/2}\hbar^4\rho\varepsilon_0^3k_{\text{B}}T_L}(k_{\text{B}}T_e)^{-3/2}. \tag{21}$$

Разностная задача, соответствующая уравнениям (2), (10), (11) и граничным условиям (12)–(15), решалась численно. При этом в качестве возбуждения $g_{\text{ex}}(t)$ брался импульс гауссовой формы с шириной

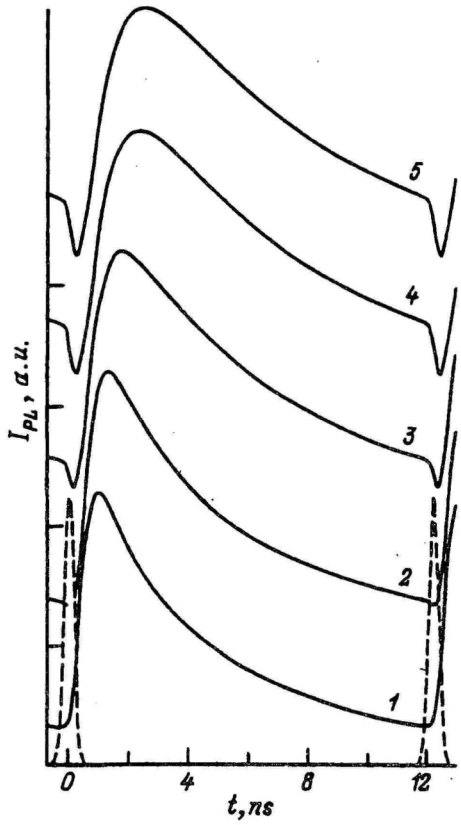

Рис. 4. Рассчитанные импульсы экситонной люминесценции при различных значениях начальной температуры электронов.
T_{ge}(K): *1* — 10, *2* — 20, *3* — 30, *4* — 50, *5* — 80. Интенсивность возбуждения 5 W/cm^2. Пунктиром показана использованная при расчете аппаратная функция.

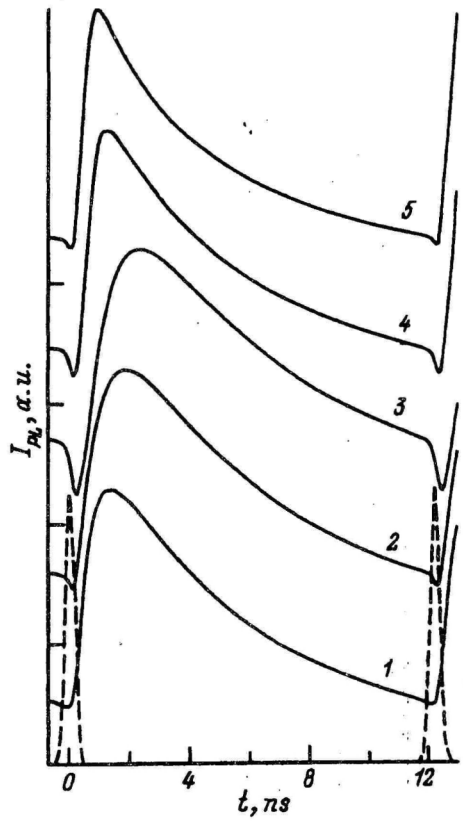

Рис. 5. Рассчитанные импульсы экситонной люминесценции при различных интенсивностях возбуждения.
1 — 0.5, *2* — 1.5, *3* — 5, *4* — 15, *5* — 30 W/cm^2. Начальная температура электронов T_{ge} = 50 K. Пунктиром показана использованная при расчете аппаратная функция.

$\Delta t_p = 5$ ps. Для моделирования периодического возбуждения с периодом 12.2 ns вычисления продолжались с новым импульсом возбуждения до тех пор, пока концентрации и температуры не стали периодичными. Были использованы следующие параметры GaAs: $\hbar\omega_{LO} = 36.7$ meV, $\varepsilon_\infty = 10.63$, $\varepsilon_0 = 12.56$, $e_{14} = 4.8 \cdot 10^4\,\mathrm{cm}^{-1/2}\cdot\mathrm{g}^{1/2}\cdot\mathrm{s}^{-1}$, $\rho = 5.32\,\mathrm{g}\cdot\mathrm{cm}^{-3}$, $E_1 = 7$ eV, $a_D = 100$ Å, $E_D = 4.4$ meV, $M = 1.2m_0$, $E_{cv} = 9.8$ eV. Параметры, соответствующие экспериментальным условиям: $N_D = 10^{12}\,\mathrm{cm}^{-3}$, $T_L = 1.7$ K, $l = 10\,\mu$, $\alpha_{ex} = 10^4\,\mathrm{cm}^{-1}$. Параметр T_{ge} есть начальная температура электронов, устанавливаемая сразу после фотовозбуждения, а значит, связанная с энергией возбуждающего кванта света. Аналогичный параметр для экситонов мы взяли равным $T_{gx} = 36$ K, что соответствует разнице энергий возбужденного и основного состояний экситона (мы полагаем, что экситон образуется через возбужденное состояние). Остальные параметры варьировались, и результаты приведены для следующих значений: $D_e = 10\,\mathrm{cm}^2/\mathrm{s}$, $D_x = 5\,\mathrm{cm}^2/\mathrm{s}$, $\tau_e = 3.3$ ns, $\tau_x = 10$ ns, $s_e = 5 \cdot 10^5$ cm/s, $s_x = s_{Te} = s_{Tx} = 0$.

После определения координатных и временны́х зависимостей спектр экситонной фотолюминесценции рассчитывается в соответствии с выражением

$$I(E,t) \sim \int \frac{n_x}{T_x^{3/2}} \exp\left(-\frac{E-E_T}{k_B T_x}\right) \exp(-\alpha z) dz. \qquad (22)$$

Здесь E_T — энергия дна экситонной зоны, α — коэффициент поглощения люминесценции. Результирующий импульс люминесценции получается сверткой рассчитанной временно́й зависимости и аппаратной функцией, выбранной в виде гауссовой с полушириной 0.3 ns.

На рис. 4, 5 показаны рассчитанные импульсы люминесценции для энергии излучаемого фотона $E - E_T + 0.1$ meV и коэффициента поглощения $\alpha = 5 \cdot 10^4\,\mathrm{cm}^{-1}$. Как видно из рис. 4, увеличение начальной температуры электронов приводит к появлению и возрастанию провала на фронте импульса люминесценции. С увеличением интенсивности возбуждения величина провала меняется немонотонно, достигая максимума при $\sim 5\ \mathrm{W/cm}^2$.

3. Обсуждение

Предложенная модель объясняет основные экспериментальные проявления эффекта динамического гашения экситонной люминесценции. Учет экситон-электронного взаимодействия приводит к появлению провала на фронте рассчитанного импульса люминесценции. С увеличением энергии возбуждающих квантов света выше края запрещенной зоны увеличивается начальная температура электронного газа, что, как показывает расчет, вызывает больший разогрев и соответственно гашение люминесценции экситонов. Модель объясняет и немонотонную зависимость эффекта от интенсивности возбуждения. Действительно, сначала с ростом интенсивности возбуждения увеличивается концентрация электронов и экситоны более эффективно разогреваются электронами, что приводит к росту величины провала. При достаточно больших интенсивностях возбуждения экситон-электронное взаимодействие помимо разогрева экситонов приводит к более быстрому охлаждению в электронной подсистеме. В результате разогрев экситонов и гашение люминесценции происходят на более коротких временах, и с учетом конечного временно́го разрешения они перестают наблюдаться. Обращает на себя внимание хорошее соответствие между экспериментальной и расчетной интенсивностями возбуждения, при которой наблюдается максимум эффекта динамического гашения.

Отметим, что экситон-электронное взаимодействие представляет собой новый механизм энергетической релаксации электронов. Дело в том, что экситоны как более массивные частицы, эффективнее взаимодействуют с акустическими фононами, тогда как для электронов рассеяние на акустических фононах почти упругое. В результате передача энергии электронов экситонам при достаточной концентрации последних приводит к эффективному охлаждению электронов.

Обратим внимание на то, что в расчете использовалось нулевое значение для скорости поверхностной рекомбинации экситонов. Дело в том, что при ее большой величине экситоны отсутствуют вблизи поверхности к моменту прихода очередного импульса фотовозбуждения, рождающего электроны в приповерхностной области. Таким образом,

экситоны и электроны оказываются разделенными в пространстве и их взаимодействие неэффективно. Расчет в этом случае показывает отсутствие провала на фронте импульса возбуждения. Предположение о малой скорости поверхностной рекомбинации экситонов кажется реалистичным для сверхчистого GaAs, в котором приповерхностное электрическое поле, являющееся причиной диссоциации экситона, невелико.

Конечно, использованные упрощения могут быть причиной некоторого несоответствия теории эксперимента. Особенно это касается использования максвелловской функции распределения для экситонов. Строго говоря, следовало бы определить эту функцию распределения, решив кинетическое уравнение. Неучет поляритонных эффектов не позволил получить достаточно большую задержку импульсов люминесценции, наблюдаемую в эксперименте и связанную с эффектом «бутылочного горла» для поляритонов. Однако полученные результаты вполне подтвеждают правильность предложенного объяснения наблюденного эффекта динамического гашения экситонной люминесценции.

При расчете считалось, что коэффициент диффузии не зависит от эффективной температуры. Подобный расчет был проведен также и для линейной зависимости коэффициента диффузии от температуры. В этом случае основные уравнения имеют более громоздкий вид, однако результат оказался примерно таким же, как и в приведенном варианте.

Таким образом, экситон-электронное взаимодействие оказывает существенное влияние на кинетику экситонной люминесценции. Обнаруженный эффект динамического гашения экситонной люминесценции связан с разогревом экситонов, оставшихся от предыщушего импульса возбуждения вновь рожденными горячими электронами. Расчет динамики экситонов и электронов после короткого импульса фотовозбуждения с учетом экситон-электронного взаимодействия показал немонотонную зависимость эффекта от интенсивности возбуждения в соответствии с экспериментом. При больших интенсивностях возбуждения появляется новый эффективный канал охлаждения электронов за счет их рассеяния на экситонах.

Работа выполнена при поддержке Российского фонда фундаментальных исследований, проект № 92-02-2373.

ПРИЛОЖЕНИЕ

Процесс экситон-электронного рассеяния может быть описан в координатной системе центра масс как упругое рассеяние частицы с приведенной массой $\mu = m_e M/(m_e + M)$ и волновым вектором $\mathbf{Q} = (M\mathbf{k}_e - m_e\mathbf{k}_x)/(M + m_e)$ в потенциале взаимодействия, усредненном по внутреннему движению в экситоне. При этом суммарный волновой вектор $\mathbf{K} = \mathbf{k}_e + \mathbf{k}_x$ сохраняется. Скорость обмена энергией между электронной и экситонной подсистемами, усредненная по их максвелловским распределениям, может быть записана в виде

$$S_{e-x} = \left\langle \left\langle \int \frac{\hbar Q}{\mu} \sigma_{e-x} \Delta E_x d\Omega_Q \right\rangle_{\mathbf{k}_{xi}} \right\rangle_{\mathbf{k}_{ei}} n_x n_e, \qquad (\text{П}.1)$$

где σ_{e-x} — дифференциальное сечение рассеяния, $\mathbf{k}_{ei}$ и $\mathbf{k}_{xi}$ — начальные волновые векторы взаимодействующих электрона и экситона. Ин-

тегрирование производится по всем направлениям приведенного волнового вектора $\mathbf{Q}$. Энергия ΔE_x, которая передается экситону, и усреднения $\langle\rangle$ описываются выражениями

$$\Delta E_x = \frac{\hbar^2}{2M}(k_{xf}^2 - k_{xi}^2), \qquad \mathbf{k}_x = -\mathbf{Q} + \frac{M}{M+m_e}\mathbf{K}, \tag{П.2}$$

$$\langle F\rangle_{\mathbf{k}} = \int \exp\left(-\frac{E}{k_{\mathrm{B}}T}\right) F \frac{d^3\mathbf{k}}{(2\pi)^3} \left[\int \exp\left(-\frac{E}{k_{\mathrm{B}}T}\right)\frac{d^3\mathbf{k}}{(2\pi)^3}\right]^{-1}. \tag{П.3}$$

Здесь $\mathbf{k}_{xf}$ — конечный волновой вектор экситона в результате процесса рассеяния; усреднение может проводиться по функции распределения как экситонов, так и электронов (соответствующий индекс опущен).

В качестве сечения рассеяния σ_{e-x} используем выражение, полученное для рассеяния электрона на нейтральном доноре [16], так как эффективная масса дырки значительно больше эффективной массы электрона

$$\sigma_{e-x} = \frac{5}{\pi}\frac{s_x}{Q}. \tag{П.4}$$

Наконец, после прямых вычислений (П.4) получаем

$$S_{e-x} = \gamma_{e-x} n_e n_x \frac{3}{2} k_{\mathrm{B}}(T_e - T_x), \qquad \gamma_{e-x} = 40\frac{\hbar a_x}{M+m_e}. \tag{П.5}$$

Список литературы

[1] Shank C.V., Fork R.L., Leheny R.F., Shah J. // Phys. Rev. Lett. 1979. V. 42. N 2. P. 112–115.
[2] Fehrenbach G.W., Schäder W., Treusch J., Ulbrich R.G. // Phys. Rev. Lett. 1982. V. 49. N 17. P. 1281–1284.
[3] Leite R.C.C., Shah J., Gordon J.P. // Phys. Rev. Lett. 1969. V. 23. N 23. P. 1332–1335.
[4] Sell D.D., Stokowski S.E., Dingle R., DiLorenzo I.V. // Phys. Rev. B. 1973. V. 7. N 10. P. 4568–4586.
[5] Aoki K., Kinugasa T., Yamamoto K. // Phys. Lett. A. 1979. V. 72. N 1. P. 63–66.
[6] Aoki K., Okuyama Y., Kobayashi T., Yamamoto K. // J. Phys. C. 1979. V. 12. N 4. P. 647–654.
[7] Rossin V.V., Christianen P.C.M., Travnikov V.V. // Sol. St. Commun. 1993. V. 87. N 7. P. 623–626.
[8] Shultheis L., Kuhl J., Honold A., Tu C.W. // Phys. Rev. Lett. 1986. V. 57. N 13. P. 1635–1638.
[9] Аавиксоо Я.Ю., Рейманд И.Я., Россин В.В., Травников В.В. // ФТТ. 1991. Т. 31. № 8. С. 2408–2412.
[10] Aaviksoo J., Reimand I., Rossin V.V., Travnikov V.V. // Phys. Rev. B. 1992. V. 45. N 3. P. 1473–1476.
[11] Голубев В.Г., Жиляев Ю.В., Иванов-Омский В.И., Маркарян Г.Р., Осутин А.В., Челноков В.Е. // ФТП. 1987. Т. 21. № 10. С. 1771–1776.
[12] Weisbuch C. // Solid St. Electr. 1978. V. 21. N 1. P. 179-183.
[13] Ulbrich R. // Phys. Rev. B. 1973. V. 8. N 12. P. 5719–5727.
[14] Tait W.C., Weigher R.L. // Phys. Rev. 1969. V. 178. N 5. P. 1404–1410.
[15] Абакумов В.Н., Перель В.И., Яссиевич И.Н. // ЖЭТФ. 1980. Т. 78. № 3. С. 1240–1252.
[16] Erginsoy C. // Phys. Rev. 1950. V. 79. N 6. P. 1013–1014.

Физико-технический институт
им. А.Ф.Иоффе РАН
Санкт-Петербург

Поступило в Редакцию
14 декабря 1993 г.

X

С. О. Когновицкий, В. В. Травников, Я. Аавиксоо, И. Рейманд,
“Рассеяние света электронами в области экситонного
поглащения GaAs”,
ФТТ том 39, стр. 1011, (1997).

Рассеяние света электронами в области экситонного поглощения GaAs

© С.О. Когновицкий, В.В. Травников, Я. Аавиксоо, И. Рейманд

Физико-технический институт им.А.Ф.Иоффе Российской академии наук,
194021 Санкт-Петербург, Россия
Институт физики Академии наук Эстонии,
EE-2400 Тарту, Эстония

(Поступила в Редакцию 14 августа 1996 г.
В окончательной редакции 4 октября 1996 г.)

Исследовано влияние дополнительной генерации фотовозбужденных электронов на спектры экситонного поглощения и люминесценции сверхчистых образцов GaAs при $T = 2$ K. Показано, что обнаруженное увеличение коэффициента поглощения для основного ($n = 1$) экситонного состояния связано с поляритонным характером энергетического спектра этого состояния и обусловлено увеличением поляритонного затухания. Рост затухания при генерации электронов вызывается процессами рассеяния поляритонов на горячих электронах в процессе термализации последних. При этом происходит нагрев поляритонов. Причиной изменений, обнаруженных в спектрах люминесценции, является обратный процесс–нагрев электронов и охлаждение поляритонов.

Энергетические состояния экситонов и свободных носителей формируют энергетический спектр в области собственного поглощения полупроводников. При фотовозбуждении носители и экситоны могут взаимодействовать между собой. Это взаимодействие носит двоякий характер. С одной стороны, воздействие свободных носителей за счет экранирования кулоновского взаимодействия может изменять энергетический спектр полупроводника (положение края запрещенной зоны, энергию связи и силу осциллятора экситона и т.д.). С другой стороны, экситон-электронное взаимодействие может приводить к рассеянию экситонов и электронов друг на друге в пределах своих зон. Экранирование обычно проявляется при больших интенсивностях фотовозбуждения. В частности, в спектрах поглощения экранирование может приводить к полному исчезновению экситонных линий [1–3]. Рассеяние экситонов и электронов друг на друге проявляется при умеренных интенсивностях возбуждения. До сих пор оно исследовалось при изучении спектров люминесценции и проявлялось в основном либо в особенностях формы линий излучения основного экситонного состояния [4,5], либо в особенностях кинетики излучения этого состояния [6,7]. Целью данной работы являлось выяснение влияния экситон-электронного рассеяния на спектры поглощения света.

1. Экспериментальные результаты

В настоящей работе исследовались тонкие (~ 500 nm) кристаллы GaAs, которые получались путем полировки и последующего химического травления из образцов, аналогичных сверхчистым образцам, использованным в работах [6–8]. Спектры поглощения исследовались при $T = 2$ K в спектральной полосе "пробного" пучка света, выделяемой монохроматором МДР-12 из сплошного спектра лампы накаливания. Полоса подбиралась таким образом, чтобы свести к минимуму возбуждение свободных носителей и надежно измерять линии поглощения основного ($n = 1$) и возбужденного ($n = 2$) экситонных состояний. Накачка свободных носителей осуществлялась двумя способами. В первом случае она выполнялась с помощью непрерывного гелий-неонового или аргонового лазера ($\lambda = 632.8$ или 514.5 nm). Излучение в этом случае регистрировалось с помощью стандартной методики счета фотонов. Во втором случае для генерации носителей использовался импульс лазера на красителе длительностью 5 ps, а полуширина аппаратной функции системы регистрации составляла 300 ps. Импульсное возбуждение и регистрация использовались нами также и при исследовании временной кинетики люминесценции. Накачка носителей приводит не только к изменению пропускания, но и к появлению в области экситонных резонансов люминесценции, интенсивность которой в некоторых случаях была сравнимой с интенсивностью сигнала пропускания. Далее представлены результаты измерения "чистого" пропускания, которые получались вычитанием сигнала люминесценции из суммарного регистрируемого сигнала.

На рис. 1 спектр *1* является исходным спектром пропускания, полученным без дополнительной подсветки. Спектр *2* получен в тех же условиях, но при одновременной генерации носителей непрерывным He–Ne-лазером (интенсивность фотовозбуждения (I_{ex}) в этом случае равнялась $I_{ex} = 1\,\mathrm{W/cm^2}$). Дополнительная генерация носителей существенным образом меняет спектр пропускания. Характер изменения поглощения для основного и возбужденного состояний диаметрально противоположен. В области основного состояния поглощение при генерации свободных носителей увеличивается, а в области максимума возбужденного состояния оно уменьшается. Аналогичные результаты получены и при импульсной подсветке.

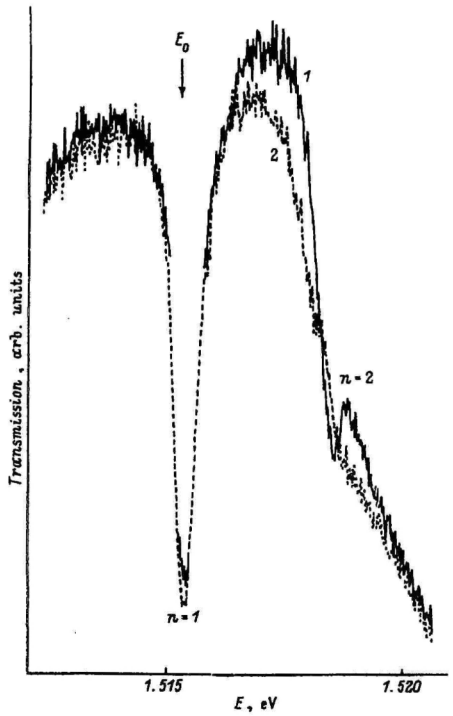

Рис. 1. Спектр пропускания тонкого образца GaAs без (*1*) и при (*2*) одновременной добавочной фотогенерации носителей. Стрелка E_0 соответствует энергии дна зоны основного экситонного состояния.

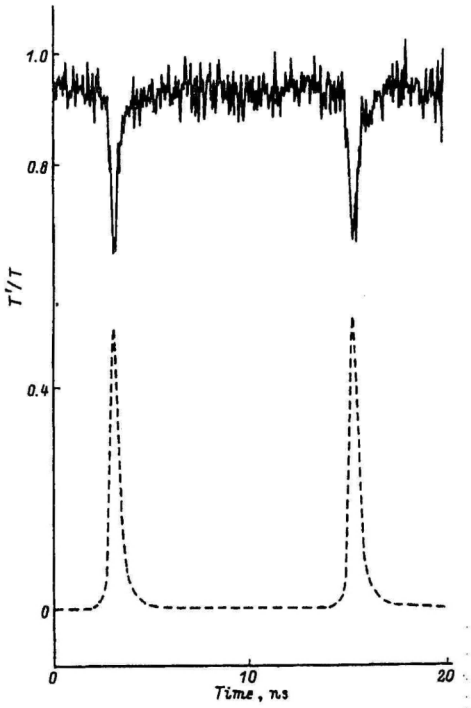

Рис. 2. Временна́я зависимость отношения сигнала пропускания с подсветкой к величине сигнала пропускания без подсветки. Штриховой линией представлен импульс возбуждающего лазера.

На рис. 2 представлена развертка во времени величины отношения сигнала пропускания с подсветкой (T') к величине сигнала пропускания без подсветки (T). Сигнал пропускания регистрировался на длине волны, соответствующей максимуму поглощения основного состояния. Из рис. 2 видно, что при импульсной подсветке, как и в случае непрерывной, поглощение в области основного состояния возрастает.

С ростом накачки наряду с изменениями в спектре пропускания происходят изменения и в спектре люминесценции исследованных тонких образцов. На рис. 3 представлены спектры люминесценции одного из тонких образцов при двух значениях интенсивности возбуждающего света. Спектр *1* соответствует спектру люминесценции тонкого образца, полученному при минимально возможной интенсивности подсветки, когда никаких изменений в спектре поглощения не наблюдается. Спектр *2* получен при $I_{ex} = 7\,\mathrm{W/cm^2}$, когда изменения в спектре поглощения весьма существенны. Рис. 3 показывает, что интенсивности подсветки, существенно меняющие спектр поглощения, изменяют заметным образом и спектр люминесценции. Несмотря на некоторые отличия (связанные в основном с уменьшением относительной интенсивности излучения связанных экситонов [9]) общей формы спектров люминесценции тонких образцов от формы спектров люминесценции толстых образцов, исследованных нами ранее [8], общие закономерности изменения спектров люминесценции с ростом накачки одинаковы. Наиболее примечательной особенностью этого изменения является возникновение в области ниже энергии E_0 (E_0 — энергия дна экситонной зоны основного состояния) интенсивного длинноволнового хвоста линии поляритонной люминесценции (спектр *2* на рис. 3). При минимальной I_{ex} этот хвост практически отсутствует (спектр *1*). В толстых образцах хвост проявляется как "подставка" для линий D^0X, D^+X, A^0X, соответствующих излучению связанных экситонов. Спектральное положение линий излучения связанных

экситонов для кристаллов GaAs на рис. 3 указано стрелками. Сопоставление с положением стрелок показывает, что появляющийся с ростом I_{ex} хвост длинноволнового излучения располагается в спектральной области, соответствующей излучению связанных экситонов. Чтобы исключить сомнения, обусловленные возможной связью рассматриваемого хвоста с излучательной рекомбинацией связанных экситонов, мы провели исследование временно́й кинетики люминесценции одного из тонких образцов, в спектре люминесценции которого присутствовала отчетливая линия D^+X. Интегрированный по времени спектр люминесценции этого образца, полученный при импульсном возбуждении, представлен на вставке к рис. 4. Стрелками *a, b, c, d* на этой вставке указаны точки спектра, для которых исследовалась временна́я кинетика. Импульс люминесценции *1* на рис. 4 соответствует кинетике поляритонного излучения на энергии E_0 (стрелка *a*), а импульс *2* — кинетике излучения связанного экситона D^+X (стрелка *c*). Кинетика излучения в точках, отмеченных стрелками *b* и *d*, практически неотличима от кинетики резонансного поляритонного излучения (импульс *1*), и поэтому соответствующие им-

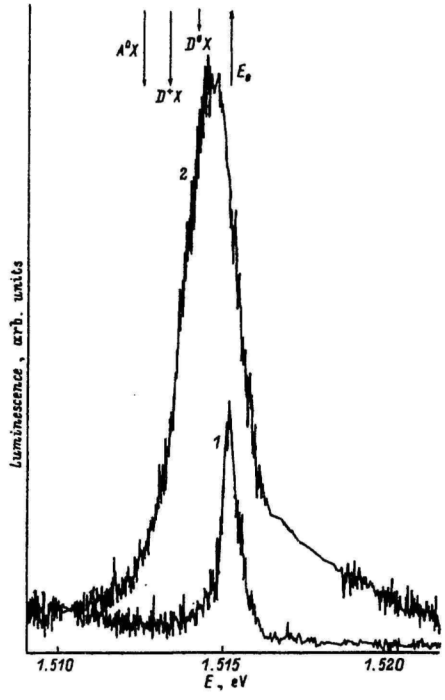

Рис. 3. Спектры люминесценции тонкого образца при двух значениях интенсивности возбуждающего света.

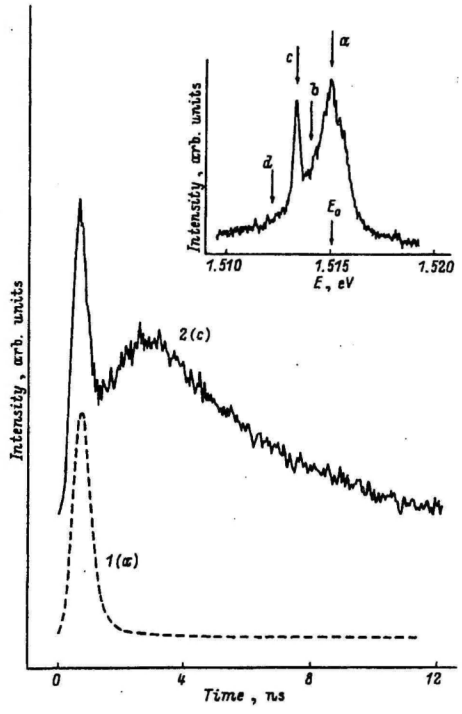

Рис. 4. Кинетика излучения для разных участков спектра поляритонной люминесценции одного из исследованных тонких образцов GaAs. На вставке представлен спектр люминесценции образца. Стрелками указаны участки спектра, для которых измерялась временна́я зависимость интенсивности излучения.

пульсы на рис. 4 не представлены. Затянутый во времени спад излучения D^+X соответствует большим временам излучательной рекомбинации, характерным для связанных экситонов [10]. Одинаковость кинетики для излучения, соответствующего разным точкам длинноволнового хвоста, и излучения из области резонанса свидетельствует в пользу их одинакового происхождения.

2. Обсуждение результатов

Результаты по изменению поглощения при генерации носителей являются довольно необычными. В выполненных ранее экспериментах дополнительная подсветка фотонами с энергией $E > E_g$ приводила не к увеличению, а к уменьшению поглощения в области максимума основного экситонного состояния. Это наблюдалось как при воздействии короткими импульсами большой интенсив-

ности [1–3], так и при модуляции поглощения на малых частотах слабо интенсивными потоками фотонов [11].

В экспериментах по фотопоглощению [11] наблюдаемая модуляция пропускания объяснялась изменением эффективной глубины поглощения в результате изменения приповерхностного поля за счет перезарядки поверхностных центров. Изменение приповерхностного поля довольно медленный процесс [11], и в нашем случае оно вряд ли может отвечать за основной эффект воздействия подсветки, поскольку, как это видно из рис. 2, максимальная модуляция пропускания происходит за короткие времена, сопоставимые с временны́м разрешением установки. Следует, однако, отметить, что существует и длинновременна́я компонента воздействия подсветки на спектр пропускания. На это указывает отличие величины T'/T от единицы в промежутке между импульсами возбуждения. В данной работе мы не будем обсуждать механизм этой длинновременно́й модуляции пропускания. Что же касается быстрой компоненты воздействия подсветки, то остается предположить, что она связана с воздействием носителей на объемный коэффициент поглощения.

Основным параметром, определяющим коэффициент экситонного поглощения, является затухание экситонов Γ. Для выделенного экситонного резонанса в зависимости от соотношения величины Γ и некоторой критической величины затухания Γ_c, определяемой силой осциллятора рассматриваемого экситонного резонанса, существуют две альтернативные возможности рассмотрения свойств экситонного резонанса [12,13]. При $\Gamma < \Gamma_c$ необходим учет поляритонного эффекта. Коэффициент поглощения поляритонов α прямо пропорционален величине затухания Γ [14]

$$\alpha = \Gamma/v, \qquad (1)$$

где v — групповая скорость поляритонов. Если $\Gamma > \Gamma_c$, экситоны и фотоны в кристалле могут рассматриваться как независимые квазичастицы. В этом случае линия экситонного поглощения аппроксимируется лоренцевским контуром, и величина коэффициента поглощения на частоте резонанса обратно пропорциональна величине Γ ($\alpha(E_0) \sim 1/\Gamma$).

Результаты, представленные на рис. 1, с учетом вышесказанного однозначно указывают на то, что генерация носителей приводит к увеличению затухания экситонов. Для состояния $n = 1$ реализуется поляритонный подход ($\Gamma < \Gamma_c$) [8], и поэтому генерация носителей приводит к возрастанию коэффициента поглощения. Для возбужденного состояния ситуация соответствует случаю $\Gamma > \Gamma_c$. Это и понятно, поскольку сила осциллятора состояния $n = 2$ в 8 раз меньше силы осциллятора состояния $n = 1$, а его затухание за счет возможности перехода в $n = 1$ существенно больше. В дальнейшем мы будем анализировать лишь изменения, происходящие в области состояния $n = 1$, для которого справедлив поляритонный подход и для которого возможна оценка параметров, определяющих величину экситонного коэффициента поглощения.

Для экспериментальной оценки изменения величины экситонного затухания ($\Delta\Gamma$) нами измерена величина изменения экситонного поглощения на частоте, соответствующей максимуму поглощения линии $n = 1$. Оказалось, что коэффициент поглощения при $I_{ex} = 5\,\mathrm{W/cm^2}$ увеличивается на величину, равную $\Delta\alpha = 0.5 \cdot 10^4\,\mathrm{cm^{-1}}$. При оценке величины $\Delta\alpha$ нами учитывалось измеренное изменение коэффициента отражения, которое также имеет место при подсветке. Используя значение групповой скорости для поляритонов нижней ветви на энергии, соответствующей максимуму поглощения, находим, что затухание в области резонанса возрастает на величину, равную $\Delta\Gamma = 7.4 \cdot 10^9\,\mathrm{s^{-1}}$.

Величина экситонного затухания определяется всеми процессами ухода поляритонов из состояния с заданными энергией и волновым вектором. Схематически процессы, определяющие затухание поляритонов, представлены на рис. 5. Обычно (см., например, [14,15]) при рассмотрении процессов, определяющих Γ, учитывались процессы ухода в другие поляритонные состояния за счет неупругого рассеяния на фононах (акустических (LA) и оптических (LO)) и упругого рассеяния на примесях (imp), а также процессы безызлучательной (nr) гибели экситонов (рис. 5,*a*):

$$\Gamma = \Gamma_{LA} + \Gamma_{LO} + \Gamma_{\mathrm{imp}} + \Gamma_{\mathrm{nr}}. \qquad (2)$$

В принципе дополнительное возбуждение носителей может изменять все указанные в уравнении (2) парциальные величины Γ. За счет антистоксовых процессов рассеяния на фононах (LA^+, LO^+) (рис. 5,*a*), рождающихся в ходе энергетической релаксации свободных носителей, могут увеличиваться значения Γ_{LO} и Γ_{LA}. Однако использованные нами небольшие интенсивности возбуждения не могут привести к существенному изменению чисел заполнения в фононной подсистеме [16], и поэтому взаимодействие с фононами вряд ли может быть причиной увеличения Γ. При дополнительной генерации носителей могут меняться и величины затухания, обусловленные взаимодействием экситонов с примесями. С одной стороны, с ростом концентрации фотовозбужденных носителей происходит насыщение центров безызлучательной гибели экситонов, и величина Γ_{nr} может уменьшаться. С другой стороны, может возрастать величина Γ_{imp}, обусловленная упругим рассеянием экситонов на различных центрах, поскольку после локализации на них носителей они из центров захвата могут превращаться в центры упругого рассеяния [8,17]. Оценить изменение затухания за счет взаимодействия экситонов с примесями практически невозможно, поскольку нам неизвестны ни тип, ни концентрация центров, определяющих величины Γ_{nr} и Γ_{imp}. Можно лишь сказать, что подходящее для объяснения экспериментальных результатов увеличение Γ_{imp} должно компенсироваться соответствующим уменьшением величины Γ_{nr}, что ставит под сомнение объяснение наблюдаемого эффекта и за счет взаимодействия с примесями.

При генерации носителей в полупроводнике вклад в затухание поляритонов помимо рассмотренных процессов могут вносить также процессы ухода поляритонов

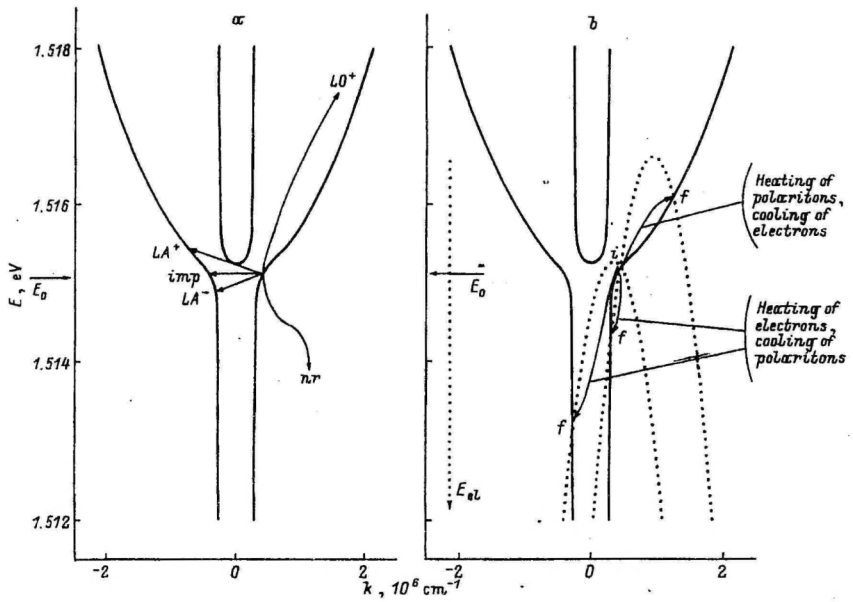

Рис. 5. Энергетическая диаграмма процессов, ответственных за затухание поляритонов. Сплошными линиями представлены дисперсионные кривые поляритонов, а пунктиром — параболы, соответствующие зоне проводимости.

в другие состояния за счет непосредственного рассеяния поляритонов на носителях. В первом приближении величина соответствующего затухания может быть оценена как вероятность рассеяния экситона (без учета поляритонных эффектов) на носителях [7,18]

$$\Gamma = 20\hbar a_x n/m, \qquad (3)$$

где a_x — боровский радиус экситона, n и m — концентрация и эффективная масса носителя. Формула (3) показывает, что эффективность взаимодействия возрастает с увеличением боровского радиуса и уменьшением эффективной массы носителя. В GaAs боровский радиус экситона доволно велик ($a_x = 14$ nm), а эффективная масса электрона мала ($m_e = 0.06m_0$), она существенно меньше эффективной массы дырки ($m_h = 0.5m_0$). Это приводит к эффективному взаимодействию экситонной и электронной подсистем в GaAs, наблюдавшемуся ранее в особенностях временной кинетики экситонной люминесценции примерно при таких же интенсивностях фотовозбуждения [6,8], которые использованы нами для дополнительной подсветки.

Оценим, каким концентрациям электронов соответствует измеренное значение $\Delta\Gamma$, если предположить, что оно полностью обусловлено экситон-электронным взаимодействием. Для этого воспользуемся формулами (1), (3), взяв величину групповой скорости на энергии, соответствующей максимуму поглощения. В результате получаем $n = 1.5 \cdot 10^{13}\,\mathrm{cm}^{-3}$. Это вполне разумное значение концентрации для использованных нами интенсивностей накачки. Для $I_{ex} = 5\,\mathrm{W/cm}^2$ такая концентрация электронов соответствует времени жизни свободных электронов, равному $\tau = 1 \cdot 10^{-11}$ s. Это время заметно меньше величины τ, использованной нами ранее для толстого образца. Такое уменьшение обусловлено, очевидно, увеличением влияния поверхностной рекомбинации на время жизни в тонком образце.

Таким образом, приведенные оценки разумно согласуются с предположением о том, что наблюдаемые при генерации носителей изменения в спектре поглощения обусловлены экситон-электронным рассеянием.

Веским доводом в пользу того, что наблюдаемые в эксперименте изменения спектров экситонного поглощения связаны с экситон-электронным рассеянием, а не с процессами взаимодействия экситонов с фононами и примесями, является и то, что ни один из этих процессов не может объяснить возникновение длинноволнового хвоста излучения, появляющегося при генерации носителей. В то же время в рамках модели экситон-электронного рассеяния появление хвоста находит естественное объяснение.

Схематически процессы рассеяния, приводящие к образованию хвоста, представлены на рис. 5, *b*. На этом рисунке для наглядности начальная точка для процесса рассеяния в зоне проводимости и начальная точка на нижней поляритонной ветви совмещены в точке *i*. В связи с тем, что в силу закона сохранения энергии знаки изменения энергии поляритонов и электронов противоположны, ось кинетической энергии электронов на рисунке направлена вниз. Рис. 5, *b* ясно показывает, что в результате взаимодействия с электронами поляритоны могут непрерывным образом заселять состояния в области существенно ниже резонанса, формируя таким образом хвост линии поляритонной люминесценции. Поскольку заселение участков в области ниже резонанса происходит за счет рассеяния поляритонов, скапливающихся в области резонанса, кинетика излучения поляритонов в различных участках длинноволнового хвоста должна быть примерно одинаковой, что и наблюдается в эксперименте.

В [6,7] показано, что электрон-экситонное рассеяние может приводить к существенному гашению поляритонной люминесценции на ранних стадиях энергетической релаксации горячих электронов. На рис. 5, *b* этому соответствуют процессы, представленные в верхней части рисунка. Эти процессы сопровождаются охлаждением электронов и разогревом экситонной подсистемы. За формирование длинноволнового хвоста поляритонного излучения отвечает обратный процесс–разогрев электронов и охлаждение экситонной подсистемы (нижняя часть рисунка). Несмотря на то что этот обратный процесс весьма заметно проявляется в наблюдаемых спектрах люминесценции, основное влияние на величину экситонного затухания оказывает, очевидно, процесс разогрева экситонной подсистемы, поскольку плотность конечных состояний для этого процесса существенно превышает плотность фотоноподобных состояний в области ниже резонанса.

Эффекты экситон-электронного рассеяния играют, по-видимому, существенную роль и при больших плотностях возбуждения, когда влияние на спектр экситонного поглощения оказывают эффекты экранирования [1–3]. Экранирование уменьшает энергию связи экситона, приводя к увеличению его боровского радиуса, что наряду с увеличением концентрации электронов приводит к увеличению вероятности экситон-электронного рассеяния.

Таким образом, в отличие от ранее выполненных экспериментов при подсветке фотонами, создающими носители, обнаружено существенное уменьшение пропускания света в области основного экситонного состояния кристаллов GaAs. Наблюдаемый эффект объясняется ростом величины затухания экситонов за счет их рассеяния на электронах. Отличие от выполненных ранее экспериментов связано с тем, что в использованном диапазоне интенсивностей подсветки в наших сверхчистых образцах для основного состояния реализуется поляритонный подход, в котором увеличение затухания приводит к росту коэффициента поглощения.

Авторы признательны Л.М. Федорову за предоставленные для исследований сверхчистые кристаллы GaAs и Н.Д. Ильинской за изготовление тонких образцов.

Работа выполнена при поддержке Российского фонда фундаментальных исследований и Международного научного фонда.

Список литературы

[1] J. Shah, R.F. Leheny, W. Wiegmann. Phys. Rev. **B16**, *4*, 1577 (1977).
[2] C.V. Shank, R.L. Fork, R.F. Leheny, J. Shah. Phys. Rev. Lett. **42**, *2*, 112 (1979).
[3] G.W. Fehrenbach, W. Schafer, J. Treusch, R.G. Ulbrich. Phys. Rev. Lett. **49**, *17*, 1281 (1982).
[4] K. Aoki, T. Kinugasa, K. Yamamoto. Phys. Lett. **72A**, *1*, 63 (1979).
[5] E. Gobel, K.L. Shaklee, R. Epworth. Solid State Commun. **17**, *9*, 1185 (1975).
[6] J. Aaviksoo, I. Reimand, V.V. Rossin, V.V. Travnikov. Phys. Rev. **B45**, *3*, 1473 (1992).
[7] Я. Аавиксоо, И. Рейманд, В.В. Россин, В.В. Травников. ФТТ **36**, *5*, 1470 (1994).
[8] Ю.В. Жиляев, Г.Р. Маркарян, В.В. Россин, Т.В. Россина, В.В. Травников. ФТТ **28**, *9*, 2688 (1986).
[9] W.L. Bloss, E.S. Koteles, E.M. Brody, B.J. Sowell, J.P. Salerno, J.V. Cormly. Solid State Commun. **54**, *1*, 103 (1985).
[10] Э.И. Рашба. ФТП **8**, *7*, 1241 (1974).
[11] А.В. Варфоломеев, Р.П. Сейсян, Ю.Л. Шелехин. ФТП **10**, *6*, 1063 (1976).
[12] W.C. Tait. Phys. Rev. **B5**, *2*, 648 (1972).
[13] M. Matsushita, I. Wicksted, H.Z. Cummins. Phys. Rev. **B29**, *6*, 3362 (1984).
[14] W.C. Tait, R.L. Weiher. Phys. Rev. **178**, *3*, 1404 (1969).
[15] В.В. Травников, В.В. Криволапчук. ЖЭТФ **85**, *12*, 2087 (1983).
[16] J. Shah. Sol. State Electron. **21**, *1*, 43 (1978).
[17] В.В. Травников, В.В. Криволапчук. ФТТ **28**, *4*, 1210 (1986).
[18] R.C.C. Leite, J. Shah, J.P. Gordon. Phys. Rev. Lett. **23**, *23*, 1332 (1969).

XI

I. Reimand, E. Gminder, M. Kirm, V. Kisand, B. Steeg,
D. Varding, G. Zimmerer,
"An analysis of electron-hole recombination in solid Xenon with
time-resolved luminescence spectroscopy",
Phys. Stat. Sol. (b), vol. 214, no 1, p. 81 (1999).

phys. stat. sol. (b) **214**, 81 (1999)

Subject classification: 71.35.Aa; 78.47.+p; 78.55.Hx; S5.2

An Analysis of Electron–Hole Recombination in Solid Xenon with Time-Resolved Luminescence Spectroscopy

I. REIMAND (a), E. GMINDER (b), M. KIRM (b), V. KISAND (b), B. STEEG (b), D. VARDING (b), and G. ZIMMERER[1]) (b)

(a) Institute of Experimental Physics and Technology, Tartu University, Tähe 4, EE-2400 Tartu, Estonia

(b) II. Institut für Experimentalphysik der Universität Hamburg, Luruper Chaussee 149, D-22761 Hamburg, Germany

(Received July 27, 1998; in revised form April 1, 1999)

The formation of free excitons in solid Xe from photogenerated electron–hole pairs was investigated with time-resolved luminescence spectroscopy. The initial kinetic energy of the photocarriers was varied over a large range by an appropriate choice of photon energy of excitation. The decay curves of the free-exciton luminescence yield a cascade-type behaviour. The experimental results were reproduced with model calculations including thermalization via scattering on acoustic phonons and a recombination cross-section which depends on the actual carrier temperatures. Good agreement between experiment and theory was found.

1. Introduction

The onset of optical absorption of solid Xe in the vacuum ultraviolet spectral range is governed by excitonic excitations [1 to 4]. Recently, it was possible to resolve up to six members of the exciton series in the reflectivity spectra of samples with high structural quality [5]. The energetic positions of the excitons are well described by the Wannier formula, $E_n = E_g - B/n^2$ (band gap energy $E_g = (9.298 \pm 0.005)$ eV, binding energy $B = (0.94 \pm 0.05)$ eV, both values at $T = 5$ K; n being the main quantum number).

Several methods to create excitons in rare-gas solids, and in particular in solid Xe, have already been used, (i) direct photon excitation [1 to 4], (ii) energy loss of either excess electrons (external electron beam [6]) or of 'hot' photo electrons [7], (iii) creation of electronic polaron complexes [7], and (IV) recombination of electron–hole pairs [8]. The purpose of the present paper is a more detailed analysis of electron–hole recombination. There is a general need to understand the microscopic mechanism of electron–hole recombination because this is one of the most important steps in the scintillation process of scintillators [9].

The lack of optical phonons in the atomic f.c.c. lattice is responsible for unique transport properties of (photo-) carriers. Thermalization of 'hot' electrons is slowed down dramatically compared to other insulators and semiconductors. This was demonstrated in, e.g., time-resolved transient conductivity measurements [10]. At $T = 157$ K, Sowada

[1]) Corresponding author. Tel.: 040-8998 2288, Fax: 040-8998 2787, e-mail: georg.zimmerer@desy.de

et al. [10] observed a thermalization time $\tau_{th} = 4.4$ ns. Taking into account that τ_{th} is proportional to $T\mu_0$ (μ_0 being the low field mobility) with μ_0 proportional to $T^{-3/2}$ (scattering on acoustic phonons), the thermalization time at $T = 5$ K is of the order of 20 ns (this estimate is rough because other scattering mechanisms like scattering on defects and impurities speed up thermalization).

The low thermalization rates for hot electrons in rare-gas solids lead to unique properties of the electron mobility as a function of an applied electric field. The mobility is independent of the field strength only at low fields [11 to 13]. At a field strength of less than 1 kV/cm, the electric field starts heating up electrons. For solid Xe, electrons gain kinetic energy of the order of 10 eV at a field strength of less than 10^5 V/cm [14]. This should enable the construction of solid Xe-VUV lasers which are driven by an electric field [15].

In the present paper, a luminescence technique has been used for the analysis of the dynamical properties of photocarriers. Solid Xe has a strong luminescence line at $h\nu = 8.359$ eV originating from free excitons [8]. It is not only observed following primary excitation of excitons themselves (photon energy of excitation, $h\nu_{ex} < E_g$) but also following primary excitation of free electron–hole pairs ($h\nu_{ex} > E_g$). The temporal behaviour of the so-called FE-line of solid Xe was analyzed for a set of photon energies of excitation covering the range $E_g < h\nu_{ex} \leq 10.8$ eV. In other words, the initial kinetic energy of the photocarriers has been varied over a large range. Varding et al. [8] already showed that the decay curves sensitively depend on the initial kinetic energies of the carriers. The purpose of the present paper is an analysis of the results of Varding et al. The decay curves will be explained taking into account models for thermalization via scattering on acoustic phonons on one side and recombination of electron–hole pairs into excitons on the other side. The kinetics are so slow that the nanosecond techniques in connection with repetitive synchrotron radiation applied by Varding et al. [8] are well suited to observe thermalization and recombination of free carriers. Although the experimental curves have already been published [8], they are included because otherwise comparison with theory would be obsolete.

2. Experiment

The experiments were performed at the SUPERLUMI station [16] of the Hamburger Synchrotronstrahlungslabor HASYLAB at DESY. All decay curves shown in this paper were obtained with a resolution interval $\Delta\lambda = 0.25$ nm in excitation and $\Delta\lambda = 1.5$ nm in luminescence analysis. The basis of time resolution is the pulsed nature of synchrotron radiation. At the storage ring DORIS in Hamburg, the light pulses have a FWHM of 130 ps. The number of photons per pulse was $\approx 10^5$ excluding two-photon processes. The measured FWHM of the pulses was 0.4 ns. The broadening arises from a convolution of the temporal behaviour of the excitation pulse, the response of the detector and of the electronics. Time-correlated single-photon counting was used. The photon detector was a channel-plate detector sensitized with a CsI coating.

The crucial part of the experiment was the sample preparation. With the set-up described in [17], samples were grown under nearly thermal equilibrium conditions at $T = 118$ K. The growing rate was $\approx 10^3$ nm/min, the preparation time was up to 18 h. In this way, bulk clear samples were obtained with a thickness up to ≈ 1 mm. The background pressure in the sample chamber was in the low 10^{-10} mbar range.

3. Experimental Results

In Fig. 1, a time-integrated luminescence spectrum of solid Xe is reproduced [8]. It was measured at T = 4.7 K, following primary excitation with $h\nu$ = 8.86 eV. This is well below the energy of n = 2 excitons (9.07 eV). In this way, electronic relaxation within the exciton series is avoided. On the other hand, the chosen photon energy of excitation is sufficiently away from the photon energy of the FE-line at 8.359 eV. In this way, the amount of scattered light from excitation spectrally overlapping with luminescence is minimized (but – as will be shown below – not zero!). The spectral resolution interval was 0.08 nm.

Besides the pronounced FE-line, a broad, Stokes shifted band centered around 7.2 eV is observed. It arises from self-trapped excitons (STE-band) and will not be discussed in this paper. The inset shows the decay curve of the spectrally selected FE-line. The decay is non-exponential. The rise is compatible with the temporal resolution of the experiment, however, scattered light from excitation may contribute to the measured rise. Note, the spectral resolution interval of the monochromator–detector system for the time-resolved measurements was much larger than for the time-integrated but spectrally resolved measurements.

The decay curves of the FE-line following primary selective excitation at and above the bandgap energy are displayed in Fig. 2. The parameter given in the figure is the excess energy

$$E_{\text{excess}} = h\nu_{\text{ex}} - E_g \,. \tag{1}$$

The decay curve obtained with $E_{\text{excess}} = 0$ deviates more from a single exponential behaviour but is still of the same type than the one shown in Fig. 1. With increasing E_{excess}, the shape develops into a cascade-type behaviour. Moreover, the kinetics are slowed down. The width of the narrow spike around delay = 0 yields the temporal reso-

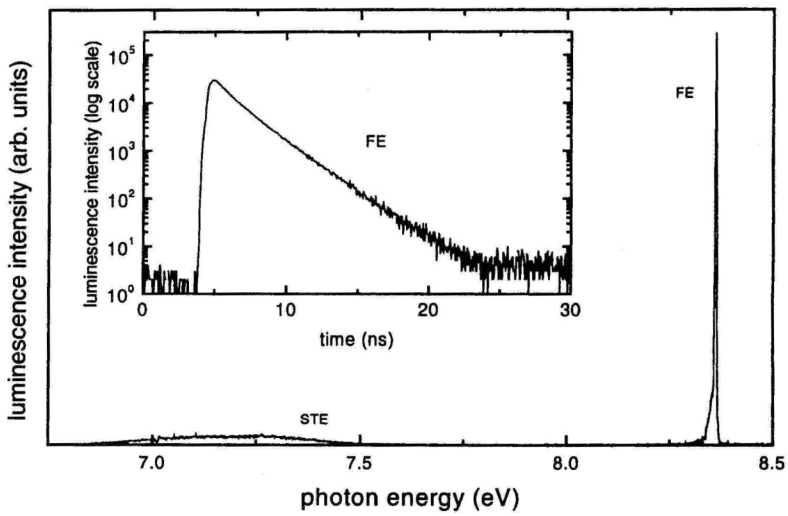

Fig. 1. Luminescence of solid Xe at T = 4.7 K, excited with synchrotron radiation (photon energy 8.86 eV). The inset shows a time-resolved spectrum of the FE-line at 8.359 eV. The figure was taken from Ref. [8]

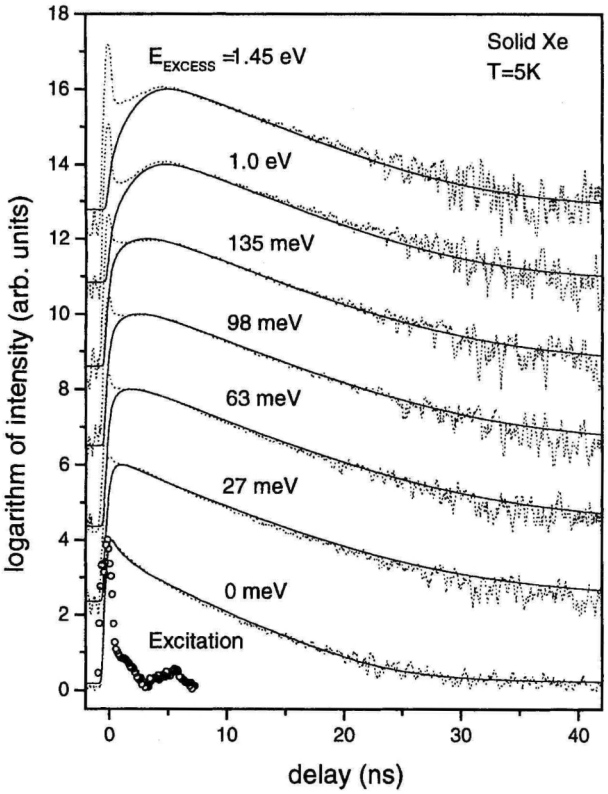

Fig. 2. Decay curves of the FE-luminescence line of solid Xe at $T = 5$ K, excited with different photon energies of excitation, $h\nu_{ex}$. The parameter given in the figure is the excess energy, $E_{excess} = h\nu_{ex} - E_g$ (E_g is the band gap energy). The dotted lines are measurements, the full curves are results of model calculations. For comparison purposes, the apparatus function (open circles) is included

lution of the experiment (scattered light). In contrast to the result in Fig. 1, in the curves of Fig. 2, scattered light plays a more pronounced role because the time-integrated intensity of the FE-line is approximately an order of magnitude lower following primary excitation of free electron–hole pairs compared to primary excitonic excitation. The full curves in Fig. 2 are results of the model calculations (see the following section).

4. Model Calculations

The observation of FE-luminescence following primary excitation of free electron–hole pairs clearly shows that free excitons are formed in electron–hole recombination. This is by far non-trivial because in the past it was assumed that the holes are trapped within some ps and than capture electrons forming *self-trapped* excitons. The latter mechanism is not ruled out by our results, but it is at least not the only recombination process. Whether or not the self-trapped excitons observed following excitation of free electron–hole pairs originate exclusively from self-trapping of free excitons or also from the capture of electrons by self-trapped holes cannot be decided on the basis of the results.

The description of the model requires a discussion of the initial conditions (kinetic energies and spatial density of the photocarriers immediately following the excitation pulse). According to energy and momentum conservation rules, at a given excess energy the electrons and holes (effective masses m_e and m_h) get an initial kinetic energy

E_e and E_h, respectively,

$$E_{e,h} = \frac{m_{h,e}}{m_e + m_h} E_{excess} . \tag{2}$$

The initial carrier density may be estimated from the absorption coefficient α (penetration depth of the exciting light $\sim 1/\alpha$) at the respective photon energy of excitation, from the photon flux, and from the size of the focus of the exciting radiation at the sample. The estimate is hampered by the fact that the literature values for α range between $\approx 3 \times 10^5\,cm^{-1}$ [18], $\approx 5 \times 10^5\,cm^{-1}$ [19], and $\approx 10^6\,cm^{-1}$ [20]. The absolute value of reflectivity is uncertain as well. An experimental parameter, namely the width of the strongly asymmetric focus (length = 0.4 cm, width = 0.02 to 0.04 cm) is also uncertain. Taking into account all uncertainties, an initial carrier density of the order of 10^{12} to $10^{13}\,cm^{-3}$ is estimated. As was shown by experiments on hot electron relaxation in semiconductors [21], on a short time scale (far below the time resolution of the present experiment), a redistribution of carriers which is attributed to carrier–carrier interaction results in quasi-equilibrium electron and hole temperatures (T_e and T_h). For semiconductors, the time required to establish Maxwellian-like velocity distributions is estimated to be in the sub-picosecond regime [22]. The carrier density N_0, established during redistribution, is treated in our model as an adjustable parameter.

From this point on, energy relaxation of charge carriers is mainly going on due to scattering on acoustic phonons, described by the deformation potential E_d. The averaged energy loss rate per electron (hole) in a Maxwellian distribution of temperature T_e (T_h) is given by [23, 24],

$$\left\langle \frac{dE_{e,h}}{dt} \right\rangle_{ac} = -\frac{8\sqrt{2}\, E_d^2 m_{e,h}^{5/2}}{\pi^{3/2}\hbar^4 \varrho} (kT_{e,h})^{3/2} \left(\frac{T_{e,h} - T_L}{T_{e,h}} \right) . \tag{3}$$

Here, ϱ is the crystal mass density, $\varrho = 3.781\,g/cm^3$ [4], k is the Boltzmann constant. The value of $E_d = 0.79$ eV, was given by Ratner [25]. This value is different from the one of excitons [4]. At the beginning, E_d was used in the calculations as an adjustable parameter. It turned out that the calculations are not sensitive for E_d within the more severe limitations to be discussed below. An important feature of the relaxation arises from the $m^{5/2}$ law. With $m_e = 0.35 m_0$ (m_0 being the free electron mass) and $m_h = 2.1 m_0$ [3, 4] it turns out that holes loose their kinetic energy at least two orders of magnitude faster than electrons. Therefore, in the following we assume $T_h = T_L$ (lattice temperature).

The creation of excitons from charge carriers is a complicated many-body quantum problem which in principle could be modelled by Monte-Carlo calculations [26]. However, the information obtained from our experimental curves is not sufficient for a reasonable modelling. We treated exciton formation from electrons and holes with a simple set of Boltzmann kinetic equations because the parameters involved have a clear physical sense, and because it is possible to describe the processes in the effective temperature approximation, including all temperature effects in the cross-section and in the relative velocities,

$$\frac{dn_{e,h}}{dt} = G(t) - \sigma(T_e)\, n_e n_h v_{rel}(T_e) , \tag{4a}$$

$$\frac{dn_{ex}}{dt} = \sigma(T_e)\, n_e n_h v_{rel}(T_e) - R(t) . \tag{4b}$$

Here, n_e, n_h and n_{ex} are the electron, hole, and exciton densities. $G(t)$ is the generation rate for electrons and holes. It is treated as δ-like. The shape of the apparatus function (see Fig. 2) is indeed narrow compared to the kinetics under discussion. Starting from initial quasi-equilibrium conditions means, $G(t)$ describes the δ-like creation of carriers with density N_0. $R(t)$ is the decay function of excitons. For $R(t)$, we took an experimental decay curve of FE-luminescence which was excited with a photon energy (9.29 eV) just below the band gap value [8]. In this way, all further relaxation processes *within* the exciton manifold including non-radiative decay channels, are taken into account. The mean relative velocity of electrons and holes, v_{rel}, is a function of T_e. The time dependence of T_e was calculated from Eq. (3) via

$$T_e(t) = \frac{2}{3k} E_e(t) . \tag{5}$$

The set of equations is not complete. Capture of carriers in traps and, e.g., non-radiative surface recombination are neglected (see below).

The calculation of the cross-section σ for electron–hole recombination is based on the theory by Abakumov et al. [27] in which exciton formation is treated as a continuation of energy relaxation of charge carriers into the *negative* excess energy region, i.e. into the bound states. Abakumov et al. assumed thermal equilibrium between holes and electrons. In the present case, electrons and holes are clearly not in equilibrium. In the Abakumov approach, the particle temperatures enter the final result *only* via the distribution functions and particle velocities. The parameter describing the magnitude of energy loss via scattering on LA phonons (energy loss rate per propagation length) does not depend on the particle energy. Consequently, in Eq. (11) of the paper of Abakumov et al. we can ad hoc modify the expression for the distribution $f(E)$ for the pairs at positive temperatures, replacing T^3 by $T_e^{3/2} T_L^{3/2}$ ($T_h = T_L$, see above). Then it follows

$$\sigma(T_e) = \frac{16\sqrt{2}\, e^6 E_d^2}{3\sqrt{3\pi}\, \hbar^4 s \varrho \varepsilon^3} \frac{m_e^3}{\sqrt{m_h}} \frac{1}{\sqrt{kT_L}\,(kT_e)^2} . \tag{6}$$

Here, e is the electron charge, s is the sound velocity, s = 830 m/s (averaged value) [1], and ε is the dielectric permeability, ε = 2.22 [4]. The model was solved numerically. The results are included in Fig. 2 as full lines. The measured data are reproduced quite well. $N_0 = 6 \times 10^{10}$ cm^{-3} was obtained from the fits. This value is smaller by a factor of ≈20 to 200 compared to the density estimated for the excitation process itself. Note, however, N_0 represents the carrier density *after* redistribution by carrier–carrier interaction [21]. As was already pointed out, the initial excitation volume has a thickness of the order of $1/\alpha \approx 10$ to 30 nm. Then, even the mean free path of a carrier may exceed $1/\alpha$ (an electron with a kinetic energy of 1 eV has a mean free path of the order of 60 to 600 nm for a scattering rate between 10^{13} to 10^{12} Hz). Moreover, as a consequence of the transverse size of the excitation volume (length, width $\gg 1/\alpha$), the diffusion of carriers can be treated as a one-dimensional problem. Under these particular excitation conditions, carrier diffusion during redistribution establishing the electron and hole temperature may account for an expansion of the charge cloud into the bulk of the sample thus enlarging the excitation volume.

Capture of carriers in traps and nonradiative surface losses may also contribute to the difference between the initial excitation density and the value of N_0. Concerning *free excitons*, a crude estimate for surface quenching under the conditions of the present ex-

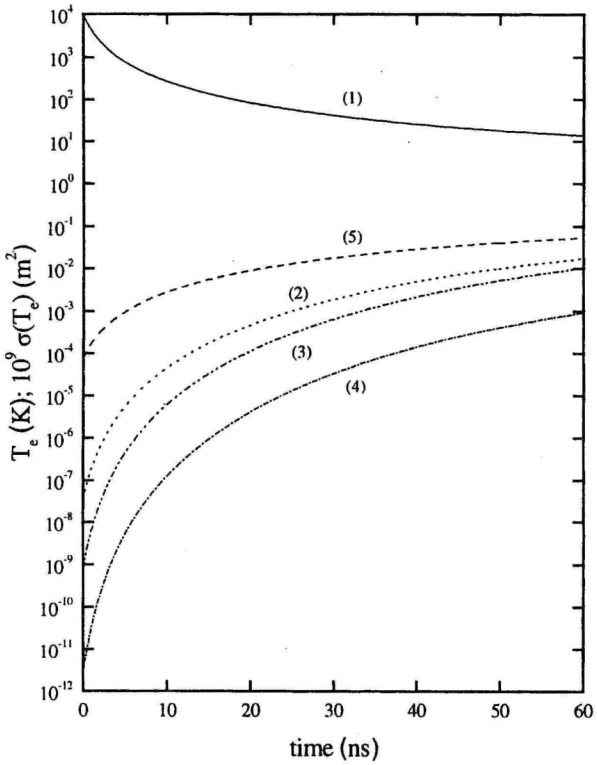

Fig. 3. (1) Electron temperature (Eq. (3)), (2) cross-section for electron–hole recombination (Eq. (6)), (3) cross-section for electron–hole recombination [27], (4) cross-section for capture of electrons at positively charged centers [30], and (5) ratio of (4) and (2). The initial electron energy was 1.24 eV. All curves are given as functions of time (the temperature is given in K, the cross-sections are given in 10^{-9} m^2)

periment brought about a factor of two [8]. It is already included in the treatment as was shown above. Detailed information on nonradiative surface recombination of *free carriers* is missing for rare gas solids. Therefore, this quenching channel was omitted in the model.

Electron capture in deep traps was already observed in two-photon photoemission experiments [31]. The peculiar temperature dependence of the luminescence yield of solid Xe which is nearly constant up to T = 50 K but then increases is also an indication of electron capture (electrons being released for $T > 50$ K). Up to T = 60 K, the yield doubles [8]. Therefore, electron capture may contribute at least a factor of two to the discrepancy under discussion.

In order to get more insight into the recombination dynamics in solid Xe, we present in Fig. 3 the electron temperature (integration of Eqs. (4) and (5)) and the recombination cross-section (Eq. (6)) as a function of time. The initial conditions correspond to E_{excess} = 1.45 eV (initial electron energy 1.24 eV, T_e = 9590 K). The electrons never reach thermal equilibrium with the lattice within the time interval of observation. As a consequence of the strong variation of T_e, the recombination cross-section yields an even more pronounced variation over nearly four orders of magnitude. The other curves shown in Fig. 3 will be discussed below.

5. Discussion of Some Assumptions

In spite of the simplifications, the results of the calculations fit the experimental results quite well. Nevertheless, it is indispensable to discuss some hidden assumptions of the model.

(i) The calculation of initial kinetic energies according to Eq. (2) assumes a parabolic band approximation. This assumption is valid only for small E_{excess}. Moreover, due to the fact that the valence bands of rare gas solids are narrow, the initial kinetic energy of a hole is strongly *limited*. The total width of the valence bands (including both the $j = 3/2$ and 1/2 bands) in solid Xe, e.g., is about 3 eV [3]. From the highest value of E_{excess} used in this paper, we obtain 0.207 eV as initial kinetic energy of holes. This is within the possible range, however, the parabolic approximation may no longer be applicable for such a value.

The estimate of an initial electron temperature T_e from the initial electron energy is an upper limit because the short period of redistribution includes energy exchange between the electron and the hole subsystem. An incorrect initial T_e mainly influences the dynamical behaviour at short times in which the experimental data are uncertain due to the scattered light superimposed.

Another complication arises from the fact that the effective-mass tensor of the holes is strongly anisotropic [25, 28]. The upper valence band in the Γ–L direction of the Brillouin zone has nearly no dispersion. This would give rise to a larger initial energy for electrons than calculated from Eq. (2). Therefore, the initial energy distribution between holes and electrons calculated from Eq. (2) is only a rough estimate.

(ii) A serious hidden assumption concerns the use of Eq. (6) which is valid for *mobile* holes and electrons. For rare gas solids, it is generally assumed that holes are self-trapped after creation within pico-seconds. Only for solid Xe, recent calculations by Umehara [29] show that the self-trapped hole state may be metastable or nearly on the stability boundary. In this context we would like to mention that the self-trapping probability of *excitons* in solid Xe is very low. An upper limit for the intrinsic self trapping rate, $\Gamma_{ST,intrinsic} \approx 0.5 \times 10^8\ s^{-1}$ was given in [8]. However, the self-trapping behaviour of excitons and holes may be very different.

Nevertheless, we compared the cross-section given by Eq. (6) with the cross-section for recombination of an electron with a positively charged center in a semiconductor [30]. The result is included in Fig. 3. Again, the time dependence arises from the variation of the electron temperature. The cross-section is remarkably lower than the one calculated from Eq. (6). The ratio of both cross-sections (in Fig. 3) is nearly constant at longer times. At short times, the ratio itself depends on time. Using the cross-section for recombination at positively charged centers instead of the cross-section for recombination of mobile holes in solving Eqs. (4a) and (4b) would mainly change the value of the product $N_{0,el}N_{0,h} \approx N_0^2$. An additional change of N_0 would originate from the relative velocity which is proportional to $\sqrt{1/\mu}$ (μ is the reduced mass of free electron–hole pair) in one case, and to $\sqrt{1/m_e}$ in the other case. Apart from the change of N_0, mainly the rising part of the calculated curves would be influenced. This will be masked by the scattered light (spike).

The choice between both types of cross-section is impeded by the fact that we observe *mobile* excitons. In other words, recombination of electrons with self-trapped holes being observed in the experiment results in a free exciton. This case is not covered by the theory on recombination at a positively charged center [30].

In Fig. 3, we also included the calculation of the recombination cross-section as given in [27]. In this case, thermal equilibrium between holes and electrons is assumed. The deviations between this curve and the modified cross-section (Eq. (6)) are rather small over the entire range of time. Therefore, our modification seems to be reliable.

(iii) The bimolecular-type recombination as described by Eq. (4b) could be checked, of course, with a variation of the excitation density over a large range. This is beyond the present experimental possibilities at HASYLAB. The variation of the excitation density which is compatible with the sensitivity of the experiment covers at most a factor of two which is by far too small to perform a systematic study. The new VUV free-electron laser under construction at HASYLAB [32, 33] will change the situation drastically.

6. Conclusions

The recombination dynamics of electron–hole pairs in a wide bandgap material without optical phonons have been investigated for the first time with time-resolved luminescence experiments. Free excitons have been used as a probe of recombination. The initial excess energy of the carriers was varied over a large range, $E_{\text{excess}} \gg kT_{\text{L}}$. In this way, rather slow thermalization of carriers via scattering on acoustic phonons comes into play. In spite of many simplifications, it was possible to fit the experimental curves with the results of model calculations taking into account exclusively acoustic phonons. The evolution of the electron temperature as a function of time is the key for an understanding of the strong variation of the recombination cross-section that governs the observed kinetics. Good agreement concerning thermalization of hot photoelectrons with earlier results obtained with other methods like electrical conductivity was found.

A quite natural extension of the measurements concerns the temporal behaviour of the luminescence of self-trapped excitons in rare gas solids. In solid Ar, Kr, and Xe, a fast STE luminescence band (lifetime of the order of 1 ns) originating from $^1\Sigma_u^+ \rightarrow {}^1\Sigma_g^+$ transitions of the molecular-type STE is known [1, 3, 4]. This band should be well suited to study the recombination dynamics and in particular to answer the question whether or not the free excitons are the only precursors of the self-trapped excitons. Such experiments are in progress now.

Acknowledgements The work was supported by the Bundesministerium für Bildung und Forschung (BMBF) of Germany (grant No. 05 650GUB), and by the Deutsche Forschungsgemeinschaft DFG (grant No. Zi 159/2-1). M.K. is grateful for financial support from the STINT Foundation (Sweden), and I.R. acknowledges financial support from the exchange programme of the universities of Tartu and Hamburg.

References

[1] I.Ya. Fugol, Adv. Phys. **27**, 1 (1978); **37**, 1 (1988).
[2] V. Saile, Appl. Optics **19**, 4115 (1980).
[3] N. Schwentner, E.-E. Koch, and J. Jortner, Electronic Excitations in Condensed Rare Gases, Springer Tracts Mod. Phys., Vol. 107, Springer-Verlag, Berlin 1985.
[4] G. Zimmerer, in: Excited State-Spectroscopy in Solids, Eds. U.M. Grassano and N. Terzi, North-Holland Publ. Co., Amsterdam 1987 (p. 37).
[5] G. Zimmerer, J. Low-Temp. Phys. **111**, 629 (1998).
[6] J.D. Nuttall, T.E. Gallon, M.G. Devey, and J.A.D. Matthew, J. Phys. C **8**, 445 (1975).
[7] B. Steeg, M. Kirm, V. Kisand, S. Körding, S. Vielhauer, and G. Zimmerer, J. Low-Temp. Phys. **111**, 739 (1998).
[8] D. Varding, I. Reimand, and G. Zimmerer, phys. stat. sol. (b) **185**, 301 (1994).
[9] V.V. Mikhailin, Nucl. Instrum. and Methods **B97**, 530 (1995).
[10] U. Sowada, J.M. Warman, and M.P. de Haas, Phys. Rev. B **25**, 3434 (1982).

[11] L.S. MILLER, S. HOWE, and W.E. SPEAR, Phys. Rev. **166**, 871 (1968).
[12] E.M. GUSHCHIN, A.A. KRUGLOV, and I.M. OBODOVSKII, Soviet Phys. – J. Exper. Theor. Phys. **55**, 650 (1982).
[13] S. KUBOTA, T. TAKAHASHI, and J. RUAN(GEN), J. Phys. Soc. Jpn. **51**, 3274 (1982).
[14] E.B. GORDON, V.V. KHMELENKO, and O.S. RZHEVSKY, Chem. Phys. Lett. **217**, 605 (1994).
[15] E.B. GORDON, O.S. RZHEVSKII, and V.V. KHMELENKO, Quantum Electronics **21**, 209 (1994).
[16] G. ZIMMERER, Nucl. Instrum. and Methods **A308**, 178 (1991).
[17] W. LAASCH, H. HAGEDORN, T. KLOIBER, and G. ZIMMERER, phys. stat. sol. (b) **158**, 753 (1990).
[18] S.R. SCHARBER and S.E. WEBBER, J. Chem. Phys. **55**, 3985 (1971).
[19] I.T. STEINBERGER, C. ATLURI, and O. SCHNEPP, J. Chem. Phys. **52**, 2723 (1970).
[20] J.L. SUBTIL, P. LAPORTE, R. REININGER, and V. SAILE, phys. stat. sol. (b) **143**, 783 (1987).
[21] D.W. SNOKE, W.W. RÜHLE, Y.-C. LU, and E. BAUSER, Phys. Rev. B **45**, 10 979 (1992).
[22] S. BAR-AD, P. KNER, M.V. MARQUEZINI, and D.S. CHEMLA, Phys. Rev. Lett. **77**, 3177 (1996).
[23] R. ULBRICH, Phys. Rev. B **8**, 5719 (1973).
[24] E.M. CONWELL, in: Solid State Physics, Suppl. 9, Eds. H. EHRENREICH, F. SEITZ, and D. TURNBULL, Academic Press, New York/London 1967.
[25] A.M. RATNER, Phys. Rep. **269**, 197 (1996).
[26] P.E. SELBMANN, M. GULIA, F. ROSSI, E. MOLINARI, and P. LUGLI, Phys. Rev. B **54**, 4660 (1996).
[27] V.N. ABAKUMOV, V.I. PEREL, and I.N. YASSIEVICH, Soviet Phys. – J. Exper. Theor. Phys. **51**, 626 (1980).
[28] N.C. BACALIS, D.A. PAPACONSTANTOPOULOS, and W.E. PICKETT, Phys. Rev. B **38**, 6218 (1988).
[29] M. UMEHARA, Phys. Rev. B **33**, 4245 (1986).
[30] V.N. ABAKUMOV and I.N. YASSIEVICH, Soviet Phys. – J. Exper. Theor. Phys. **44**, 345 (1977).
[31] T. VANESS, Dissertation, The University of Hamburg, 1990; Internal Rep. DESY F41 HASYLAB 90-04, November 1990.
[32] J. ROSSBACH, Nucl. Instrum and Methods **A375**, 269 (1996).
[33] B. SONNTAG and J. FELDHAUS, in: Annu. Rep. I of HASYLAB 1997, Eds. T. MÖLLER, W. LAASCH, and J.R. SCHNEIDER, Deutsches Elektronensynchrotron DESY, Hamburg 1998 (p. 95).

XII

I. Reimand, J. Aaviksoo,
"Exciton interaction with hot electrons in GaAs"
(**submitted** to Phys. Rev. B, October 1999).

Exciton Interaction with Hot Electrons in GaAs

I. Reimand and J. Aaviksoo

Institute of Physics, Tartu University, Riia 142, Tartu 50415, Estonia

Abstract

The dynamics of exciton interaction with charge carriers in GaAs, excited by a CW light source and subjected to collisions with free carriers, which are independently created by a picosecond light pulse, is studied by a novel time-resolved dual channel modulated luminescence correlation technique.

The dynamics reveals a decreased exciton generation rate at a higher temperature of charge-carriers, and a strong exciton scattering on hot free carriers that heats the excitons and effectively quenches luminescence due to smaller exciton-photon coupling at an elevated temperature of excitons.

In spite of an intense interest in excitons, some aspects of exciton dynamics are, due to their complexity, not yet well known. The dynamics of the formation of bound states, and more generally, exciton interaction with charge carriers, is one of these aspects. In recent years, several works [1 – 9] have been published on exciton formation and relaxation in quantum wells (QW), which have greater exciton oscillator strength and binding energy compared to bulk material. In bulk, experiments are made with materials with a large exciton-LO-phonon coupling [10]. Only few experimental works address exciton creation in bulk GaAs [11,12]. From the theory, we know no comprehensive model with a quantitative agreement. Therefore, every additional experimental feature could contribute to the understanding about this.

The current work presents some experimental results on exciton luminescence kinetics depending on simultaneously generated charge carriers' properties. This work was initiated by a luminescence quenching effect, found by us earlier, due to interaction between hot electrons and free excitons in bulk undoped GaAs [11]. Excitons generated by previous laser excitations were killed or heated up by the next ongoing laser pulse causing luminescence quenching. The effect had a strong dependence on the excitation energy and power.

Experimental

The sample was an ultra pure vapour phase epitaxy grown GaAs sample with the residual donor concentration of about 10^{-12} cm^{-3} [13].

Luminescence was excited by two light sources: a synchronously pumped mode-locked cavity-dumped Styryl-8 dye laser and a semiconductor (diode) CW laser. The optical pulse duration was about 5 ps with the repetition rate of 4 MHz and spectral linewidth of 0.7 meV tuneable at exciton energies and above. The semiconductor laser had a fixed wavelength of 815 nm with the linewidth of 0.1 nm (corresponds to the electron excess energy of 3 meV). The excitation power intensity was about 0.01 – 1 W/cm^2 for the pulsed laser (time averaged power) and 6 W/cm^2 for the diode laser. Photoluminescence was measured at the temperature of 2 K. The semiconductor laser had a step-like modulation of 50 kHz, thus being a quasi-CW light source for our time scales. All the luminescence kinetics curves were recorded simultaneously into two channels (corresponding to the phase of CW laser modulation) by a time-correlated photon counting system. The temporal and spectral resolution of the registering system was about 100 ps and 0.2 meV, respectively.

The chosen parameters of the modulation scheme of photon counting allow us to eliminate the effects of dead time difference for each channel of photon counting (the modulation frequency is higher than the photon count frequency) and slow time-scale laser drifts. So we can directly and quantitatively compare the luminescence intensities, depending on whether the diode laser is illuminating or not.

To the best of our knowledge, no one has ever reported using such an experimental set-up for investigating exciton luminescence. Modulation schemes have been used for registering luminescence in the spectral domain [4,9]. Our experimental set-up uses a similar idea as in ref. [4] *in the time domain* and gives us a new dimension for registering the processes.

On the other hand, such an experiment is complementary to the Four Wave Mixing experiments with a pre-injection of excitations [14, 15], but it registers inherently incoherent luminescence.

Results

In Fig. 1, luminescence kinetics curves have been shown for three different pulse intensities. The pulse photon energy is E_g+15 meV, well below the optical phonon (E_{LO}=36 meV) replica of the band (E_g - electron conduction band energy). The solid line marks the temporal dependence of luminescence when both (the diode and pulsed) lasers are exciting the crystal. The dashed line marks luminescence for the case the crystal is excited only by the pulsed laser.

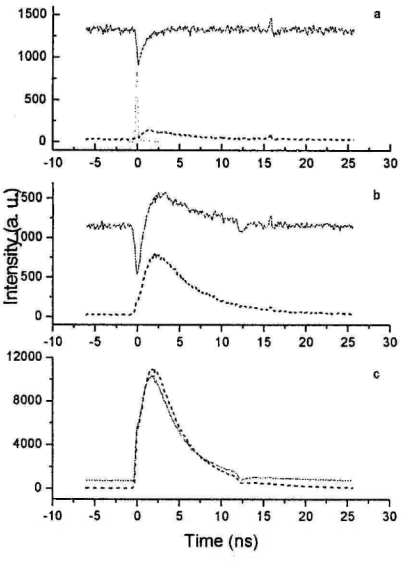

Figure 1. Experiment: temporal behaviour of the photoluminescence of the sample for excitation by the pulsed laser with (solid line) and without (dashed line) CW laser illumination in the case of three pulsed laser intensities: a - 0.01 W/cm^2, b - 0.2 W/cm^2 and c – 1 W/cm^2. The incident pulse is depicted by dots in part a.

At the lowest pulse intensity (part a) of 10 mW/cm^2 (about 10^{14} excited electrons per cubic cm per pulse) a stationary luminescence is emitted by the crystal until the pulse fires. In response to the pulse, the luminescence momentarily (below the temporal resolution of the experiment) decreases and afterwards slowly relaxes to the stationary state. The integral of the "hole" in the luminescence is approximately 80% compared to the integral of luminescence when exciting only with the pulsed laser. In other words, the excited amount of electrons, being able to create one registered exciton is able to "kill" 1.8 otherwise registered excitons. The difference kinetics is shown in the upper part of Fig. 2.

It is remarkable that no maximum appears in the kinetics, although additional excitations where injected by pulse. Where do the excitons disappear? We can analyse whether the excitons were permanently destroyed, or they moved only temporarily out of sight -- thrown to somewhere up into their evolution track (heated or ionised to charge carriers) -- and will later also take part in luminescence.

If the excitons were destroyed, we can calculate the exciton decay time in the following way. The stationary number of excitons is determined by the balance between the generation rate (due to diode-laser), and lifetime τ_x of excitons. At the moment of the pulse an unknown process quickly changes the number of excitons. Now the system approaches to the balance again, and, additionally, new excitons, generated by pulse, will play a role in the luminescence.

$$\frac{dN_1}{dt} = G_P(t) - \frac{N_1}{\tau_x}$$

$$\frac{dN_2}{dt} = G_S + G_P(t) - R(I)\delta(t)N_{2,stats} - \frac{N_2}{\tau_x}$$

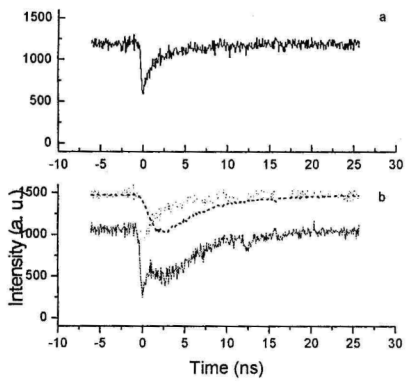

Figure 2. Solid lines: temporal behaviour of the photoluminescence difference at a low pulse intensity (0.01 W/cm^2 – upper part) and intermediate intensity (0.2 W/cm^2 – lower part). Dotted line -- the contribution of smaller exciton coupling with photons due to the exciton temperature change, dashed line – the contribution of the changed exciton generation rate due to the electron temperature change.

Here N_1 and N_2 are the number of excitons created by pulsed-laser-only and by both lasers, respectively. G_P, G_S are the exciton generation rates from a pulsed and stationary source, R(I) is the number of lost excitons depending on the pulse intensity I, $\delta(t)$ is the delta-function. For the sake of simplicity we use stationary value of N_2 considering the number of lost excitons.

The solution gives us the number of excitons, proportional to our measured luminescence for either case:

$$N_1 = \exp(-\frac{t}{\tau_x}) \int G_p(t) \exp(\frac{t}{\tau_x}) dt$$

$$N_2 = N_{2,stats} \left(1 - H(t) R(I) \exp(-\frac{t}{\tau_x}) \right) + N_1$$

Subsequently the difference of the two measured luminescence kinetics should give us a pure exponential curve. Consequently, we get exciton lifetime extracted from all other processes. H(t) is the Heaviside function.

This idea holds in the zeroth order of approximation, assuming that the exciton generation function from the pulse-excited charge carriers $G_P(t)$ does not differ for different experiments (which means that the additional charge carrier concentration, caused by pulse, is small compared to the stationary one). For testing of the applicability of the idea we subtracted the luminescence curves, corresponding to N_1, from N_2. In the pulse intensity range of 0.01 mW to 0.05 mW the character of the difference kinetics does not change essentially, indicating that using this idea at our lowest intensities is reasonable. The decay time fitted from the difference kinetics (assuming excitons were destroyed) is τ=2 ns.

If the excitons were not permanently destroyed (a part of "lost excitons" will return to the stationary state), then τ fitted from difference kinetics is a function of the exciton decay time τ_x and round trip time τ_r. In the simplest case, when losses during the round trip are equal to the stationary exciton losses, we will get $\tau^{-1} = \tau_x^{-1} + \tau_r^{-1}$. But in any case $\tau_x \geq \tau$. A qualitative analysis says that if losses during the round trip are smaller than in the stationary case, then the luminescence kinetics excited by both lasers will always have a maximum.

On the other hand, we do have independent data for exciton decay time (measured on the same sample, where excitons were created directly by a laser pulse at a low intensity), $\tau_x \approx 4$ ns. Due to an essential difference between τ and τ_x, we can conclude that the excitons, disappearing from the luminescence band at the moment of an additional laser excitation, will be excited to a state with a higher energy (a hot exciton or a free charge carrier pair) and will later return to their previous state. The absence of a maximum in luminescence (at excitation of both lasers) lets us conclude, that the averaged losses (both non-radiative and radiative) at these upper states are bigger than in the stationary case.

At an intermediate intensity of 0.2 W/cm^2 (Fig. 1 b) when excited both by a diode and pulsed laser, at the moment of pulse excitation the stationary luminescence also decreases, but later the luminescence grows higher than the stationary one. For the pulsed-only excitation, a steep rise of luminescence is taking place followed by a slower component. In luminescence kinetics this steep step-like or even spike-like behaviour is often attributed to an experimental artefact (scattered exciting laser pulse), but in the current experiment we do not see the feature on other simultaneously registered kinetics – indicating to the real nature of the effect. We think that the step-like behaviour may be caused by a small fraction of excitons created by a LO-phonon mediated process (the initial hot distribution of the charge carriers generated by photons with an excess energy of 15 meV may have a sufficiently high-energy tail). The relative share of the step-like feature increases with the pulse intensity, as it should be in a bimolecular process, thus, confirming the interpretation. The LO-mediated exciton generation is important in GaAs QW structures [3,7]. The Monte-Carlo calculations made by Selbmann et. al. [16] predicted an essential share of the LO-process in exciton creation also in bulk GaAs. In our earlier experiment [11] we, as well as the authors of ref. [12] have not seen a distinct evidence of the LO-phonon mediated exciton generation in bulk GaAs. This may be caused by the fact that in the experiments of [11,12] the excitation intensity is about an order of magnitude lower and the bimolecular process (depending on the carrier concentration as n^2) had too small probability. In our earlier unpublished measurements, we often saw this spike-like behaviour, but attributed it to a scattered laser light.

The difference kinetics in the case of an intermediate pulse intensity is shown in the lower part of Fig. 2. A two-component structure is clearly seen. At the moment of excitation, a similar luminescence quenching is going on as in the low-intensity case. Later, another component, roughly proportional to the exciton luminescence signal, also reveals itself. We interpret the further component as a contribution of a smaller exciton coupling with photons due to an exciton temperature change (photons can be emitted only at $k \cong 0$, at an elevated temperature the share of such excitons decreases). The other

component may be due to a changed exciton generation rate with an electron temperature increase.

At a high pulse intensity of 1 W/cm^2 (Fig. 1 c), no initial decrease takes place. Instead, at the first moment, a step-like rise in luminescence is found for both cases. A striking fact is that the maximum luminescence intensity, if exciting with both light sources, is lower than if exciting only with a pulsed laser. The character of difference kinetics (not shown) does not change, compared with the intermediate pulse intensity, except that the slower component reveals a different (slower) form than the corresponding pulsed-only luminescence. This seems to be natural, considering the bimolecular process of exciton formation and the reduced exciton generation rate at a higher carrier temperature.

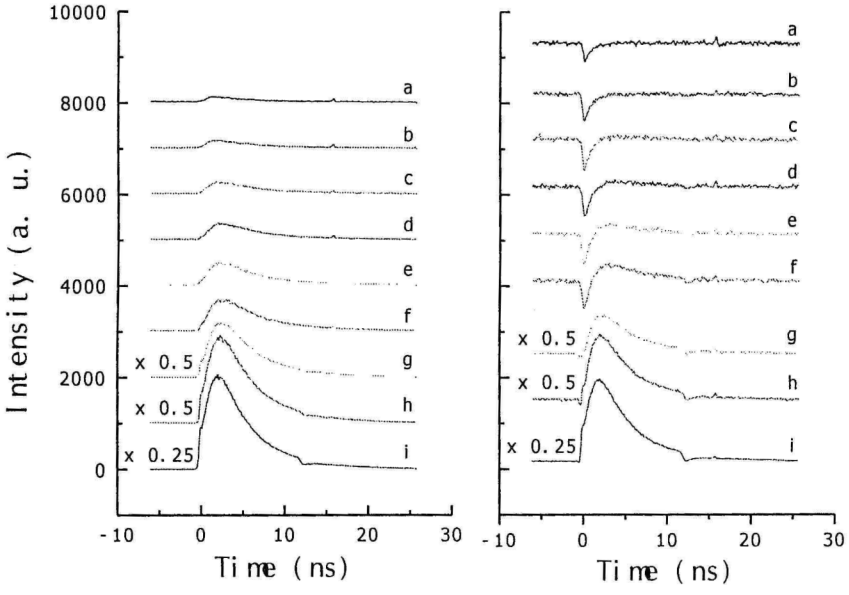

Figure 3. A series of luminescence kinetics for different intensities of pulse excitation without (left part) and with (right part) CW background illumination. a - 0.01 W/cm^2, b - 0.03 W/cm^2, c – 0.05 W/cm^2, d - 0.08 W/cm^2, e - 0.12 W/cm^2, f - 0.15 W/cm^2, g - 0.3 W/cm^2, h - 0.8 W/cm^2 and i – 0.8 W/cm^2. The excess energy of pulse excitation was 15 meV.

In Fig. 3, a series of kinetics depending on the pulse intensities are shown. At higher excitation intensities another hole in the luminescence kinetics is pronounced (at 12 ns delay). The second hole originates from the excitation by a replica of the laser pulse (due to a imperfection of the cavity-dumper), which has approximately 1.5% of the main pulse intensity.

For comparison, similar experiments were performed with the photon energy of the pulsed laser tuned into the exciton energy zone and below the exciton

resonance energy. In the case of exciting excitons directly by the laser pulse, no significant changes in the luminescence kinetics' shape, depending on the background lightening, were found. In this case, however, the rise of the luminescence is so fast that the quenching effect could be hidden under it. In case of exciting the crystal below the exciton resonance the stationary luminescence was totally unaffected by the presence of the pulsed laser. That rules out the possibility of a direct interaction between a laser pulse and the excitons created by the diode laser.

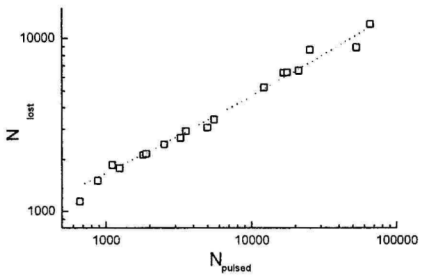

Figure 4. Open squares: fraction of excitons "getting lost" when an additional CW excitation is present, compared to the luminescence intensity for the pulsed excitation. With the dotted line a fit $q \propto \sqrt{N_{pulsed}}$ is shown.

In Fig. 4, the number of lost excitations (N_{lost}) depending on N_{pulsed} is shown, calculated by formula:

$$N_{lost} = N_{stationary} + N_{pulsed} - N_{both}$$

where $N_{stationary}$ is the integral of stationary luminescence when excited only with a diode laser, N_{pulsed} is the integral of luminescence when excited only with a pulsed laser and N_{both} is the integral when both excitations are in use. We do not have an explanation to the dependence, but it is interesting to note that N_{lost} depends on N_{pulsed} as square root. The dotted line in Fig. 4. marks the dependence

$N_{lost} = a + b*(N_{pulsed})^{1/2}$.

To model the interaction of charge-carriers and excitons including thermal exchange, we used the following set of Boltzmann rate equations for particle concentrations n and mean energies E (subscripts eh and x denote charge carriers and excitons, respectively):

$$\frac{dn_{eh}}{dt} = G - \frac{n_{eh}}{\tau_{eh}} - \sigma n_{eh}^2$$

$$\frac{dn_x}{dt} = -\frac{n_x}{\tau_x} + \sigma n_{eh}^2$$

$$\frac{2}{3k}\frac{dE_{eh}}{dt} = GT_g - \frac{n_{eh}}{\tau_{eh}}T_{eh} - \left\langle \frac{dE_{eh}}{dt} \right\rangle_{ph} - \sigma n_{eh}^2 T_{eh} + \gamma n_{eh} n_x (T_x - T_{eh})$$

$$\frac{2}{3k}\frac{dE_x}{dt} = -\frac{n_x}{\tau_x}T_x - \left\langle \frac{\overline{dE_x}}{dt} \right\rangle_{ph} + \sigma n_{eh}^2 (T_{eh} + T_B) - \gamma m_{eh} n_x (T_x - T_{eh})$$

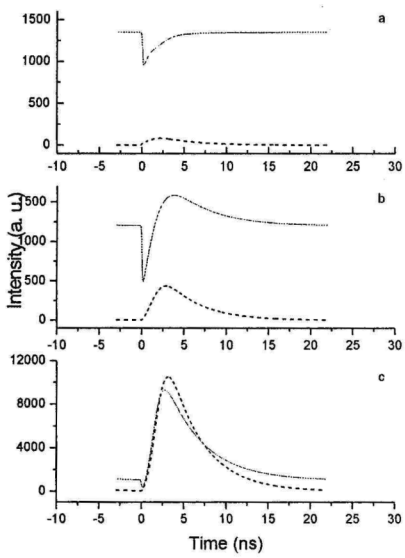

Figure 5. Model calculations basing on Boltzmann' rate equations (see text): temporal behaviour of the photoluminescence of the sample for excitation by the pulsed laser with (solid line) and without (dashed line) CW laser illumination in the case of different pulsed laser intensities: a – low pulse intensity, b – intermediate pulse intensity and c – high intensity.

Here T_g is the charge carrier temperature at excitation and T_B is the temperature corresponding to the Rydberg' energy of the exciton. $\left\langle \frac{\overline{dE}}{dt} \right\rangle_{ph}$ is the mean energy loss rate of a particle in all the scattering processes on phonons (for charge carriers we considered the deformation potential and piezoelectric LA phonon and polar LO phonon scattering, for excitons deformation potential LA scattering, the corresponding rates were taken from literature [17,18]). γ stands for an exciton probability to lose energy by colliding with a charge carrier (we considered the thermal exchange, not exciton dissociation). For γ we used the hydrogen-electron collision efficiency $\gamma_0 = 20a_0\frac{h}{m_e}$, taken from [19], multiplied by the mean energy exchange fraction at collision $\frac{2m_e}{m_e + m_x}$.

$$\gamma = 40a_0\frac{h}{m_e + m_x}$$

a_0 is the Bohr radius of an exciton.

For bimolecular coupling constant σ we used a formula from Ref. [20], which we modified for the case when the temperature of the charge carriers differs from that of the lattice. To our knowledge, this is the only model describing the exciton creation cross section depending on (carriers effective) temperature (in 3D). In our calculations the essential feature was the temperature behaviour of the cross section $\sigma \propto T_e^{-1.5}$, which follows from the acceptable assumption of

charge carriers Boltzmann' distribution. For 2D case in QW, the dependence $\sigma \propto T_e^{-1}$ is used by ref. [6].

In Fig. 5 the calculated kinetic curves are presented. The model qualitatively explains the experimental features. At a low pulse intensity no maximum appears in the luminescence with a CW background excitation. At a high excitation the luminescence without a background CW excitation has a higher intensity than the one with that. We could not find an opportunity for the model to take into account the proposed LO phonon mediated exciton creation mechanism, so the model does not reproduce the initial steep rise.

Comparison with the results of other authors

The results of our experiment are related to Excitation Induced Dephasing (EID) experiments, made by Four Wave Mixing (FWM) techniques with a pre-injection of incoherent excitations [14,15]. The authors of Ref. [14,15] determine the excitons dephasing rate $1/T_2$ depending on the concentration of the additionally injected excitations. They indicate that exciton-free-carrier scattering is 10 times as efficient as exciton-exciton scattering. As the FWM experiment measures the phase-coherence dephasing, it says nothing explicit about the energy (heat) exchange, the heat exchange in exciton-free-carrier scattering is evident. Our experiment, measuring the incoherent part of the secondary emission, thus gives some complementary information to FWM EID experiments.

Robart et. al. [21] have also seen a significant energy exchange between the charge carriers and excitons. They have even concluded a thermodynamic equilibrium with equal temperatures and chemical potentials of the subsystems. In a bulk crystal, we cannot apply the method of ref. 21 to check this idea.

To the authors' knowledge, the most comprehensive calculation of the involved processes is published in Ref. [16] using the Monte-Carlo ensemble method for solving Boltzmann' rate equations for coupled free-carriers and excitons. The authors of ref. [12] report a good accordance of the experimental data with the calculations (except for the calculations' conclusion about the exciton creation through a LO phonon). In the theoretical consideration, however, no process was involved for the charge-carrier-exciton heat exchange and for the exciton dissociation depending on the charge-carrier distribution. Basing on our experiment, and on the FWM results of [14], we note, however, that exciton dephasing processes should play an important role in the experimental results of Ref. 12 as well. These processes do reveal themselves in a less evident way, retarding the onset of luminescence until the hot charge carriers are cooled down.

However, the Monte-Carlo ensemble' approach, used by the authors of Refs. [12, 16], after including the thermal exchange between excitons and carriers, is evidently a more appropriate method for trying to quantitatively fit the experimental results.

Piermarocchi et. al. [8, 22], calculating exciton creation dynamics in QW, also neglect the heat exchange effect while operating with hot charge carrier distributions with quite a high concentration up to $n=10^{12}\,cm^{-2}$ (the corresponding bulk concentration would be $n=10^{18}\,cm^{-3}$). We think that one should expect an essential influence of exciton dephasing on carriers.

Aschkinadze et. al. [4] have also investigated the exciton heat exchange with charge carriers in GaAs QW. A very interesting result was obtained, revealing exciton *cooling* by the carriers (although the carriers were initially generated at a high temperature). We think that in their experiment the excitons, created directly in the exciton band, had normally a higher effective temperature, compared with the carriers' effective temperature establishing dynamically in the process of charge-carrier generation and their energy relaxation.

Baars et. al [9], in their modulation experiment on exciton creation in GaAs QW, have detected a broadening and blue-shift of the exciton line depending on the excitation intensity of the charge carriers. They have attributed the exciton broadening to exciton-carrier scattering and the blue-shift to a quantum-confined Stark effect. We think that if there is an effective exciton-carrier scattering (as they propose), then the carriers may heat excitons as well, with a blue-shift of the exciton line. Certainly, a detailed analysis of the origin of the blue-shift is needed to establish the contributions of each process.

Summary

Exciton luminescence quenching in bulk GaAs was investigated using a new experimental technique. This technique gives complementary information to the FWM experiments with pre-pulse, studying excitation induced dephasing in semiconductors.

The quenching effect consists of two contributions: a decreased exciton coupling with photons due to an exciton temperature change and a changed exciton generation rate due to an electron temperature change. The effect can be explained qualitatively using Boltzmann' rate equations, if the exciton heating by the charge carriers is taken into account.

The steep luminescence onset, often attributed to an experimental artefact, may be an evidence of a LO phonon mediated exciton creation process.

Acknowledgement

We gratefully thank V. V. Travnikov and V. V. Rossin for providing us with the sample.

The present work has been supported by Estonian Science Foundation grant no G2338.

References

1. T. C. Damen, J. Shah, D. Y. Oberli, D. S. Chemla, J. E. Cunningham, J. M. Kuo, Phys. Rev. B **12**, 7434 (1990).
2. J. Kusano, Y. Segawa, Y. Aoyagi, S. Namba, H. Okamoto, Phys. Rew. B **40**, 1685 (1989).
3. P. W. M. Blom, P. J. van Hall, C. Smit, J. P. Cuypers, J. H. Wolter, Phys. Rev. Lett. **71**, 3878 (1993).
4. B. M. Ashkinadze, E. Linder, E. Cohen, Arza Ron, L. N Pfeiffer, Phys. Rev. B **51**, 1938 (1995).
5. J. Kovač, H. Schweizer, M. H. Pilkuhn, H. Nickel, Phys. Rev. B **54**, 13440 (1996).
6. R. Kumar, A. S. Vengurlekar, S. S. Prabhu, J. Shah, L. N. Pfeiffer, Phys. Rev. B **54**, 4891 (1996).
7. M. Gulia, F. Rossi, E. Molinari, P. E. Selbmann, P. Lugli, Phys. Rev. B **55**, R16049 (1997).
8. C. Piermarocchi, F. Tassone, V. Savona, A. Quattropani, P. Schwendimann, Phys. Rev. B **55**, 1333 (1997).
9. T. Baars, M. Gal, Phys. Rev. B **57**, 3974 (1998).
10. S. S. Prabhu, A. S. Vengurlekar, J. Shah, Phys. Rev. B **53**, R10465 (1996).
11. J. Aaviksoo, I. Reimand, V. V. Rossin, V. V. Travnikov, Phys. Rev. B **45**, 1473 (1992).
12. M. Gurioli, P. Borri, M. Colocci, M. Gulia, F. Rossi, E. Molinari, P. E. Selbmann, P. Lugli, Phys. Rev. B **58**, R13403 (1998).
13. V. G. Golubev, Yu. V. Zhilyaev, V. I. Ivanov-Omskii, G. R. Markaryan, A. V. Osutin, V. E. Chelnokov, Sov. Phys. Semicond. **21**, 1074 (1987).
14. L. Shultheis, J. Kuhl, A. Honold, C. W. Tu, Phys. Rev. Lett. **57**, 1635 (1986).
15. A. Honold, L. Shultheis, J. Kuhl, C. W. Tu, Phys. Rev. B **40**, 6442 (1989).
16. P. E. Selbmann, M. Gulia, F. Rossi, E. Molinari, P. Lugli, Phys. Rev. B **54**, 4660 (1996).
17. J. Shah, Ultrafast Spectroscopy of Semiconductors and Semiconductor Nanostructures, Springer, 1996.
18. "Semiconductors Probed by Ultrafast Laser Spectroscopy", vol.1, edited by R. R. Alfano, Academic Press Inc., 1984.
19. Erginsoy, Phys. Rev. **79**, 1013 (1950).
20. V. N. Avakumov, V. I. Perel, I. N. Yassievich, Sov. Phys. JETP **51**, 626 (1980).
21. Robart, X. Marie, B. Baylac, T. Amand, M. Brousseau, G. Baquet, G. Debart, R. Planel, J. M. Gerard, Sol. Stat. Comm. **95**, 287 (1995).
22. C. Piermarocchi, F. Tassone, V. Savona, A. Quattropani, P. Schwendimann, Phys. Rev. B **53**, 15834 (1996).

CURRICULUM VITAE

Indrek Reimand

Citizenship:	Estonian
Date of birth:	July 5, 1964
Personal status:	Married, one child
Address:	Institute of Physics, University of Tartu, Riia 142, 50415 Tartu, ESTONIA
Phone:	(372) 7 383028
Fax:	(372) 7 383033
E-mail	indrek@fi.tartu.ee

Education

1971–1979	Tartu Secondary School No 5
1979–1982	Nõo Secondary School. Finished in 1982.
1982–1983	University of Tartu, Faculty of Physics and Chemistry
1983–1985	Regular service in the Soviet Army
1985–1989	University of Tartu, Faculty of Physics and Chemistry. Graduated *cum laude* in solid state physics

Employment

1989–1992	Institute of Physics, Estonian Academy of Sciences, junior research fellow
1992–1996	Tartu University, post-graduate student
1996–	Institute of Physics, engineer
1994, 1996, 1997	University of Hamburg, Germany, visiting scientist

Research

His scientific interests lie in the field of optics and spectroscopy of solid states: time-resolved laser spectroscopy of semiconductors and cryo-crystals, dynamics of photo-excitations in bulk crystals and low-dimensional structures.

Has 20 scientific publications.

ELULUGU

Indrek Reimand

Kodakondsus:	Eesti
Sünniaeg:	5. juuli 1964
Perekonnaseis:	Abielus, peres üks laps
Aadress:	Tartu Ülikooli Füüsika Instituut, Riia 142, Tartu 50415, Eesti.
Telefon:	(372) 7 383028
Faks:	(372) 7 383033
E-meil	indrek@fi.tartu.ee

Hariduskäik

1971–1979	Tartu 5. Keskkool
1979–1982	Nõo Keskkool
1982–1983	Tartu Ülikool, Füüsika-keemia teaduskond
1983–1985	Teenistus Nõukogude armees
1985–1989	Tartu Ülikool, Füüsika-keemia teaduskond; lõpetas 1989 kiitusega füüsikaosakonna tahkisefüüsika erialal

Erialane teenistuskäik

1989–1992	TA Füüsika Instituut, nooremteadur
1992–1996	Tartu Ülikool / Füüsika Instituut, doktorant
1996–	Füüsika Instituut, insener
1994, 1996, 1997	Hamburgi Ülikooli külalisteadlane

Teadustegevus

Teaduslikud huvid on seotud tahkiste optika ja spektroskoopiaga: aeglahutusega pooljuhtide ja krüokristallide laserspektroskoopia, fotoergastuste dünaamika kristallides ja madaladimensioonilistes struktuurides.

On avaldanud 20 teaduspublikatsiooni.

LIST OF PUBLICATIONS BY THE AUTHOR

1. J. Aaviksoo, J. Kuhl, I. Reimand, "Time-resolved reflection of light from InP crystals", Solid State Comm., vol. 72, no. 1, p. 49 (1989).
2. Я. Ю. Аавиксоо, И. Я. Рейманд, В. В. Россин, В. В. Травников, "Пикосекундная кинетика энергетической релаксации и образования экситонов в GaAs", Тезисы докладов, XII Всесоюсная конференсия по физике полупроводников, Киев, ч. 2, стр. 6, (1990).
3. И. Рейманд, Я. Аавиксоо, "Отражение коротких световых импульсов от поверхности полупроводников в области экситонного резонанса", Тезисы докладов, XII Всесоюсная конференсия по физике полупроводников, Киев, ч. 2, стр. 165, (1990).
4. J. Aaviksoo, J. Kuhl, I. Reimand, "Time resolved resonant reflection of light", abstr. of the IV USA-USSR Symp. On Laser Spectroscopy, Jan. 26, - Feb. 1, 1990, Irvine, p. 3, (1990).
5. J. Aaviksoo, J. Kuhl, I. Reimand, "Time resolved resonant reflection of light", Laser Optics of Condensed Matter, vol. 2, Plenum New York, pp. 61-69 (1991).
6. A. Reznitsky, A. Naumov, S. Verbin, J. Aaviksoo, I. Reimand, "Exciton and pair recombination through alloy trapped states in $CdS_{1-x}Se_x$ solid solutions", J. Lumin, vol. 47, no. 6, p. 297, (1991).
7. Я. Ю. Аавиксоо, И. Я. Рейманд, В. В. Россин, В. В. Травников, "Кинетика образования и энергетической релаксации экситонов в GaAs", Письма в ЖЭТФ, том 53, вып. 7, стр. 377, (1991).
8. I. Reimand, J. Aaviksoo, "Surface polarization dynamics revealed by time-resolved resonant reflection of light", Opt. Commun., vol. 86, no. 2, p. 142, (1991).
9. Я. Ю. Аавиксоо, И. Я. Рейманд, В. В. Россин, В. В. Травников, "Гашение экситонной люминесценции горячими электронами в GaAs", ФТТ, том 33, вып. 8, стр. 2408, (1991).
10. J. Aaviksoo, I. Reimand, V. V. Rossin, V. V. Travnikov, "Kinetics of free exciton luminescence in GaAs", Phys. Rev. B, vol. 45, no. 3, p. 1473, (1992).
11. J. Aaviksoo, I. Reimand, V. Rossin, V. Travnikov, "Kinetics of free exciton formation and relaxation in GaAs", J. Lumin., vol. 53, p. 423, (1992).
12. J. Aaviksoo, I. Reimand, V. Rossin, V. Travnikov, "Hot photoexcited electrons and exciton kinetics in GaAs", Proc. SPIE, vol. 1677, p. 192, (1992).
13. D. Varding, I. Reimand, G. Zimmerer, "Monte-Carlo-Simulation zur Exzitonendiffusion und Vergleich mit zeitaufgelösten Lumineszenz-

untersuchungen freier Exzitonen in festem Xenon", HASYLAB Jahresbericht, 1993.
14. D. Varding, I. Reimand, G. Zimmerer, "Time-resolved luminescence of exciton-polaritons in solid xenon", Physica Status Solidi B, vol. 185, no. 1, p.301, (1994).
15. Я. Ю. Аавиксоо, И. Я. Рейманд, В. В. Россин, В. В. Травников, "Влияние экситон-электронного взаимодействия на кинетику экситонной люминесценсии", ФТТ, т. 36, № 5, стр. 1470, (1994).
16. J. Aaviksoo, I. Reimand, V. V. Travnikov, S. O. Kognovitskii, "Polariton-electron interaction in GaAs", Proc. 23rd Int. Conf. On the Physics of Semiconductors, Berlin, July 1996, pp. 357-360, (M.Scheffer and R.Zimmermann eds.), World Scientific Singapore.
17. С. О. Когновицкий, В. В. Травников, Я. Аавиксоо, И. Рейманд, "Рассеяние света электронами в области экситонного поглащения GaAs", ФТТ том 39, стр. 1011, (1997).
18. R. Jaanisoo, H. Lipsanen, I. Reimand, M. Sopanen, "Photoluminescence decay and upconversion of stressor-induced GaInP Quantum Dots", Proceedings of the X international conference "Ultrafast Processes in Spectroscopy", Tartu, 1997, p. 81.
19. I. Reimand, J. Aaviksoo, "Exciton interaction with hot electrons in GaAs", Technical digest of X International Conference on Ultrafast Phenomena in Spectroscopy, Tartu, 1997, p. 82.
20. I. Reimand, E. Gminder, M. Kirm, V. Kisand, B. Steeg, D. Varding, G. Zimmerer, "An analysis of electron-hole recombination in solid Xenon with time-resolved luminescence spectroscopy", Phys. Stat. Sol. (b), vol. 214, no 1, p. 81 (1999).
21. I. Reimand, J. Aaviksoo, "Exciton interaction with hot electrons in GaAs" (**submitted** to Phys. Rev. B, October 1999).

DISSERTATIONES PHYSICAE UNIVERSITATIS TARTUENSIS

1. Andrus Ausmees. XUV-induced electron emission and electron-phonon interaction in alkali halides. Tartu, 1991.
2. Heiki Sõnajalg. Shaping and recalling of light pulses by optical elements based on spectral hole burning. Tartu, 1991.
3. Sergei Savihhin. Ultrafast dynamics of F-centers and bound excitons from picosecond spectroscopy data. Tartu, 1991.
4. Ergo Nõmmiste. Leelishalogeniidide röntgenelektronemissioon kiiritamisel footonitega energiaga 70–140 eV. Tartu, 1991.
5. Margus Rätsep. Spectral gratings and their relaxation in some low-temperature impurity-doped glasses and chrystals. Tartu, 1991.
6. Tõnu Pullerits. Primary energy transfer in photosynthesis. Model calculations. Tartu, 1991.
7. Olev Saks. Attoampri diapasoonis voolude mõõtmise füüsikalised alused. Tartu, 1991.
8. Andres Virro. AlGaAsSb/GaSb heterostructure injection lasers. Tartu, 1991.
9. Hans Korge. Investigation of negative point discharge in pure nitrogen at atmospheric pressure. Tartu, 1992.
10. Jüri Maksimov. Nonlinear generation of laser VUV radiation for high-resolution spectroscopy. Tartu, 1992.
11. Mark Aizengendler. Photostimulated transformation of aggregate defects and spectral hole burning in a neutron-irradiated sapphire. Tartu, 1992.
12. Hele Siimon. Atomic layer molecular beam epitaxy of A^2B^6 compounds described on the basis of kinetic equations model. Tartu, 1992.
13. Tõnu Reinot. The kinetics of polariton luminescence, energy transfer and relaxation in anthracene. Tartu, 1992.
14. Toomas Rõõm. Paramagnetic H^{2-} and F^+ centers in CaO crystals: spectra, relaxation and recombination luminescence. Tallinn, 1993.
15. Erko Jalviste. Laser spectroscopy of some jet-cooled organic molecules. Tartu, 1993.
16. Alvo Aabloo. Studies of crystalline celluloses using potential energy calculations. Tartu, 1994.
17. Peeter Paris. Initiation of corona pulses. Tartu, 1994.
18. Павел Рубин. Локальные дефектные состояния в CuO_2 плоскостях высокотемпературных сверхпроводников. Тарту, 1994.
19. Olavi Ollikainen. Applications of persistent spectral hole burning in ultrafast optical neural networks, time-resolved spectroscopy and holographic interferometry. Tartu, 1996.

20. Ülo Mets. Methodological aspects of fluorescence correlation spectroscopy. Tartu, 1996.
21. Mikhail Danilkin. Interaction of intrinsic and impurity defects in CaS:Eu luminophors. Tartu, 1997.
22. Ирина Кудрявцева. Создание и стабилизация дефектов в кристаллах KBr, KCl, RbCl при облучении ВУФ-радиацией. Тарту, 1997.
23. Andres Osvet. Photochromic properties of radiation-induced defects in diamond. Tartu, 1998.
24. Jüri Örd. Classical and quantum aspects of geodesic multiplication. Tartu, 1998.
25. Priit Sarv. High resolution solid-state NMR studies of zeolites. Tartu, 1998.
26. Сергей Долгов. Электронные возбуждения и дефектообразование в некоторых оксидах металлов. Тарту, 1998.
27. Kaupo Kukli. Atomic layer deposition of artificially structured dielectric materials. Tartu, 1999.
28. Ivo Heinmaa. Nuclear resonance studies of local structure in $RBa_2Cu_3O_{6+x}$ compounds. Tartu, 1999.
29. Aleksander Shelkan. Hole states in CuO_2 planes of high temperature superconducting materials. Tartu, 1999.
30. Dmitri Nevedrov. Nonlinear effects in quantum lattices. Tartu, 1999.
31. Rein Ruus. Collapse of 3d (4f) orbitals in 2p (3d) excited configurations and its effect on the x-ray and electron spectra. Tartu, 1999.
32. Valter Zazubovich. Local relaxation in incommensurate and glassy solids studied by Spectral Hole Burning. Tartu, 1999.

ISSN 1406–0647
ISBN 9985–56–475–8